An investigation into the influence of microstructural condition on the superelastic behaviour in Ti-Nb-based alloys.

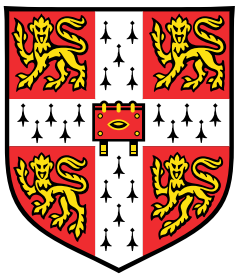

Emma Hildyard

Supervisor: Dr N.G. Jones

Department of Materials Science and Metallurgy

University of Cambridge

This dissertation is submitted for the degree of

Doctor of Philosophy

Robinson College

September 2019

I dedicate this piece of work to my mum, dad and brother, who have continued to support my work, despite me constantly shifting my goal posts!

I wonder what the next challenge will be...

Declaration

This dissertation is the result of my own work and includes nothing which is the outcome of work done in collaboration except as declared in the Preface and specified in the text. It is not substantially the same as any that I have submitted, or, is being concurrently submitted for a degree or diploma or other qualification at the University of Cambridge or any other University or similar institution except as declared in the Preface and specified in the text. I further state that no substantial part of my dissertation has already been submitted, or, is being concurrently submitted for any such degree, diploma or other qualification at the University of Cambridge or any other University or similar institution except as declared in the Preface and specified in the text. This dissertation contains fewer than 60,000 words, including the abstract, tables, footnotes and appendices, but excluding table of contents, photographs, diagrams, figure captions, list of figures/diagrams, list of abbreviations/acronyms, bibliography and acknowledgements.

The following papers have been published, or are in the process of being submitted:

E.M. Hildyard, L.D. Connor, L. Owen, D. Rugg, N. Martin, H.J. Stone and N.G. Jones, On the influence of microstructure on the $\beta \rightarrow \alpha''$ transformation in Ti-24Nb (at.%), Acta Materialia (in process of being submitted for review)

E.M. Hildyard, L.D. Connor, T. Whitfield, N. Martin, D. Rugg, H.J. Stone and N.G. Jones, On the effect of microstructural features on the superelastic behaviour in Ti-24Nb (at.%), Acta Materialia (in process of being submitted for review)

E.M. Hildyard, L.D. Connor, N. Martin, D. Rugg, H.J. Stone and N.G. Jones, The nature of the $\beta \rightarrow \alpha''$ transformation in Ti-Nb alloys, Proceedings of the 14th World Conference on Titanium, 2019 (accepted)

N.G. Jones, E.M. Hildyard, and L.D. Connor, The influence of ternary and quaternary alloy additions on the superelastic behaviour of metastable Ti-Nb based alloys, Proceedings of the 14th World Conference on Titanium, 2019 (under review)

J.M. Bennett, E.M. Hildyard, L.D. Connor, M.G. Tucker, D. Rugg, H.J. Stone, On the $\beta \rightarrow \alpha''$ transformation in Ti-15 Mo (wt%), Materials Science and Engineering A (under review)

E.L. Pang, E.M. Hildyard, L.D. Connor, E.J. Pickering, N.G. Jones, Unusual aspects of the $\beta \rightarrow \alpha''$ martensitic transformation in Ti-Nb alloys, Materials Science and Engineering A (under review)

Emma Hildyard

September 2019

Acknowledgements

A silly old bear was once told to always remember:

"You're braver than you believe, stronger than you seem, and smarter than you think"

- A.A. Milne

I would like to thank the people that have helped me to remember this too.

Firstly, thank you to my supervisor Nick for his guidance over the past 4 years. We have had some cracking discussions, which have made my brain hurt way too much, but, some great science has resulted from them. Thank you to the EPSRC and Rolls Royce for funding the project and to Nigel Martin and Dave Rugg, at Rolls Royce, for reminding me of the significance of my work in the real world. Meetings with you all have made me really proud of my work and I look forward to presenting our ideas to the wider community at the World Conference on Titanium in June 2019.

The RR UTC group have been a brilliant bunch of people to work with. Thank you for all of the help in the lab, your contributions to scientific discussions and cups of tea. In particular, I'd like to acknowledge Lewis, Kathy, Caspar, James and Tamsin, who have made the office a fun place to be. You have all become really true friends.

Thank you to the technicians in the department that helped me to run all of my experiments. A particular thanks goes to Paul Stokes for his patience whilst cutting hundreds of tensile samples and Sue Rhodes for encapsulating all of them, and HT Pang for fixing everything that I broke! The synchrotron experiments could not have been conducted without Howard Stone

and Leigh Connor, who ran the experiments during the day to let me get a few hours of sleep.

It's funny, I have spent months and months writing this document, and the part that I am about to write is by far the most difficult. I would like to thank my mum, dad and brother, who have been there since the very beginning. When Jason Drewett first mentioned that I should apply to Cambridge, we all thought that he was barking mad, but look how wrong we were. Thank you Jason, without you, I wouldn't be sat here.

I could not have completed this PhD without my wonderful friends Dan, Henri, Konstantin and Mark, who have helped me at the times when I needed help to be braver than I believed. Thank you to the college bar staff, especially Catherine and Nick, and Gary the porter, who have picked me up on the days when I have needed it most. Robinson is so so lucky to have you all.

Lastly, and by definitely no means least, James. There aren't enough words in the dictionary (or in the Emma-dictionary!) to tell you how much your support over the past 3 years has meant to me. Thank you for helping me to be brave, and helping me to find a strength that I didn't realise I had. Thank you for always believing in me, especially when I had lost faith in myself. I love you.

Abstract

Ti-Nb based alloys exhibit superelastic and shape memory properties over a wide range of temperatures, making them attractive for industrial applications. However, within the literature there are significant variations in the reported martensite start temperatures and associated behaviour that have not been fully explained. These variations are problematic to engineering design, thereby limiting the industrial uptake of these alloys. To investigate the source of these discrepancies a model alloy, Ti-24Nb (at.%), has been studied in two different microstructural conditions, cold rolled and solution heat treated, using a variety of different analytical techniques. Initial characterisation of the material was performed using X-ray diffraction and electron microscopy. Information relating to the evolution of the material in response to changes in stress and temperature were obtained *in situ* using synchrotron radiation. These diffraction data were used to directly characterise the phase constitution of the alloy during a five step thermomechanical cycle. To expand this dataset, this cycle was repeated a number of times to enable loading at different temperatures in the range of -196°C to 30°C. The α'' martensite was observed to form when cold rolled material was cooled. In contrast, no evidence of the β to α'' transformation was observed in material that had been solution heat treated, despite cooling to -196°C under identical conditions. Further transformation could be induced in both samples through the application of an external stress. In light of these results, it was proposed that the martensitic transformation that gives rise to superelastic behaviour can be explained in terms of type I, II and III stresses rather than being solely dependent on the key transformation temperatures. The observed results highlight that the transformation behaviour in Ti-24Nb (at.%) is significantly influenced by microstructural condition. To elucidate this further, the effect of grain size and dislocation density on the transformation behaviour in Ti-24Nb-4Zr-8Sn (wt.%) have been briefly investigated. The results indicated that the grain size did not alter the transformation behaviour as significantly as the dislocation

density, however, these experiments were preliminary and further investigations into the microstructural features that change the superelastic properties exhibited by these alloys are required. The use of *in situ* synchrotron diffraction experiments are recommended to identify the true martensitic start temperature for an alloy in a given microstructural condition. Finally, the effect of niobium content on the true martensitic start temperatures and form of the stress-strain behaviour were obtained and compared with previously reported datasets in literature. The new total stress based mechanism was then used to rationalise why there is a significant amount of variation in the previously reported martensite start temperatures.

Table of contents

List of figures

List of tables

List of symbols and definitions

Ti metallurgy terms

bcc - body-centred cubic

β - body-centred cubic beta phase

α'' - orthorhombic martensite phase

ω - omega phase

ω_{ath} - athermal omega phase

ω_{iso} - isothermal omega phase

Experimental techniques

XRD - X-ray diffraction

SXRD - synchrotron X-ray diffraction

SEM - scanning electron microscopy

TEM - transmission electron microscopy

DSC - Differential scanning calorimetry

ICP-OES - inductively coupled plasma-optical emission spectrometry

Sample abbreviations

CR - cold rolled

ST - solution treated

Ti-2448 - Ti-24Nb-4Zr-8Sn (wt.%)

Transformation temperatures

A_f - Austenite finish temperature

A_s - Austenite start temperature

M_s - Martensite start temperature

M_f - Martensite finish temperature

Transformation stresses

σ_{SIM} - critical value for the applied stress required to induce the martensitic transformation

σ_{DT} - critical value for the applied stress required to induce detwinning

σ_y - yield stress

Alloy compositions

at.% - atomic percent

(in this work, all compositions are given in atomic percent unless stated otherwise)

wt.% - weight percent

(Ti-2448 is the only alloy expressed in weight percent in this work)

Chapter 1

An introduction to the superelastic effect in Ti-Nb alloys

Alloys that exhibit shape memory and superelastic properties belong to a class of material commonly known as smart materials. Alternatively referred to as adaptive or functional materials, these alloys can change shape according to the temperature of their surroundings and the amount of stress that they are subjected to [1]. Shape memory alloys are used in a wide variety of applications ranging from glasses frames to heart stents [1–3] to the use in the aerospace industry [4, 5]. The most common shape memory alloy, nitinol, was first discovered in 1953 by Buehler, Gilfrich and Wiley [6], and was based around the near-equiatomic Ti-Ni composition. Since then, the research into shape memory alloys based around this base composition has rocketed and many overviews that summarise the current research have been written [7–10]. However, recent concerns over hyper-sensitivity to Ni-containing medical implants led to significant efforts to develop transforming alloys that contained no Ni [11]. Beta-type titanium alloys have offered a potential alternative to Ni-containing alloys because the diffusionless transformation from a cubic parent phase to a lower symmetry martensite phase can give rise to superelastic behaviour. Ti-Nb based alloys have attracted particular attention since they have shown shape memory and superelastic properties over a wide range of temperatures, which can be controlled by varying the Nb contents, making them attractive for industrial applications [11–15].

Current superelastic theories use key transformation temperatures to describe the range of temperatures over which the forward, (and reverse) martensitic transformation starts and finishes during cooling (and heating). The same transformation, which can also be induced through the application of a stress, can be described in terms of critical transformation stresses, which are often related to the key transformation temperatures using the Clausius-Clapeyron relation [16, 17]. Within the literature for Ti-Nb alloys there are significant variations in the reported martensite start temperatures for a given composition that remain unexplained [11, 12, 18–20]. These variations are problematic to engineering design and may limit the industrial uptake of these alloys. To investigate the source of these discrepancies, the transformation behaviour of Ti-24Nb (at.%) in two different microstructural conditions has been studied *in situ*, using synchrotron radiation, whilst undergoing a three step thermal cycle, which involved (i) an initial heat to 350°C, (ii) a cool to -196°C, and (iii) a final reheat to 350°C. A significant difference in the transformation behaviour was observed for the same alloy in the two microstructural conditions, posing doubt on the validity of the thermally driven transformation theories in Ti-24Nb (at.%) samples that contain significant levels of internal stress. These results led to the proposal of a new stress based approach to describe the transformation behaviour for Ti-24Nb (at.%).

To further validate this theory, the transformation behaviour of Ti-24Nb (at.%) alloy in the two different microstructural conditions was studied *in situ*, using synchrotron radiation, whilst undergoing a four step thermomechanical cycle, which involved (i) cooling from 350°C to a target temperature, in the range -196 to 30°C, (ii) loading the sample at the target temperature to 300 MPa, (iii) unloading the sample at the target temperature and (iv) a final reheat to 350°C. Heating and cooling rates of 30°C min^{-1}, and loading rates of ~ 4 MPa s^{-1} were used during these experiments. The observation of full superelastic recovery approximately 550°C below the martensite start temperature, posed additional doubt on the use of current critical temperature based transformation theories to explain the superelastic behaviour observed in Ti-24Nb (at.%).

A commercial Ti-24Nb-4Zr-7.5Sn alloy (wt.%) was used to investigate the potential microstructural features that gave rise to the unusual transformation of Ti-24Nb (at.%) in the

two microstructural conditions. The dislocation density and the grain size were individually varied and the effect of each on the stress-strain behaviour was investigated.

To allow a better comparison of the datasets recorded in this work with those reported in the current literature, the effect of Nb contents in the Ti-Nb binary in the cold rolled condition, three Ti-Nb alloys with a varying concentration of Nb were investigated *in situ*, using synchrotron radiation. Each alloy was subjected to the same four step thermomechanical cycle as Ti-24Nb (at.%) at a target temperature of -196°C within the beamline allowing a direct measurement of the phase constitution for these alloys at a given temperature and when subjected to an externally applied load. The observed phase transformations were directly related to the stress-strain curves that were measured, and enabled some observations within the literature to be explained.

To finalise this work, proposals for future work are suggested, with an aim of incorporating the new total stress based mechanism into both the current literature and future investigations into similar superelastic metastable beta-titanium alloys.

1.1 Titanium alloys: phases and crystal structures

1.1.1 Thermodynamically stable phases

Titanium alloys can form two equilibrium phases, the high temperature β phase, which adopts a body-centred cubic (bcc) structure, and the low temperature α phase, which takes a hexagonal structure. Titanium alloys, as with many other alloying systems, are classified in terms of how various alloying additions effect the β transus temperature, as demonstrated by the schematic diagrams shown in figure 1.1. These temperature versus composition phase diagrams are used to identify the phases that are stable at a given temperature for a specific alloy composition are determined by the relative Gibbs energy of the β and α phases at a given temperature [21]. Different alloying additions generally act as stabilisers for either the β (e.g. Nb, Ta) or the α phase (e.g. Al, O). But, some elements are considered neutral (e.g. Sn, Zr) and do not significantly influence the β-transus temperature. In general, β-containing Ti alloys can be classified into three main categories which are dependent upon their phase constitution after being cooled from above the β-transus [22, 23]. These classifications can

be termed as (i) $(\beta + \alpha)$ alloys, (ii) metastable β-titanium alloys and (iii) stable β-titanium alloys. $(\beta + \alpha)$ alloys can be further categorised into near-α and near-β alloys, depending upon the amount of β-stabilising alloying additions that it may contain. Near-α alloys are majoritively composed of the α phase and only contain a small fraction of β, and similarly, near-β alloys contain mostly the β phase and only a small amount of α.

Titanium alloys that can exhibit superelastic properties must contain a fraction of the β phase that is sufficiently unstable to undergo a stress-induced transformation to a martensitic phase, which is why that from this point onwards, metastable β-titanium alloys are considered [23]. For example, in the phase diagram that is shown in figure 1.1, a β-isomorphous alloy that contains a concentration of β-stabilising elements below β_s (defined as shown in figure 1.1) may be able to retain the β phase if the alloy is cooled sufficiently quickly from a temperature that lies above the β-transus. Alloys that contain more than this composition, can retain a thermodynamically stable β phase at room temperature, and cannot be labelled as metastable [24].

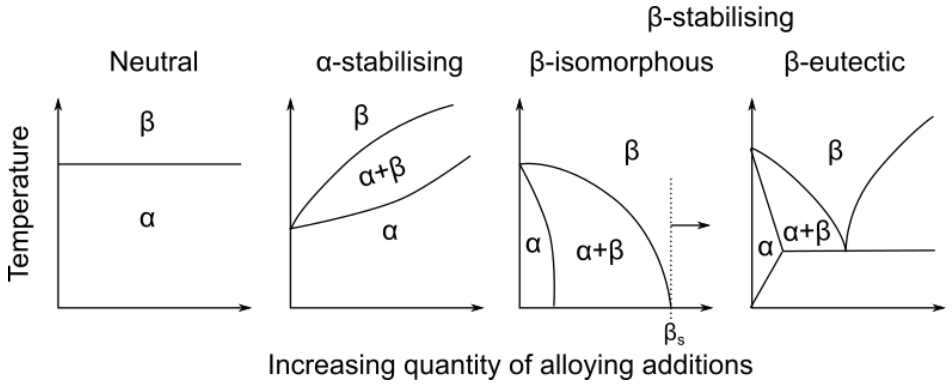

Fig. 1.1 Schematic phase diagrams for different classifications of titanium alloy. This diagram was adapted from [22]. β_s is the minimum concentration of β-stabilising elements that is required to retain a thermodynamically stable β phase alone. Above this concentration the α phase will not form.

1.1.2 Non-equilibrium phases

Martensites

Various non-equilibrium phases can form from the β phase when it is retained in its metastable state. These include two martensitic structures, α' and α'', which form via a co-operative

shear of atoms from the β phase. α' forms in alloys that contain a lean concentration of β-stabilising elements and adopts a hexagonal crystal structure that is similar to that formed by the α phase. As the concentration of β-stabilising elements are increased, the martensite that forms gradually loses its hexagonal symmetry and adopts an orthorhombic structure (α''), that is more similar to the cubic β phase [25]. The $\beta \rightarrow \alpha''$ phase transformation that can give rise to the superelastic behaviour that has been observed in metastable-β titanium alloys [2]. The crystallographic relation between the β and α'' phases were initially investigated by Hatt and Rivlin [26], who used the relations in a Ti-20 at.% Nb alloy to concluded the following lattice correspondances:

$$[100]_{\alpha''} \text{ 2° from } \langle 001 \rangle_{\beta}$$

$$[010]_{\alpha''} \text{ 2° from } \langle 110 \rangle_{\beta}$$

$$[001]_{\alpha''} \text{ parallel to } \langle 1\bar{1}0 \rangle_{\beta}$$

Figure 1.2 shows a schematic diagram demonstrating this relationship, and to improve the clarity of the diagram the angles of 2° have been ignored.

Omega

In addition to the two possible martensites that can form, the omega (ω) phase is often observed in metastable β-titanium alloys and can form during quenching from the β phase field (athermal omega, ω_{ath}), or by ageing at an appropriate temperature (isothermal omega, ω_{iso}) [27]. The ω_{ath} commonly adopts a hexagonal, but not close packed, crystal structure in alloys that are lean in β-stabilising elements, and a trigonal structure in alloys that are more solute-rich [23]. ω_{iso} has been reported to adopt the simple hexagonal structure [23, 28] and forms during ageing at low temperatures. The formation of the ω phase involves a collapse of successive $(111)_{\beta}$ planes. As demonstrated in the figure 1.3, the lattice correspondence between β and ω crystal structures [28, 29] is given by:

$$[111]_{\beta} \text{ parallel to } \langle 0001 \rangle_{\omega}$$

$$[1\bar{1}0]_{\beta} \text{ parallel to } \langle 11\bar{2}0 \rangle_{\omega}$$

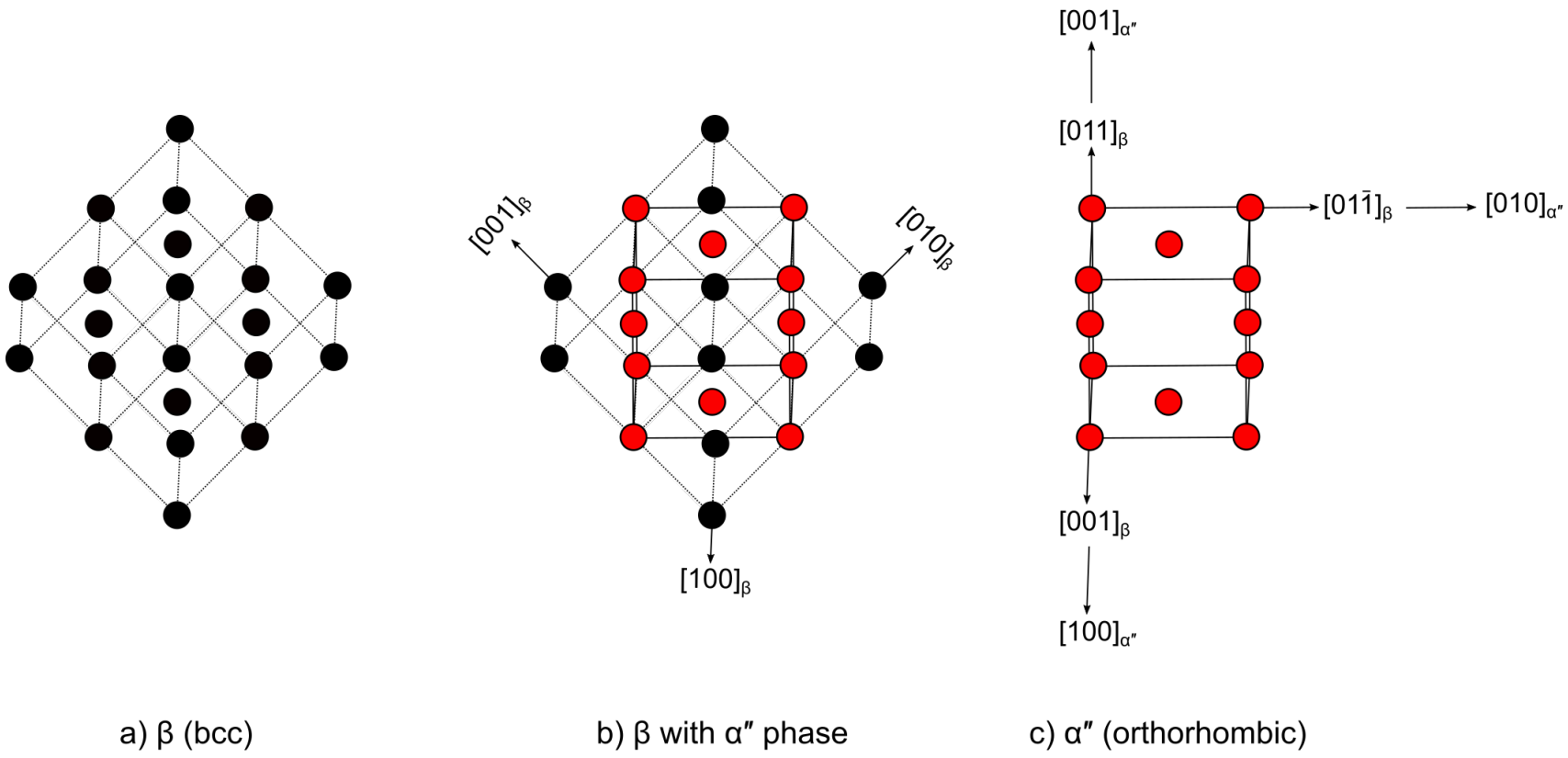

Fig. 1.2 Crystal structures of the β and α'' phases. The lattice correspondances are shown.

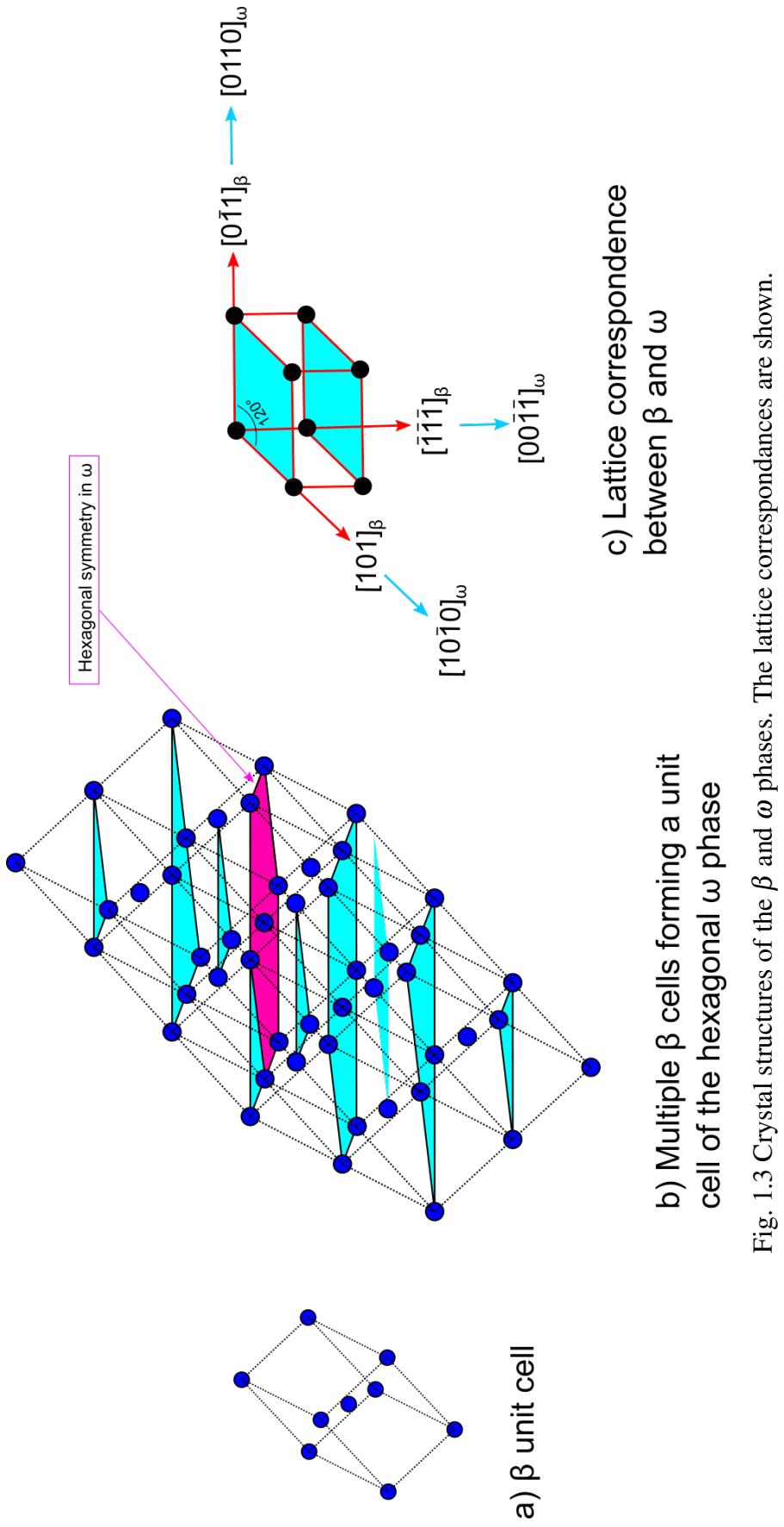

Fig. 1.3 Crystal structures of the β and ω phases. The lattice correspondances are shown.

1.2 The shape memory and superelastic effect in metastable β-titanium alloys

Metastable β-titanium alloys can undergo phase transformations that are induced through the application of a stress. Both the shape memory and superelastic effects rely upon the reversible nature of the $\beta \rightarrow \alpha''$ transformation, which may be achieved by heating (shape memory effect) or upon the removal of the stress (superelasticity) [30]. In this section, the deformation mechanisms that are associated with each effect are introduced and discussed with the aid of schematic drawings of example atomic structures.

1.2.1 Atomic movements during the shape memory effect

Figure 1.4 shows a schematic diagram that demonstrates the atomic movements as a shape memory alloy is firstly loaded, then unloaded and finally heated to regain its original shape. The initial microstructure of a shape memory alloy should be entirely composed of the α'' phase. The laths of α'' are generally twinned to minimise the elastic strain that occurs between the β and α'' boundaries [31]. Upon loading, the twinned α'' laths reorient and detwin acting to reduce the strain energy that is now associated with the applied load. Once the load is removed, the newly formed orientations of the α'' are stable and the alloy remains in the detwinned state. To recover the original shape of the initially twinned martensite, the alloy must be heated to destabilise the α'' and create a sufficient thermodynamic driving force to induce the $\alpha'' \rightarrow \beta$ transformation. Upon cooling, the forward $\beta \rightarrow \alpha''$ transformation then occurs, resulting in the initial twinned martensite being regained. The ease of movement of the martensite twin boundaries allows the initial atomic arrangement to be repeatably obtained and results in the shape memory effect [32].

1.2.2 Atomic movements during the superelastic effect

Superelasticity occurs in alloys that are deformed from the β phase. Figure 1.5 demonstrates the atomic movements that occur when a superelastic alloy is loaded and subsequently unloaded. When the sample is loaded, a stress-induced $\beta \rightarrow \alpha''$ transformation may occur

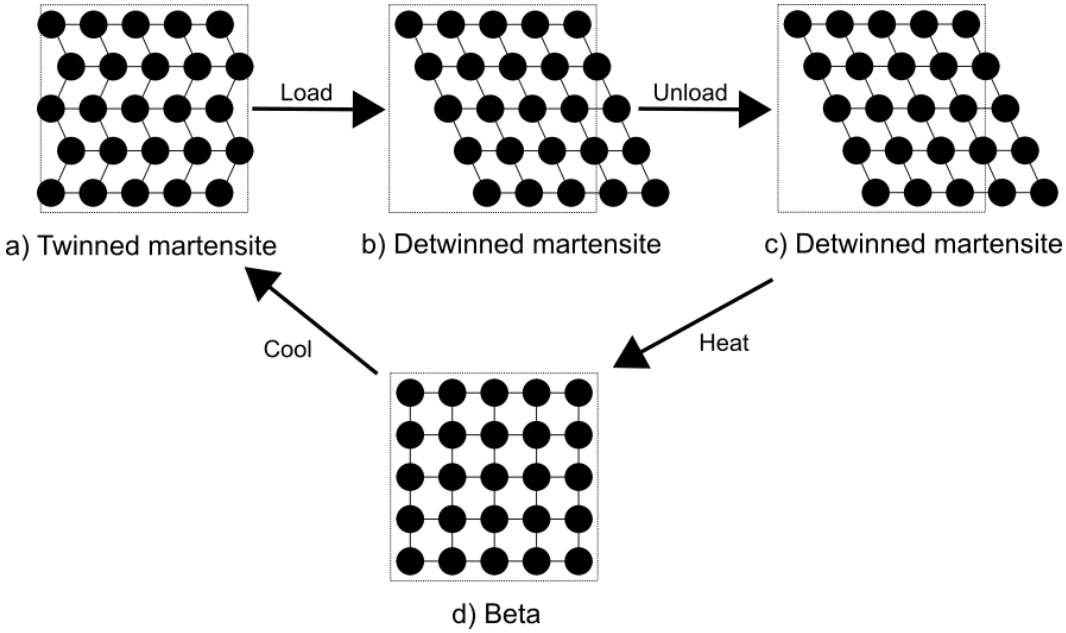

Fig. 1.4 Schematic diagram of the atomic movements during the shape memory effect.

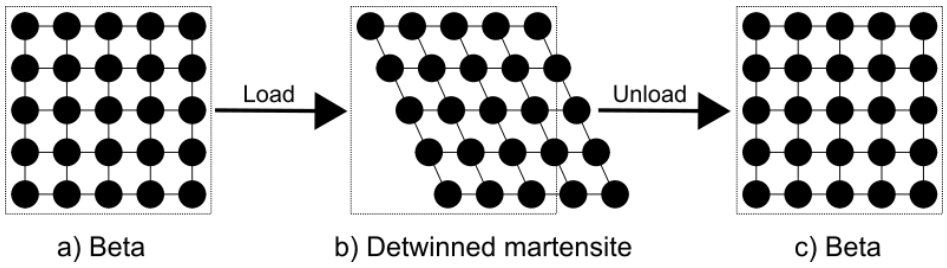

Fig. 1.5 Schematic diagram of the atomic movements that result in superelasticity.

and the strain that is associated with the transformation causes a macroscopic shape change. Then, as the load is incrementally removed, the α'' phase gradually becomes unstable and the reverse transformation from the α'' to the β phase occurs. The reversible nature of the $\beta \rightarrow \alpha'' \rightarrow \beta$ transformation results in the superelastic behaviour [32].

1.2.3 Key transformation temperatures and stresses

Definitions of transformation temperatures and stresses

Throughout the literature the terms "shape memory" and "superelasticity" are used very loosely to rationalise the non-linear elastic deformation that is observed in metastable β-titanium alloys that can form the α'' phase. It is clear from section 1.2.1 that both stress and temperature play key roles in shape memory and superelastic behaviour. As such, some fundamental transformation temperatures and stresses are often defined that enable a method for direct comparison between alloys. Figure 1.6 shows a schematic diagram that illustrates regions where an alloy possesses shape memory and superelastic properties over a range of stress and temperature. Similar diagrams have been used previously to aid the understanding of how the transformation temperatures relate to the observed deformation behaviours [17, 33, 34]. Along the temperature axis five key values are highlighted. These include the martensite start temperature, M_s, which is defined as the temperature below which the parent phase begins to transform to the martensite phase when the alloy is cooled in the absence of an externally applied load. The martensite finish temperature, M_f, is defined as the temperature below which the transformation has reached completion, and the alloy is entirely composed of the martensite phase. Similarly, the austenite start and finish temperatures, A_s and A_f, are defined as the start and finish temperatures of the reverse transformation, when the α'' transforms to the β phase. Lastly, T_s defines the temperature above which the stress-induced martensite transformation will no longer occur because slip deformation becomes more favourable than transformation.

The three solid lines in figure 1.6 demonstrate how the key transformation temperatures mentioned above can change with the alloy composition. The critical stress required to initiate slip is labelled with the commonly used σ_y. If the applied stress exceeds this value then dislocation motion will occur, and the material will undergo permanent deformation, with the

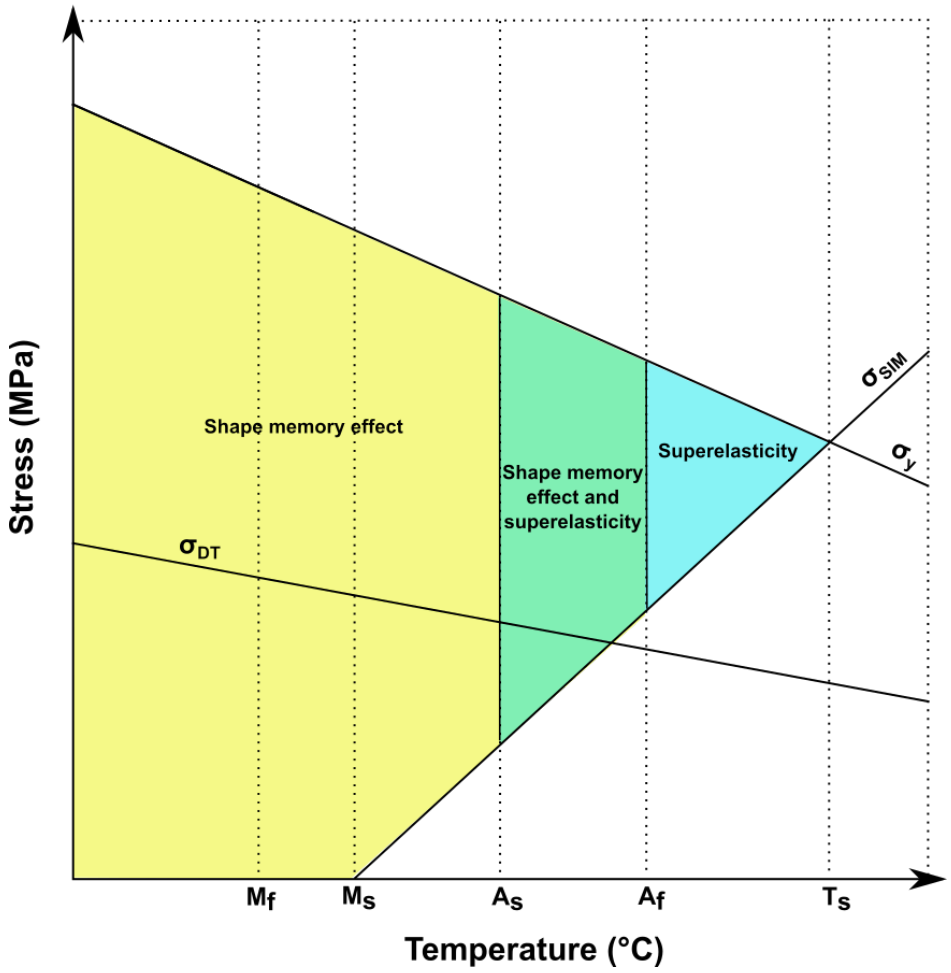

Fig. 1.6 Schematic diagram of stress-temperature space showing when the shape memory and superelastic properties are expected. This diagram has been adapted from [17] and [33].

original shape of the sample becoming unrecoverable. In a similar fashion, σ_{DT} is defined as the critical stress that is required to initiate the detwinning of a twinned α'' structure. If the applied stress exceeds σ_{DT}, but does not reach σ_y, it is expected that the original shape of the sample may be recoverable via the shape memory effect that was described above. For the purposes of this diagram, the temperature dependence of σ_{DT} and σ_y has been shown to decrease with an increasing temperature. However, it should be noted that the dependence of composition on these stress values is expected to be dependent upon the specific alloy under consideration [17]. The third stress that is defined on this diagram is the critical stress required to induce the stress-induced $\beta \rightarrow \alpha''$ transformation, σ_{SIM}. The increase in σ_{SIM} with increasing temperature follows a linear relationship that can be described using the Clausius-Clapeyron relationship [16, 17] shown in equation 1.1.

$$\frac{d\sigma_{SIM}}{dT} = \frac{\Delta \mathrm{H}}{\varepsilon \mathrm{T}} \tag{1.1}$$

where σ_{SIM} is the critical stress required to induce martensite, ΔH is the enthalpy of the transformation per unit volume, ε is the associated transformation strain and T is temperature.

Regions of stress-temperature space that define the predicted deformation behaviours

There are three main regions that are labelled with the deformation behaviours that are expected within the highlighted ranges of transformation temperatures and stresses, as shown in figure 1.6. The first, to the far left of the diagram in yellow, highlights the range of temperatures and stresses over which the shape memory effect is expected to be observed. The second, to the far right of the drawing which is shaded in blue, defines the region of temperature and stress where superelasticity is expected to occur. Thirdly, the region in between these, which is shaded green, defines a region where a combination of both effects are predicted to occur.

The grey area: when multiple deformation mechanisms can occur

In order for both of the shape memory and superelastic effects to occur in the same sample when a load is applied, the initial microstructure must contain both the β and α'' phases. Figure 1.7 shows a schematic diagram of some example atomic movements that could arise

when a multiphase alloy is loaded and subsequently unloaded. Upon loading above σ_{DT}, the self-accommodated α'' laths will begin to reorient, forming detwinned α'' and above σ_{SIM}, the $\beta \rightarrow \alpha''$ transformation can occur. As discussed in section 1.2, when the applied stress is subsequently removed, the detwinned α'' is expected to remain in its reorientated state within the sample. Additionally, whether the reverse $\alpha'' \rightarrow \beta$ transformation occurs during unloading is dependant upon the relative stability of the α'' and β phases. It is clear that the schematic diagram that is shown in figure 1.6 does not represent the more complex nature of these deformation mechanisms that can occur simultaneously in alloys that contain both the β and α'' phases initially. Therefore, a newly revised version of this diagram is proposed here. Rather than referring to the generic terms such as "shape memory" and "superelasticity", which can be limited, a modified version of stress-temperature space is shown in figure 1.8 which refers to the specific deformation mechanisms that occur.

1.3 The use of stress-temperature space to predict deformation mechanisms

In this section, figure 1.8 will be used to describe the deformation mechanisms that are expected to occur in alloys that lie within the different temperature and stress regimes. These discussions will lead to an introduction to the stress-strain curves that would be expected to be observed when an external load is applied to a sample. To improve the clarity of these discussions, only the elastic deformation region will be considered, and the hypothetical maximum stress that is reached will be sufficiently below the macroscopic yield stress of the material at the appropriate temperature.

1.3.1 A more detailed consideration of stress-temperature space

Below M_f

As previously discussed, below the M_f temperature an alloy should be entirely composed of the α'' phase. If an external load is applied, linear elastic deformation of the α'' initially occurs. Once this applied stress exceeds σ_{DT}, the martensite laths begin to reorient and grow

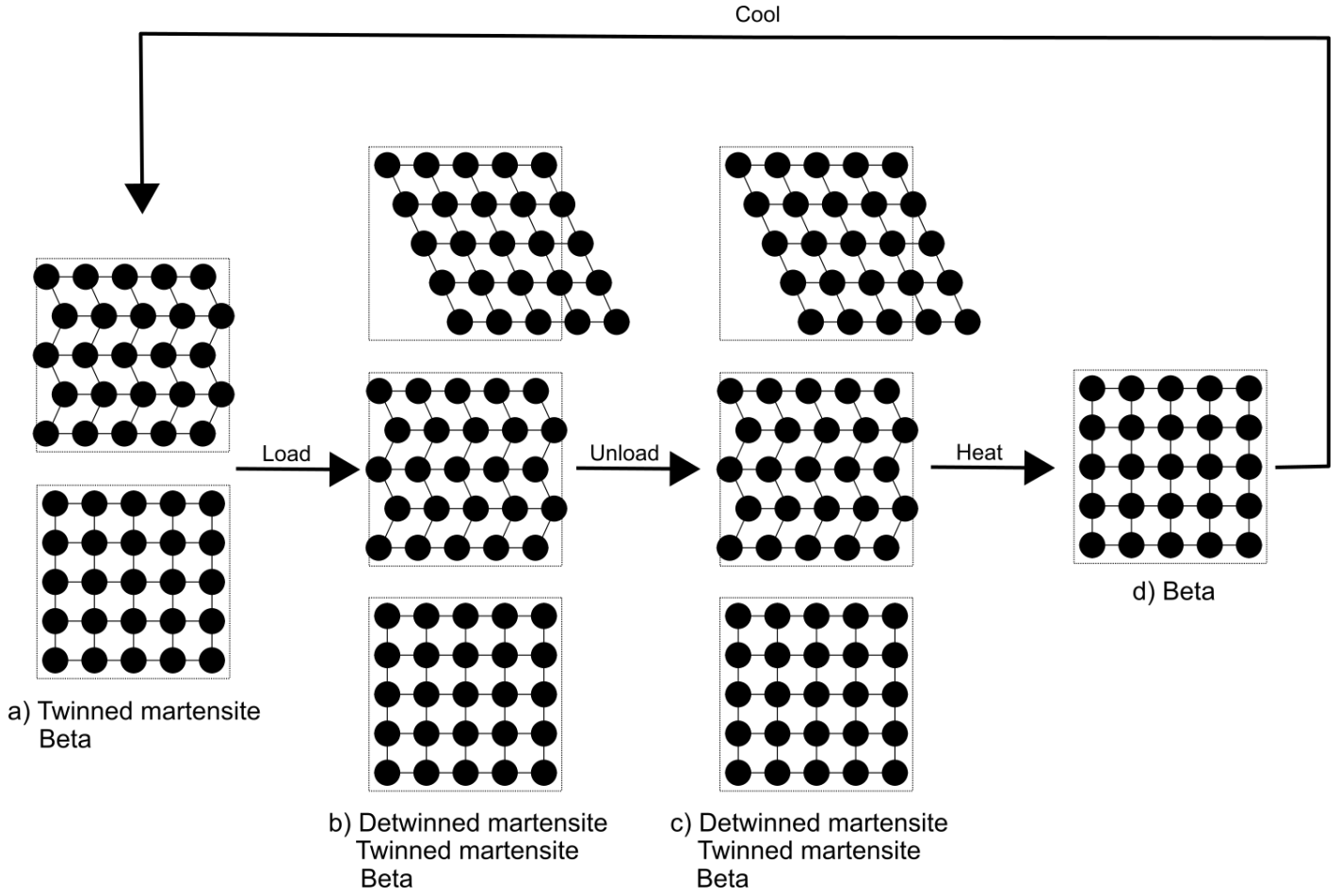

Fig. 1.7 Schematic diagram of some example atomic movements for an alloy that is loaded between M_f and A_f.

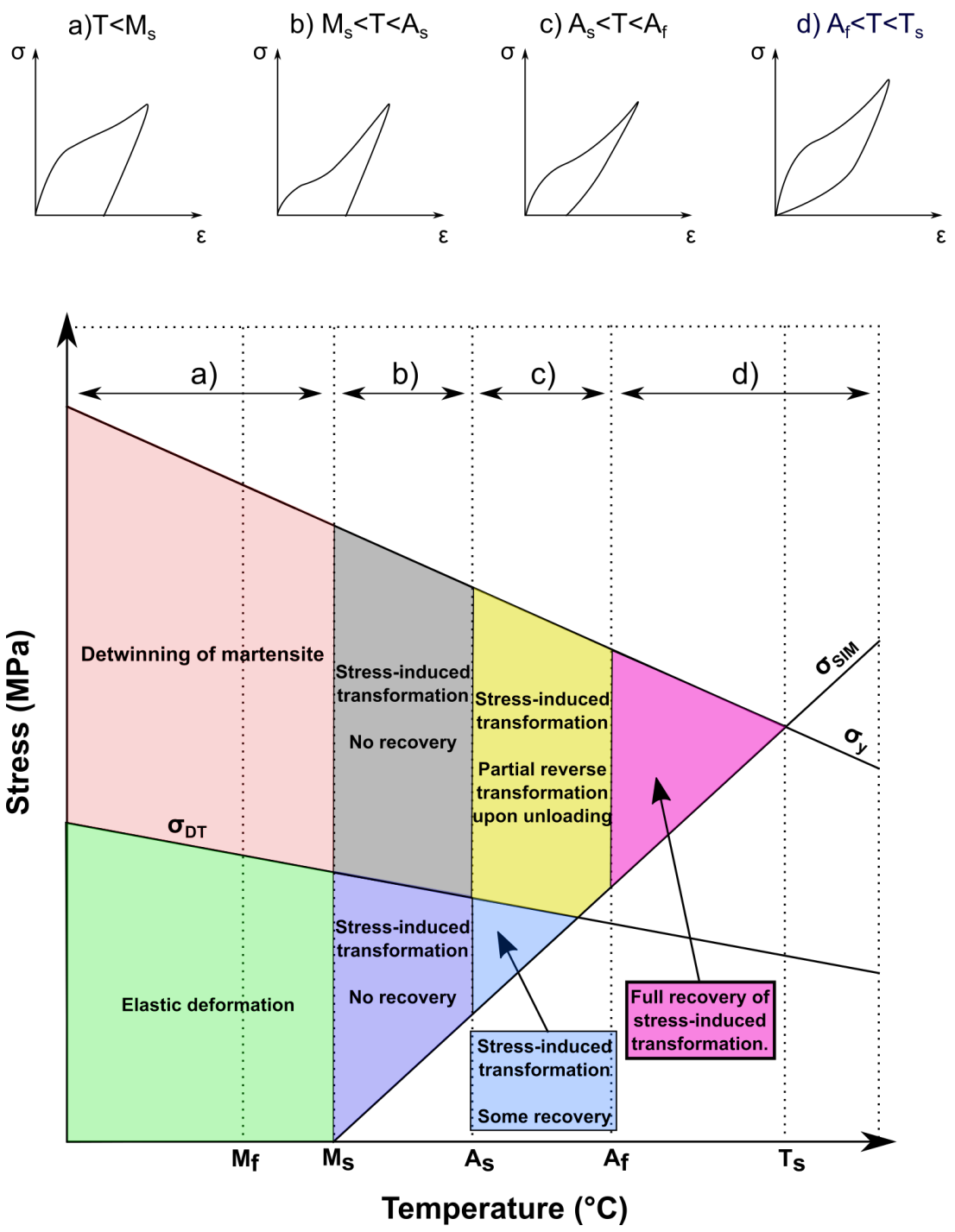

Fig. 1.8 A revised schematic diagram showing the predicted deformation mechanisms that occur over stress-temperature space. Example stress-strain curves that would be expected for a material that was loaded within each temperature range is sketched above the plot.

(detwin) to better accommodate the applied strain. This detwinning causes the stress-strain curve to change gradient, as shown in figure 1.8a. Once the target maximum stress is reached, the stress is generally removed from the sample. During this unloading, the new configuration of martensite will be retained and, consequently, the unloading section of the curve appears linear since only the elastic deformation is recovered.

Between M_f and M_s

The initial microstructure for an alloy that is cooled to a temperature between M_s and M_f is expected to contain a mixture of the β and α'' phases since the M_s temperature has been reached and the $\beta \rightarrow \alpha''$ transformation will have started to occur. However, since the M_f temperature has not been reached, the thermally-induced $\beta \rightarrow \alpha''$ transformation will not have reached completion, resulting in a microstructure that consists of both the β and α'' phases. Upon loading, the α'' that is initially present in the microstructure is predicted to detwin when the applied stress is increased above σ_{DT}. In previous reports, the potential occurrence of the $\beta \rightarrow \alpha''$ transformation in this temperature range is not considered [2], despite a fraction of the β phase still being present. Again, as the load is removed, the detwinned α'' will be retained, and only the elastic deformation will be recovered. Therefore, the stress-strain curve that is predicted for this sample is very similar to the curve observed for an alloy that lies below M_f.

Between M_s and A_s

Between M_s and A_s, the stress-induced $\beta \rightarrow \alpha''$ transformation can now occur. The initial microstructure of an alloy that lies between M_s and A_s will be dependent upon the thermal history of the sample. For example, the alloy has been cooled directly from a temperature above A_f, the microstructure is expected to contain the β phase alone. However, if the sample had been cooled to a temperature below M_s, and then reheated back into this temperature range, the sample might contain a volume fraction of the α'' phase in addition to the β phase. It is also possible that this alloy is entirely composed of α'' if it had been cooled below M_f and reheated to a temperature between M_s and A_s. When the applied stress exceeds σ_{SIM}, any β that is initially present in the microstructure can undergo the stress-induced $\beta \rightarrow \alpha''$

transformation. Since the magnitude of σ_{SIM} is expected to be fairly low when the deformation temperature is close to M_s, as it is depicted in figure 1.8, the corresponding stress-strain curve may not show an initial linear elastic region due to the stress-induced $\beta \rightarrow \alpha''$ transformation occurring as soon as a load is applied. When the applied stress reaches σ_{DT}, any twinned α'' that existed in the initial microstructure is expected to begin to detwin as the load is gradually increased to the maximum stress. The martensite variants that are present at the maximum load remain stable during the unloading of the sample. No reverse $\alpha'' \rightarrow \beta$ transformation is expected during the unload since the deformation temperature still lies below A_s. Therefore, the resultant stress-strain curve, as shown in figure 1.8b, is expected to show a small linear elastic region before curving as the $\beta \rightarrow \alpha''$ transformation occurs. And since no recovery is expected during the removal of the stress, a linear unload section of the curve is predicted.

Between A_s and A_f

Figure 1.8c shows a schematic stress-strain curve that is expected for an alloy that is subjected to an externally applied load between A_s and A_f. The initial microstructure for this sample may also differ depending upon its thermal history. For example, if the sample was cooled from above A_f into this temperature range, no α'' will be present in the sample. In contrast, if the sample was cooled below M_s and subsequently heated into this temperature range, some α'' may exist in the initial phase constitution. In addition, this temperature regime now lies above A_s, which means that it now may be favourable for the reverse $\alpha'' \rightarrow \beta$ transformation to occur during the unloading of the sample. Hence, when a stress is applied to a sample that lies between A_s and A_f, whilst the stress lies below σ_{SIM} a linear elastic deformation will be observed. Once σ_{SIM} is reached, the $\beta \rightarrow \alpha''$ transformation can occur, causing a change in the gradient of the stress-strain curve. When the maximum stress has been reached, the sample is expected to contain both the β and α'' phases. Consequently, upon unloading, some of this α'' can undergo the reverse transformation back to the β phase, however, since A_f has not been exceeded, full recovery of the β phase is not expected, and some retained strain is observed in the schematic stress-strain curve.

Above A_f and below T_s

If a stress is applied to an alloy that lies above the A_f temperature full superelastic recovery is expected upon loading and subsequent unloading. The β phase will elastically deform until σ_{SIM} is reached, above which the stress-induced $\beta \rightarrow \alpha''$ transformation begins to occur. Upon removal of the stress, the α'' phase becomes unstable and the reverse $\alpha'' \rightarrow \beta$ transformation occurs. Since the α'' phase is not expected to be stable at all above A_f, full recovery of the β phase is expected. This is observed in the stress-strain curve as a non-linear return back to the origin, as demonstrated in figure 1.8d.

Above T_s

Above the T_s temperature the value of σ_y is smaller than the value of σ_{SIM} and dislocation motion is expected to occur preferentially over the stress-induced $\beta \rightarrow \alpha''$ transformation. Consequently, no shape memory or superelastic properties are expected to be observed if an alloy is subjected to a load above the T_s temperature.

1.3.2 Summary

In section 1, a thorough introduction to the deformation mechanisms that can occur in metastable β-Ti alloys were introduced and discussed. The key transformation temperatures and stresses for alloys that exhibit shape memory and superelastic behaviour were defined and then used to predict the stress-strain curves that would be expected if an alloy were loaded between these key temperatures. This in-depth introduction to how these stress-strain curves may arise from the different deformation mechanisms enables a more detailed analysis of the observations reported in the current literature. The aim of section 2 is to provide a detailed discussion based around the deformation behaviours observed in Ti-Nb alloys, an example of a binary metastable β-titanium alloy. Gaps and discrepancies in the literature will be highlighted with reference to the concepts that were introduced in this section, and will be used to introduce the work conducted in this project.

1.4 The thermodynamics of the martensitic transformation

1.4.1 Thermally activated transformations

To predict whether a phase transformation may occur at a given temperature, the relative Gibbs energies of the phases involved are generally compared for a specific alloy composition. Therefore, the relative values of the Gibbs energies of the β and α'' phases over a range of temperatures are expected to provide an alternative perspective into why the temperature-induced, and the stress-induced $\beta \rightarrow \alpha''$ transformations may occur. To demonstrate this, figure 1.9 shows a schematic diagram of the Gibbs energy for the β and α'' phases as a function of temperature. This diagram has been adapted from similar sketches that have been previously developed to explain the martensitic transformation in Ti-Ni-based alloys [35], in steels [36] and for a more generalised viewpoint [37]. For example, if an alloy was cooled from a temperature above the transus temperature of the parent phase, initially, the Gibbs energy for the β phase lies below the equivalent line for the α''. Whilst this is the case, there is no thermodynamic driving force to drive the $\beta \rightarrow \alpha''$ transformation at these temperatures. When the alloy is cooled to the temperature where the Gibbs energy lines for the β and α'' meet, the two phases are considered to be in equilibrium. As such, this crossover temperature is considered to be the absolute M_s temperature in this work. However, due to the activation energy of the martensitic phase transformation, this absolute value cannot be directly determined through cooling experiments. In the current literature, the M_s temperature is often labelled at a temperature below this crossover point [35–38], which is often the value that is determined through experimental observations. Below this measured M_s temperature, which is highlighted with a dotted line in figure 1.9, the difference in the Gibbs energies is sufficient to exceed the activation energy required to initiate the transformation, and, consequently, upon further cooling below this value, a thermally driven $\beta \rightarrow \alpha''$ transformation will be observed.

Equivalently, if an alloy is then heated from the fully martensitic condition, whilst the Gibbs energy curve for the α'' phase lies below the β line, there is no thermodynamic driving force for the reverse $\alpha'' \rightarrow \beta$ transformation to occur. Above the crossover temperature, which, upon cooling is labelled as the absolute M_s temperature, the Gibbs energy for the β phase then lies below the α'' line. Therefore, upon heating, the crossover temperature

must relate to the absolute A_s temperature, where the two phases are in thermodynamic equilibrium. Similarly, the difference between the absolute A_s and the value that is determined experimentally can be explained in the same way as for the differences in M_s during cooling from the fully β condition. The thermodynamic driving force for the $\alpha'' \rightarrow \beta$ transformation, that is determined by the difference in the Gibbs energy values at a given temperature, must exceed the activation energy that is associated with the transformation, which gives rise to the difference in values.

1.4.2 Transformations activated through the application of a stress

The idea that the $\beta \rightarrow \alpha''$ transformation can be activated through the application of an external load has already been introduced in section 1.3.1. Figure 1.8 showed that a stress-induced transformation from β to α'' could occur when the temperature lies above M_s, but below T_s and the Clausius-Clapeyron relation (equation 1.1) was used to relate the value of the critical stress, σ_{SIM}, and the temperature. It is evident from the figure that temperatures that are closer to M_s require a smaller externally applied load to induce the $\beta \rightarrow \alpha''$ transformation. This conclusion can be used to explain how the value of σ_{SIM} can be related to the Gibbs energy diagram in figure 1.9. As the temperature is increased further above M_s the difference between the Gibbs energies of the β and α'' phases increases, with the β phase becoming increasingly more stable with an increasing temperature. Therefore, a larger amount of energy is required to be put into the system to overcome the unfavourable thermodynamic transformation, plus any activation energy. The source of this energy can be considered to come from the externally applied load, which destabilises the β phase by subjecting it to an applied stress. Hence, a larger amount of stress is required to induce the $\beta \rightarrow \alpha''$ transformation as the Gibbs energy lines deviate further apart, and the $\beta \rightarrow \alpha''$ transformation becomes less favourable as the temperature is increased away from M_s.

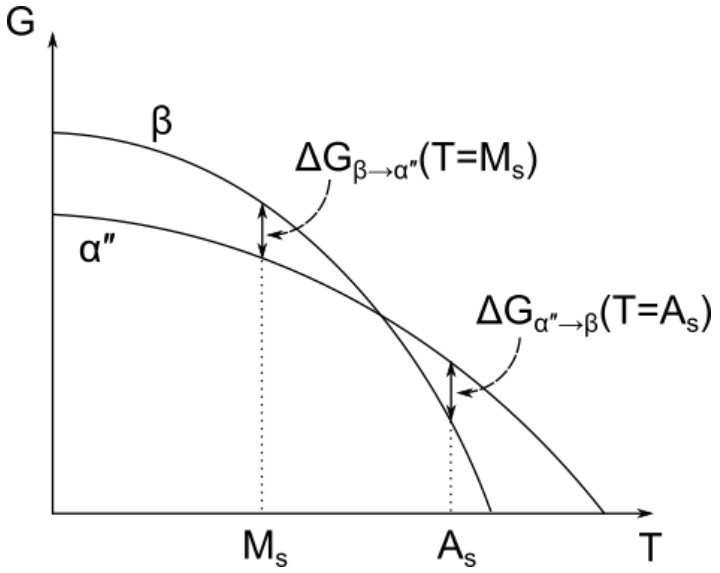

Fig. 1.9 A schematic plot of the Gibbs energy for the β and α'' phases as a function of temperature. This diagram has been adapted from diagrams in the current literature [35, 36, 38]. For simplicity, this plot does not consider the effect of increasing enthalpy as the temperature is increased.

1.5 The effect of composition on the $\beta \rightarrow \alpha''$ transformation in Ti-Nb alloys

Alloy design for engineering applications often involves adjusting the composition to adapt an alloy's mechanical properties towards the specifications of a component. The design of shape memory and superelastic materials focuses around the adjustment of the transformation temperatures to the operating temperature of the component. During the early 2000s, the majority of commercial superelastic materials were based upon near equiatomic binary NiTi [1]. However, concerns over hyper-sensitivity to Ni containing implants led to significant efforts to develop transforming alloys that were free from Ni [11, 39]. One potential alternative to NiTi alloys are the metastable beta (β) titanium alloys, often based around the binary systems Ti-V [40, 41], Ti-Mo [42–44] and Ti-Nb [11, 12, 20, 41, 45, 46], all of which are isomorphous β-stabilising elements. Of these, Ti-Nb alloys have received the most attention and have been reported to exhibit both shape memory and superelastic behaviour depending upon both the concentration of Nb [11, 12, 15, 39, 45, 47] and the deformation

temperature [14, 39, 46]. With increased Nb content, the β phase is more stable and the transformation to the α'' phase becomes less favourable.

1.5.1 The effect of Nb contents on the stability of the β phase

Early development of the Ti-Nb phase diagram

In 1951, Hansen, Kamen and Kessler [48] proposed a phase diagram for the Ti-Nb system which they obtained by annealing samples which had a range of compositions at various temperatures and quenching to retain the microstructure. Data points for temperatures lower than 750°C could not be reliably investigated due to coring of the alloys which contained higher Nb contents [48, 49]. Despite this, a trendline separating the β and $\beta + \alpha$ regions of the phase diagram were reported, and are shown by the dotted lines in figure 1.10.

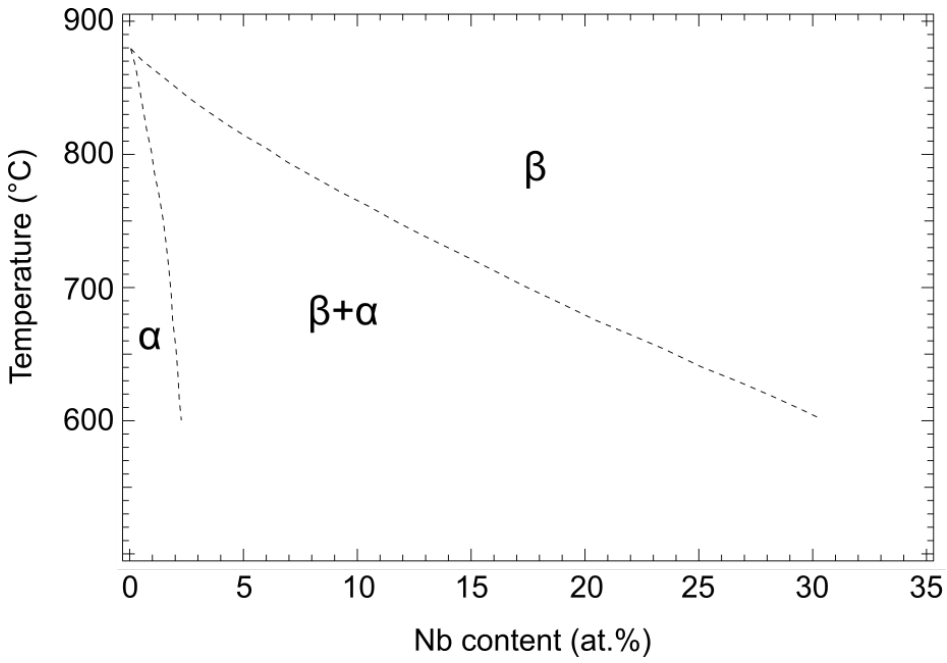

Fig. 1.10 Phase diagram for the Ti-Nb system proposed by Hansen et al. [48] in 1951.

The metastable phases that can form in Ti-Nb alloys were first investigated by Duwez in 1953 [50]. Samples of varying chemical compositions were quenched at different rates using a jet of helium gas and a chromel-alumel thermocouple that was spot welded to the sample surface was used to obtain its temperature over a given time period. Temperature-time curves were then used to identify the martensite start temperature at different cooling rates.

This method for determining the martensitic transformation temperatures is described in more detail by Greninger [51] which studied the martensite in the iron-carbon system. The study conducted by Duwez [50] investigated the M_s temperature for alloys containing between 2 and 16 at.% Nb, which are shown in figure 1.11. The range of M_s values recorded over the different cooling rates are shown using cross symbols that are connected by straight lines, and the proposed trendline is shown using a solid black line. However, M_s values for alloys that contained > 16 at.% Nb could not be obtained [50] because the method used by Greninger [51] was limited by the sensitivity of the equipment used. Alloys that contained a higher concentration of Nb form a more stable β phase, which reduces the extent of the $\beta \rightarrow \alpha''$ transformation that occurs upon cooling than in an alloy that contains less Nb. Therefore, Duwez [50] proposed that the trendline could be extrapolated to predict M_s for Ti-Nb alloys that contain > 16 at.%, and, therefore predict the M_s temperatures below 350°C.

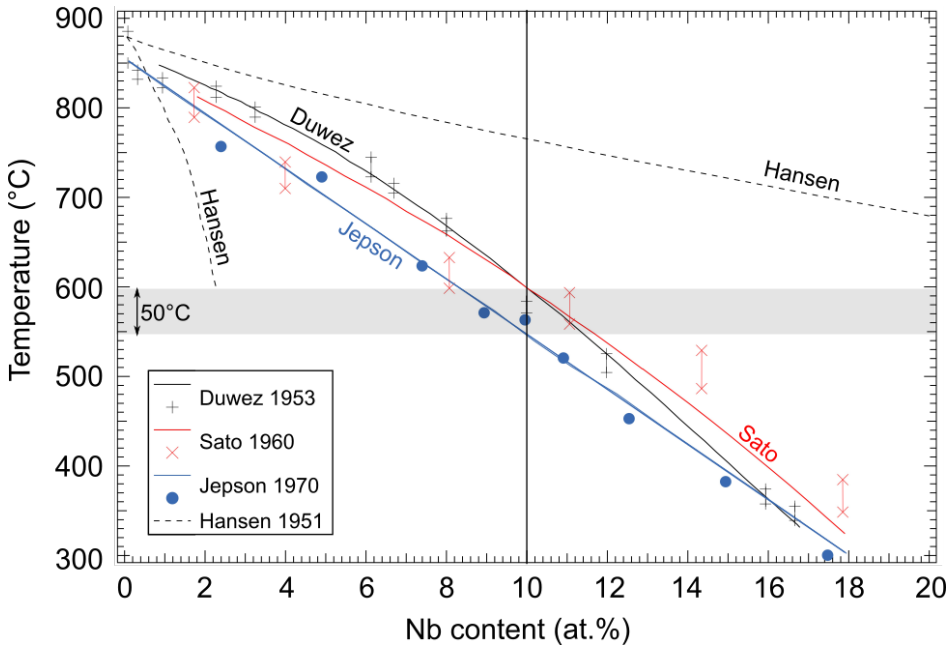

Fig. 1.11 Summary of reported transformation temperatures in literature [48, 50, 52, 53].

Sato, Seikiti and Huang [52] used a similar method to determine M_s values for Ti-(4-18) at.% Nb alloys. Similarly to the study that was conducted by Duwez [50], values for M_s could not be determined for alloys that contained > 18 at.% Nb, and correspondingly, for values of M_s below 300°C. The data from this study has also been plotted in figure 1.11 using red "×" symbols that are connected by red straight lines. The trendline that was proposed is shown

as a solid red line, and adopts a curved form, similar to that of the trendline proposed by Duwez [50].

Jepson, Brown and Gray [53] measured the M_s temperature for alloys that contain up to 17.5 at.%, which had a value of 300°C, but did not report any values for M_s lower than this temperature. These data points are shown as blue circles in figure 1.11. Jepson, Brown and Gray [53] proposed a linear trendline for these data points, which is shown as a blue line in the figure. From these earlier investigations, the lowest value for M_s for Ti-Nb alloys was reported by Brown et al. [54] for Ti-20Nb as 212°C. From the discussions above, it is clear that the equipment used for the Greninger [51] method had a limited capability and could not allow the direct measurement of lower, and arguably, the most important values of M_s. The proposed trendlines shown in figure 1.11 display a significant variation in the predicted M_s values for Ti-Nb binary alloys. For example, the collective dataset in figure 1.11 would predict that the M_s value for Ti-10Nb, which has been observed to form the orthorhombic α'' phase [53], could vary from 550°C to 600°C. A range of $\sim$ 50°C is not ideal when these transformation temperatures are used for alloy design. In addition to this, alloys that contain 14.5 at.% and 17.5 at.% could have an even larger range of proposed values for M_s. Unfortunately, these significant discrepancies result in an inability to trust these alloys in an engineering application and further investigation as to the reasons behind the variety was required. Despite this, because a number of studies had investigated the metastable transformation temperatures for this alloy system in detail [50, 52, 53, 55], various articles that collated and summarised the datasets were published [56].

The M_s temperature of Ti-Nb alloys containing a higher Nb content

More recent measurement techniques Interest in the unique properties of Ti-Nb alloys was sparked once again in the early 2000s when the demand for Ni-free shape memory materials for the use in biomaterials became apparent [11, 12]. During this time gap in the literature, between the 1980s and 2000s, more up to date methods for the determination of the martensitic transformation temperatures had been developed. Differential scanning calorimetry (DSC) is often used to identify key temperatures that are associated with phase transformations [1]. The amount of heat energy that is released during the forward $\beta \rightarrow \alpha''$

transformation, and absorbed during the reverse $\alpha'' \rightarrow \beta$ transformation, is measured as a function of temperature. The resulting heat flux is generally plotted as a function of temperature and the key transformation temperatures are measured from the points where the heat flux curve deviated from the background level. However, once the deviation of the heat flux from the background level can be measured, it is expected that a significant amount of the transformation must have occurred. Thus, the transformation temperatures that are measured using this technique are expected to be an estimation that is close to the true value. Therefore, alloys that undergo small amounts of the martensitic transformation may not always be detectable. Other indirect measurement techniques for the transformation temperatures have also been used, which are also predicted to result in values that are an over or underestimation of the true temperatures. These include measurements of the changes in the electrical resistance of samples which result from the occurrence of the $\beta \leftrightarrow \alpha''$ transformation [1].

An alternative approach measured the strain response of a sample as a function of changing temperature under a constant stress [12]. A plot of transformation temperature versus applied stress is extrapolated to a stress of 0 MPa, which then gives an M_s value for the sample. Limitations of this method include the requirement to extrapolate the data to predict a value for M_s, however, unlike the arbitrary curve used to extrapolate data by a few hundred degrees celcius that had been previously used [50, 52, 55], the relation between the stress and temperature is expected to be a straight line according to the Clausius-Clapeyron relation (see equation 1.1).

The more recent measurement techniques that have been used to determine M_s have allowed alloys with higher Nb contents to be investigated. Figure 1.12 collates values for M_s that have been reported for Ti-Nb alloys that contain > 20 at.% Nb [12, 18–20, 57–59]. Despite the use of improved techniques, a similar variation of $\sim$ 50°C is observed in the reported values for M_s when the data is collated in this manner. It is the aim of this literature review to discuss potential reasons for these discrepancies.

Effect of Nb contents on M_s Section 1.5.1 discussed the effect of Nb concentration on the M_s transformation temperature for alloys that contain less than 18 at.% Nb. Figure 1.11 summarised that Duwez [50] and Sato, Seikiti and Huang [52] used curved trendlines to relate

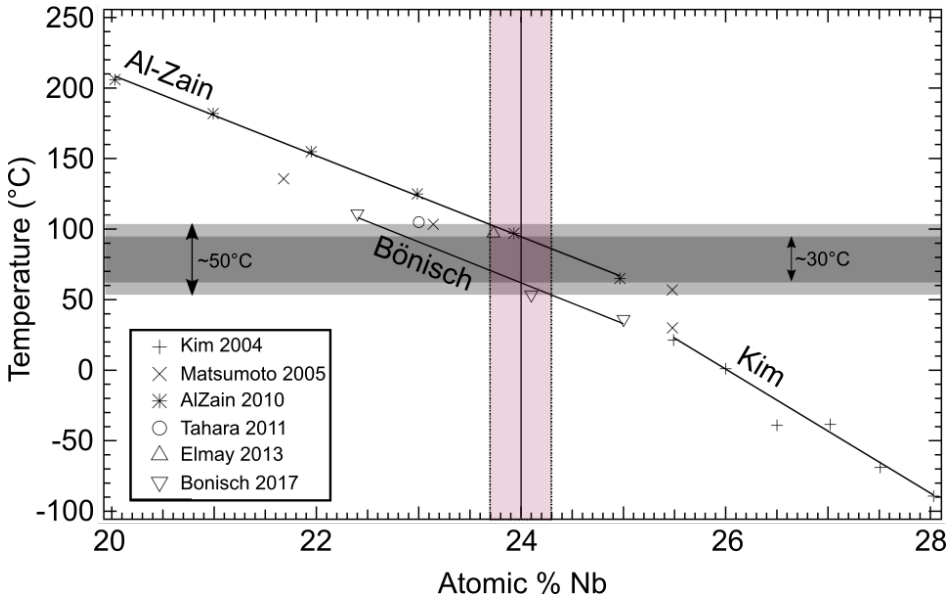

Fig. 1.12 Summary of reported transformation temperatures in literature for Ti-Nb with higher Nb contents [12, 18–20, 57–59]. The ranges in temperature that are labelled represent the difference in M_s that has been recorded for alloys with similar Nb contents.

the Nb contents to M_s, whilst Jepson, Brown and Gray [53] assumed a linear relationship. Similarly, more recent studies that have evaluated M_s for Ti-Nb alloys that contain higher Nb contents commonly use a linear relation. For example, figure 1.12 shows that the data published by Al-Zain et al. [19] is observed to follow a linear trend with increasing Nb content with a decreasing gradient of -29°C with every 1 at.% Nb added, which is in agreement with the data published by Bönisch et al. [20]. Despite the data from these studies concluding a similar relationship between Nb content and M_s, figure 1.12 shows that the values reported by Al-Zain et al. [19] lie $\sim$ 30°C above those reported by Bönisch et al. [20]. Data that has been published in other studies [18, 57, 58] has reported values for the M_s temperature that lie between the trendlines reported by Al-Zain et al. [19] and Bönisch et al. [20], as shown in figure 1.12. Since these lines appear to outline the upper and lower boundaries of the reported M_s values, these lines are used here to demonstrate the range of values that M_s has been reported to take in an example alloy of Ti-24Nb. The collation of data in figure 1.12 suggests that the M_s temperature should fall in the range from $\sim$ 60°C to $\sim$ 90°C. However, in many literature studies, the actual values of the composition are rarely reported, and it is unreasonable to assume that the target composition is representative of the actual Nb contents of the alloy. If a range of Nb contents is taken to represent Ti-24Nb, from 23.7 at.% to 24.2

at.%, the range of possible M_s values would increase to $\sim$ 50°C. This has been demonstrated in the figure, using dotted lines to show the example composition range, and grey highlights to show the range of the corresponding M_s values.

Data points published by Kim et al [12] (which are drawn in figure 1.12 using "+" symbols) were also reported to follow a linear relationship for Ti-(25-28)Nb alloys, however, the recorded gradient for this line was observed to be -43°C with every 1 at.% Nb that was added, in contrast to that observed in Ti-(20-25)Nb alloys [19, 20]. One possible reason for this discrepancy is the outlying data point that deviates from the proposed trendline, which contains 26.5 at.% Nb. The removal of this point from the from the graph in figure 1.12 results in a linear trend with a revised gradient of -44°C per 1 at.%, which was insignificantly different to the initial value.

One key difference between these three studies is the thermomechanical processing route used to manufacture the alloy prior to testing. Kim et al [12] cold rolled an arc melted bar to 95% and subsequently heat treated at 900°C for 30 minutes followed by a water quench. Al-Zain et al. [19] included an initial solution treatment of 1000°C for 2 hours after arc melting, and then cold rolled the bar to 98.5% before the final heat treatment at 700°C for 10 minutes followed by a water quench. This initial solution treatment is commonly used to ensure complete chemical homogeneity through the arc melted bar before cold working. Since both studies cold rolled their alloys to very high reduction ratios it is expected that this 2 hour heat treatment will not alter the microstructure significantly between studies. In contrast to these processing routes, Bönisch et al. [20] solution treated an alloy that had been cast in a cold crucible for 24 hours at 1000°C and water quenched, and no cold work was conducted on the alloys. These dissimilar heat treatments that have been conducted at different temperatures for different periods of time are expected to have resulted in varying levels of oxygen uptake, and consequently, a difference in the final oxygen content of the sample. Additionally, variety in the processing routes used is expected to result in samples with dissimilar initial microstructural features, such as different dislocation densities as a result of the different levels of cold rolling, and varying grain sizes as a result of the different heat treatments. Therefore, it is proposed that the microstructural condition of the initial

sample has an effect on the thermal transformation behaviours in these alloys. Both the oxygen content and microstructural features will be discussed further.

1.5.2 The effect of O contents on the stability of the β phase

Interstitial alloying elements have been reported to have a significant effect upon the stability of the phases in Ti-Nb alloys, and are therefore expected to have an influence on the transformation behaviour of these alloys [11, 15, 45, 57, 59–63]. Investigations into the effect of oxygen on the transformation behaviours of Ti-Nb alloys are particularly important given the ease of oxygen pick-up during the melting and heat treatment steps of alloy processes. Significantly, the M_s temperature for the Ti-Nb binary system has been reported to decrease by 160°C with every 1 at.% added [45]. Similarly, calorimetric data has shown evidence of the $\beta \rightarrow \alpha''$ transformation occurring below 105°C in Ti-23Nb but no evidence of the same transformation was observed in Ti-23Nb-1O at.% that was cooled below -90°C using DSC measurements [57]. It should be noted that plotting this data point on a diagram, like figure 1.12, is difficult since no value for M_s was recorded. However, if the maximum temperature that this value could take is given a value of -90°C, it can be seen that the value of M_s for an alloy composition that is labelled as Ti-23Nb, can differ by over 200°C. Tahara et al. [59] then studied the effect of oxygen on Ti-20Nb, which is expected to contain a less stable β phase, and a more stable α'' phase. Additions of 0.7 and 1 at.% O were sufficient to prevented the formation of α'' on the quench following solution treatment at 900°C, indicating that the M_s temperatures for Ti-20Nb-0.7O and Ti-20Nb-1.0O lie below room temperature. Comparing these results with those published by Al-Zain et al. [19], demonstrates another discrepancy in the recorded M_s temperature for a Ti-Nb binary alloys of the order of 200°C. Whilst these comparisons are being made, it is noted that comparisons between different studies such as these cannot provide direct conclusions for the discrepancies in the recorded M_s values. As mentioned previously, many studies do not report the actual content of the niobium and oxygen in the alloys and any comparisons made here are purely speculative. For example, since Al-Zain et al. [19] did not directly add any oxygen into the alloys, it could be assumed that they contain a negligible amount of oxygen. However, it is mentioned in the report that a light oxide layer was removed from the sample surface prior to testing, which suggests that

there was an uptake of oxygen during processing, which was significant enough to produce an oxide layer. Another example includes a study conducted by Elmay et al. [58], which reported an oxygen concentration of 2.56 at.%. in their Ti-24Nb alloy that had been arc melted and solution treated at 1000°C for 20 hours followed by water quenching, cold rolling to a reduction ratio of 95% and a final heat treatment at 900°C for 1 hour and water quenched. This processing route was very similar to the ones used by Kim et al. [45], Al-Zain et al. [19] and Tahara et al. [59]. It is clear from these comparisons how vitally important that it is to measure, and report the actual oxygen composition for any alloy under investigation.

1.5.3 Discussion of the effect of composition on M_s with the use of an example

The stability of the β phase in Ti-Nb-O alloys increases with an increasing Nb and O contents. An increase of 1 at.% has been reported to decrease the M_s temperature by 40°C and 160°C in Nb and O respectively. However, across the literature, the composition differences cannot account for the differences in M_s temperatures that were shown in figure 1.12. For example, the Ti-23.7Nb-2.56O and Ti-24.1Nb-0.3O alloys that were studied by Elmay et al. [58] and Bönisch et al. [20] were reported to take values of M_s of 97°C and 54°C respectively. However, the compositional differences predicted a much larger difference of $\sim$ 378°C (40°C/at.% $\times$ 0.4 at.% + 160°C/at.% $\times$ 2.36 at.%).

1.6 Effect of the initial microstructure on M_s

In section 1.3 the effect of the initial phase constitution on the transformation behaviour for alloys that exhibit a reversible martensitic transformation was discussed. For a microstructure that contains more than one phase, multiple deformation mechanisms are in competition when a load is applied to the sample. These include the stress-induced $\beta \rightarrow \alpha''$ transformation, the reorientation of martensite variants, twinning of both the β and α'' phases, and slip deformation [58, 64]. Therefore, it is critical that the initial microstructural condition of a sample is fully characterised prior to the application of an external load, or a change in temperature.

1.6.1 The effect of the initial phase constitution

Figure 1.8, and the accompanying discussion in section 1.3 demonstrated that an alloy can form microstructures that contain different phase constitutions depending upon their thermomechanical history. Therefore, it is unsurprising that multiple studies have investigated the effect of the processing route of an alloy upon its deformation response [13, 14, 46, 58, 65–68]. The analysis of the deformation behaviour of a superelastic alloy is often conducted using its strain response to an applied stress. The resultant stress-strain curves are often used in conjunction with X-ray diffraction (XRD) patterns which characterise the phases present in the initial, and occasionally the final microstructure.

1.6.2 The effect of cold work

Cold rolling is often used to refine the grain structure and improve the overall strength of titanium alloys [58, 65, 66, 68]. Additionally, initial investigations into the replacement of NiTi-based alloys with Ti-Nb alloys suggested that cold work was often required to achieve the desirable properties which include low elastic modulus, high strength, good workability and superelastic properties [69, 70]. Post cold working, the XRD patterns for Ti-Nb alloys commonly show peaks that correspond to the α'' phase, which was induced during the high levels of plastic deformation [65, 66, 68]. The observed diffraction peaks through these studies are generally very broad, indicating a significant defect density and high levels of microstrain in the microstructure. Despite this, non-linear elastic deformation has still been observed in these alloys [58, 65, 66], and interestingly, almost full recovery of the applied strain has been observed during the unload.

For example, a Ti-26Nb alloy was observed to contain both the β and α'' phases after being cold rolled to a reduction ratio of 90% [66]. When a sample was loaded with the tensile direction along the rolling direction, the resultant stress-strain curve was observed to follow a curved elastic deformation up to 1.5% strain. Upon the removal of the applied stress, the unloading curve followed a similar curved shape, leading to full recovery of the applied strain. Since the M_s temperature for this alloy has been reported to lie below room temperature [12], and the A_s temperature has been reported to lie above room temperature [12, 20], it seems reasonable to assume that room temperature lies between M_s and A_s for this alloy. Therefore,

the consideration of figure 1.8 suggests that when a load is applied, both the stress-induced $\beta \rightarrow \alpha''$ transformation and detwinning of the α'' already present in the alloy may occur. These deformation mechanisms may account for the curved nature of the elastic deformation region during loading. For any alloy that is unloaded below A_s, no recovery of the strain is generally expected because there is no driving force for the reverse $\alpha'' \rightarrow \beta$ transformation to occur. However, the almost full recovery observed in this study is in disagreement with this, reasons for which are not mentioned in the report [66].

Elmay et al. [58] investigated the transformation behaviour of Ti-23.7Nb-2.56O that was loaded below its M_f temperature, which they recorded as 67°C using strain measurements during temperature cycles at various stresses. After cold rolling to a reduction ratio of 95% the alloy was observed to be entirely composed of the α'' phase. When loaded, the elastic region showed a non-linear deformation, consistent with a shape memory alloy starting in the martensitic condition. As demonstrated in figure 1.8, an alloy that is loaded and subsequently unloaded below M_f, no strain recovery is predicted since the α'' is considered very stable, and generally consists of only the elastic deformation of the original martensite being recovered [1]. However, when the sample was unloaded, a significant proportion of the applied strain was recovered.

Despite current thermodynamic theories being unable to explain the non-linear unloading response, the significance of these data has seemingly been overlooked. This is as a result of the focus of the work being aimed towards the improvement of the superelastic properties using post-cold working heat treatments. Therefore, it is difficult to draw conclusions as to why this reversion occurred without the data showing the final phase constitution. In spite of this, it is clear from the discussions above that the current transformation theories for these alloys, which are often based around the key transformation temperatures, A_f, A_s, M_s and M_f, may be limited for alloys that are loaded directly from the cold rolled state. It is possible that the actual chemical composition of the Ti-26Nb alloy [66] does not lie within the predicted temperature range, however, this is not the case for the Ti-23.7Nb-2.56O alloy since the key transformation temperatures for this specific alloy were measured and reported in the study [58]. Therefore, it is proposed that this unusual behaviour may have resulted

from the high levels of plastic deformation that these alloys had previously been subjected to without subsequent heating.

1.6.3 The effect of heat treatments after cold work

As previously discussed, Ti-Nb-based alloys that have been subjected to cold rolling reduction ratios > 90% have shown evidence that they contain high dislocation densities [58, 66, 71–73]. Long solution heat treatments after such high levels of cold working can induce rapid grain growth as a result of the fast kinetic recrystallisation kinetics [65, 74]. Additionally, further phase transformations to the ω and α phases become possible. Consequently, an increase in grain size may reduce the overall strength of the alloy, in accordance with the Hall-Petch effect [75, 76], and any phase transformation is expected to result in the redistribution of β-stabilising elements in the microstructure, resulting in a more stabilised β matrix. These difficulties have driven investigations into how heat treatments that are conducted after cold working may be optimised to produce alloys with a optimal superelastic properties, whilst retaining the desired high strength [12, 14, 58, 65–68, 74, 77].

Cold rolling Ti-Nb-based alloys have been shown to exhibit non-linear elastic loading and unloading curves when subjected to an externally applied load [58, 65, 66]. Elmay et al. [58] reported a decrease in strength after solution treating Ti-23.7Nb-2.56O at 900°C for 1 hour. Short heat treatments that were conducted on the alloy directly after cold rolling were reported to significantly improve the superelastic behaviour of the alloy, whilst maintaining an ultimate tensile strength that is higher than observed for the solution treated condition. These short heat treatments at 300°C and 600°C for 10 minutes reversed all of the α'' back to the β phase, and initiated the transformation to the ω and α phases. Heating at 600°C progressed these reactions further, resulting in a more stable β matrix, and consequently poorer superelastic properties. Whilst precipitation formation may be predicted to increase the plastic yield stress of the samples aged at 600°C compared with that aged at 300°C, the stress-strain curves show a lower critical stress and it is suggested that a heat treatment at 600°C for 10 minutes was sufficient to initiate microstructural recovery.

Similar effects on the tensile properties have been observed in studies that have considered different Ti-Nb alloys. For example, a flash heat treatment applied to cold rolled Ti-26Nb for

600°C for 6 minutes has been shown to significantly improve the superelastic strain recovery, however, this is at the expense of the plastic yield stress which was reduced from 1000 MPa too 600 MPa [66]. The improved superelastic properties, and slight increase in critical stress required to induce the martensitic transformation were attributed to the precipitation of the ω and α phases, which stabilised the surrounding β phase, in turn, increasing the stress required to form α''. These observations and conclusions are in agreement with the observations by Elmay et al. [58].

The growth of the ω phase in titanium alloys is generally known to cause embrittlement and a loss of ductility [28], and is therefore generally avoided. However, some studies that have investigated the effect of ageing temperature on the superelastic behaviour in metastable β-titanium alloys have reported an improvement in the superelastic behaviour with the presence of controlled amounts of the isothermal ω phase [13, 14]. Kim et al. [13] reported an increase in the critical stress required for slip deformation in Ti-26 at.% Nb, which, in turn, increased the amount of recoverable superelastic strain, and stabilised the superelastic hysteresis with cycling. Further investigations into the effect of similar ageing routines in Ti-(26-28)Nb alloys [14] confirmed an increase in the critical stress for slip after lower temperature annealing at 600°C for 10 minutes, and consequently, observed an improvement in the observed superelatic behaviour in these alloys. Additionally, an ageing treatment at 300°C that was conducted after this short low temperature anneal was found to further improve the overall tensile strength and critical stress required to induce the martensite, which both increased with an increasing ageing time. However, longer ageing times were found to be detrimental to the superelastic elongation that could be achieved. The increase in tensile strength and embrittlement of the alloy with an increased ageing time at 300°C was attributed to the growth of the ω phase. These results suggest that whilst the formation of the ω_{iso} phase can increase the critical stress that is required for slip, which in turn increases the amount of superelastic recovery strain and tensile strength in the material, longer ageing times favour the growth of the ω_{iso} precipitates, which alters the chemical stability of the surrounding β matrix. The stabilisation of the β phase increases the critical stress required to induce the $\beta \rightarrow \alpha''$ transformation, which decreases the overall superelastic recovery strain. The general consensus through the literature proposes that a balance between the tensile strength and the

superelastic recovery must be maintained through the optimisation of the microstructure using alloy design [58, 65, 66, 74, 77].

Despite the confirmation of these conclusions across multiple studies, discrepancies between the resultant stress-strain curves for the same alloy composition, that have been subjected to very similar heat treatments still exist. An example of two data sets obtained for Ti-26Nb is shown in figure 1.13. Kim et al [13] cold rolled the alloy to a reduction ratio of 99% and subsequently heated at 600°C for 10 minutes before water quenching. In comparison, Sun et al. [66] cold rolled their alloy to 90% followed by ageing at 600°C for 6 minutes and water quenching. The figure shows a drastic difference between the resultant stress-strain hysteresis shapes, which raises significant concerns for an alloy that has the same reported composition and very similar thermomechanical treatments. This comparison alone highlights the need for further investigations into the effect of the microstructural condition on the $\beta \rightarrow \alpha''$ transformation, and in turn, the superelastic behaviour of these alloys.

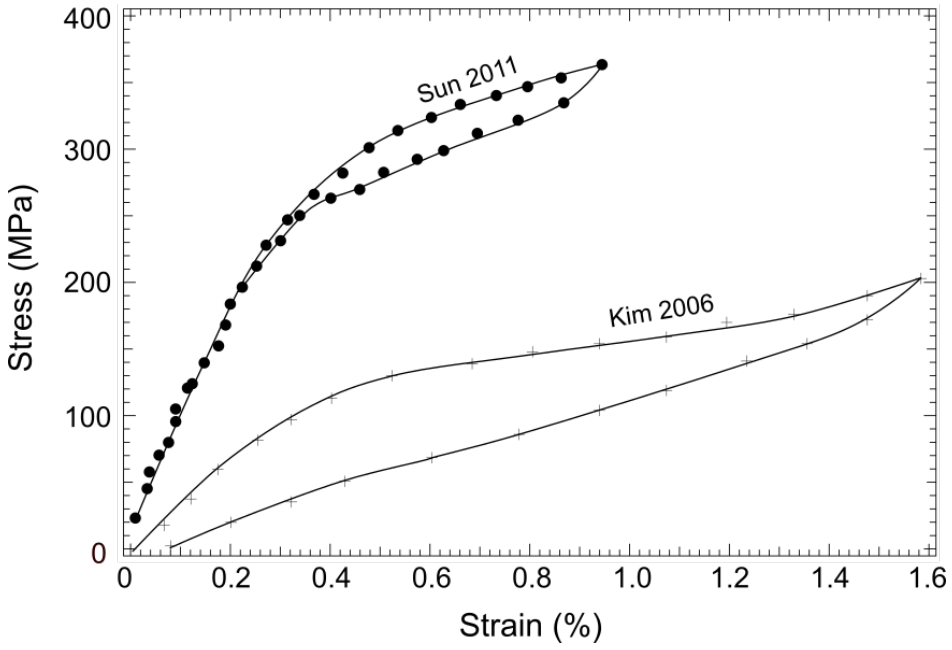

Fig. 1.13 A direct comparison between two published superelastic stress-strain responses for Ti-26Nb that has been subjected to similar thermodynamic processing routes. Data has been extracted from references [13] and [66].

1.7 Summary

This introduction has summarised the important factors of the current literature concerning the superelastic behaviour in Ti-Nb alloys. Increasing the concentration of niobium and oxygen in Ti-Nb-O alloys led to the stabilisation of the β phase, which, in turn was shown to decrease the M_s temperature for the thermally driven transformation, and increase the critical stress required to induce the transformation. The discrepancies that exist in the reported values for M_s were highlighted, and potential explanations for these were proposed and discussed. This discussion included differences in the actual composition of the alloys, and in particular, the oxygen content, since additions of 1 at.% O have been found to completely suppress the $\beta \rightarrow \alpha''$ transformation. As a result of this, the importance of the measurement and reporting of the oxygen content was expressed.

It is clear that the initial phase constitution of the alloy must have an impact on the superelastic behaviour in a Ti-Nb alloy. The effects of an initial amount of α'' and varying levels of the ω phase were introduced. The amount of α'' in the initial microstructure of a Ti-Nb alloy is dependent upon its key transformation temperatures which, in turn, are related to its composition. The presence of a twinned α'' prior to loading introduces the potential of detwinning upon loading as well as the stress-induced transformation of any β present. Small amounts of the ω phase have been shown to increase the critical stress required for slip deformation and, in turn, increase the recoverable superelastic strain. However, larger precipitates were shown to increase the stability of the surrounding β matrix as a result of the redistribution of β-stabilising elements during precipitate growth. This increased stability increased the critical stress required to induce the martensitic transformation, and resulted in lower superelastic recovery strains. The levels of α'' and ω in the initial microstructure are expected to have a significant influence on the deformation behaviour in these alloys.

It is the general consensus in the current literature that the amount of deformation and subsequent heat treatments can have a significant effect on the resultant mechanical response of a Ti-Nb alloy. However, two stress-strain curves that have been published for the same alloy, which had been subjected to very similar thermomechanical processing routes showed a difference that is worthy of attention. It is suggested that a full characterisation of these alloys, including grain structure and approximate or relative dislocation density, is required

before loading. It is clear that there are gaps in the understanding of how the form of the microstructure affects the superelastic behaviour in Ti-Nb alloys, and that further investigations are required.

Chapter 2

Methods

2.1 Microstructural characterisation

2.1.1 Fabrication of samples

Melting

Ingots of Ti-24Nb (at.%) were prepared from high-purity titanium and niobium by arc melting under an argon atmosphere. The target composition of the alloy was used to calculate the relative masses required for each element to melt a bar that weighed $\sim$ 40 g. The correct amounts of titanium and niobium were then placed onto the copper base in the arc melter. Each bar was re-melted at least 5 times to encourage macroscopic homogeneity of the elements across the bar. A significant amount of the previous literature conducted a long heat treatment after initial arc melting to ensure chemical homogeniety through out the sample. However, previous work that had been conducted in the research group suggested that these arc melted bars exhibited consistent macroscopic composition through out the bar. Figure 2.1a shows an image of the resulting bar of material, which was subsequently cut into segments using a Struers Accutom machine ready to be cold rolled.

Cold rolling

Cut segments that were $\sim$ 6 mm wide were cold rolled into long strips to refine the grain structure and introduce a high dislocation density to the sample. To achieve a minimum

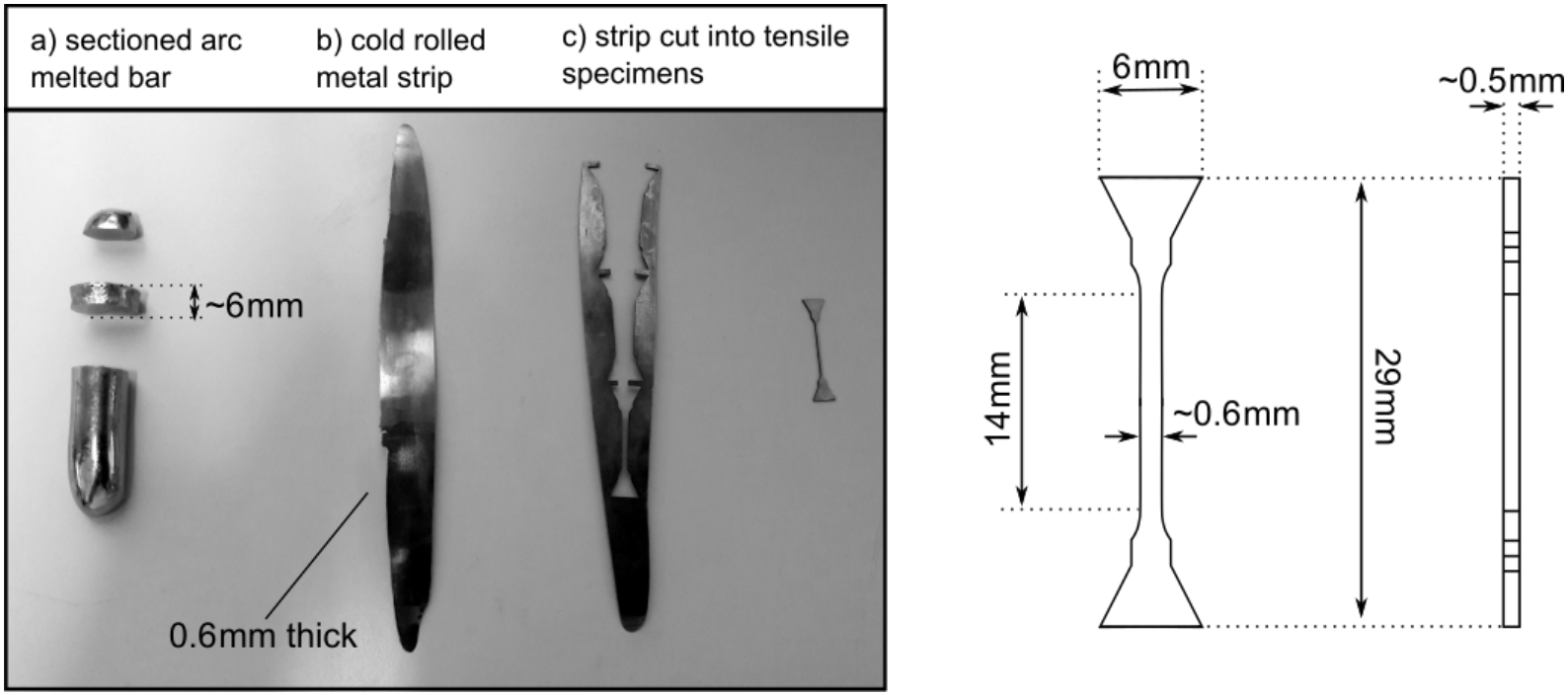

Fig. 2.1 Image and schematic diagram showing the fabrication and processing method used to produce tensile specimens

reduction ratio of 90%, the separation between the cold rolling wheels was gradually reduced from a thickness of $\sim$ 6 mm to $\sim$ 0.6 mm. In chapter 5, reduction ratios between 50% and 90% were also considered. In these cases, the original thickness of each cut piece of material was adjusted so that the final thickness of all of the samples was $\sim$ 0.6 mm. During cold rolling, each reduction in thickness resulted in the strip increasing in temperature. Therefore, between each step, the strip was allowed to cool to a temperature where it could comfortably be held by hand. The longest amount of time required for this to occur was less than a minute and prevented the metallic strip from increasing in temperature to a value that could, potentially, result in a change in microstructure as a result of the additional heat.

Solution treatment

Some of the cold rolled sample was subjected to a solution treatment at 900°C for 5 minutes followed by a water quench. This solution treatment was conducted on the sample to reduce the dislocation density and encourage recrystallisation, whilst maintaining a small grain size. These samples were cleaned with ethanol and acetone, wrapped in a tantalum foil getter and encapsulated in an evacuated quartz tube. To further reduce any potential uptake of oxygen during the solution treatment, the tubes were backfilled with argon and evacuated at least 3 times prior to final evacuation. All of the tubes were water quenched following heat treatment to achieve rapid cooling of the sample but were not broken to avoid oxidation [78]. A 12 mm outer diameter quartz tube was chosen to conduct the heat treatments to maximise the amount of the sample that was in contact with the quartz tube, allowing faster cooling rates in the evacuated tube. The preparation techniques required for the analysis of an alloy's microstructure often involves mechanical grinding and polishing to reveal the underlying microstructure. However, these polishing techniques can cause residual stresses in the surface of the material, which, in turn, might change the microstructural condition. Therefore, where possible, all preparation techniques that involved externally applied loads or slight elevations in temperature were conducted prior to any final heat treatment.

2.1.2 Synchrotron diffraction experiments

In situ synchrotron X-ray diffraction data, was used to directly measure the phase constitution of the samples during various thermomechanical cycles. Figure 2.2 shows a schematic drawing that demonstrates the set-up that was used during the synchrotron experiments, and how the two-dimensional diffraction rings were obtained.

Diamond Light Source, Oxford

A 0.5×0.5 monochromatic beam, with a wavelength of 0.15527Å, was used and the transmitted Debye-Scherrer rings were collected using a Pixium area detector at a distance of $\sim$ 1142 mm from the sample. The experimental set up is shown using a schematic drawing in figure 2.2. Diffraction images, with an expose time of 0.5 s, were recorded every 4 s, giving a temperature resolution of 2°C for the dataset.

European Synchrotron Radiation Facility (ESRF)

At the ESRF, a 0.5×0.5 mm monochromatic beam with a wavelength of 0.15804Å, was used to produce a Debye-Scherrer ring which was collected using a Frelon area detector at a distance of $\sim$ 251 mm. An exposure time of 0.5 s was used during these experiments to produce diffraction images, which were also used to obtain an image every 4 s.

Diffraction peak fitting

One-dimensional diffraction patterns were then produced by azimuthally integrating the two-dimensional diffraction data either (i) around the full 360°, or (ii) over a range of angles that lie $\pm$20° around a central angle. The drawing in figure 2.2 demonstrates how this central angle was chosen using two example segments, the first where the central angle lies along the loading axis, and the second where the central angle lies through an angle where the α'' variants were more pronounced. The integration was conducted using the Fit2D software [79] and the identification of the phases present in the irradiated samples was achieved using the Pawley refinement technique, implemented within Topas Academic. In addition, Wavemetrics IGOR Pro was used to fit individual diffraction peaks in the one-dimensional pattern with a

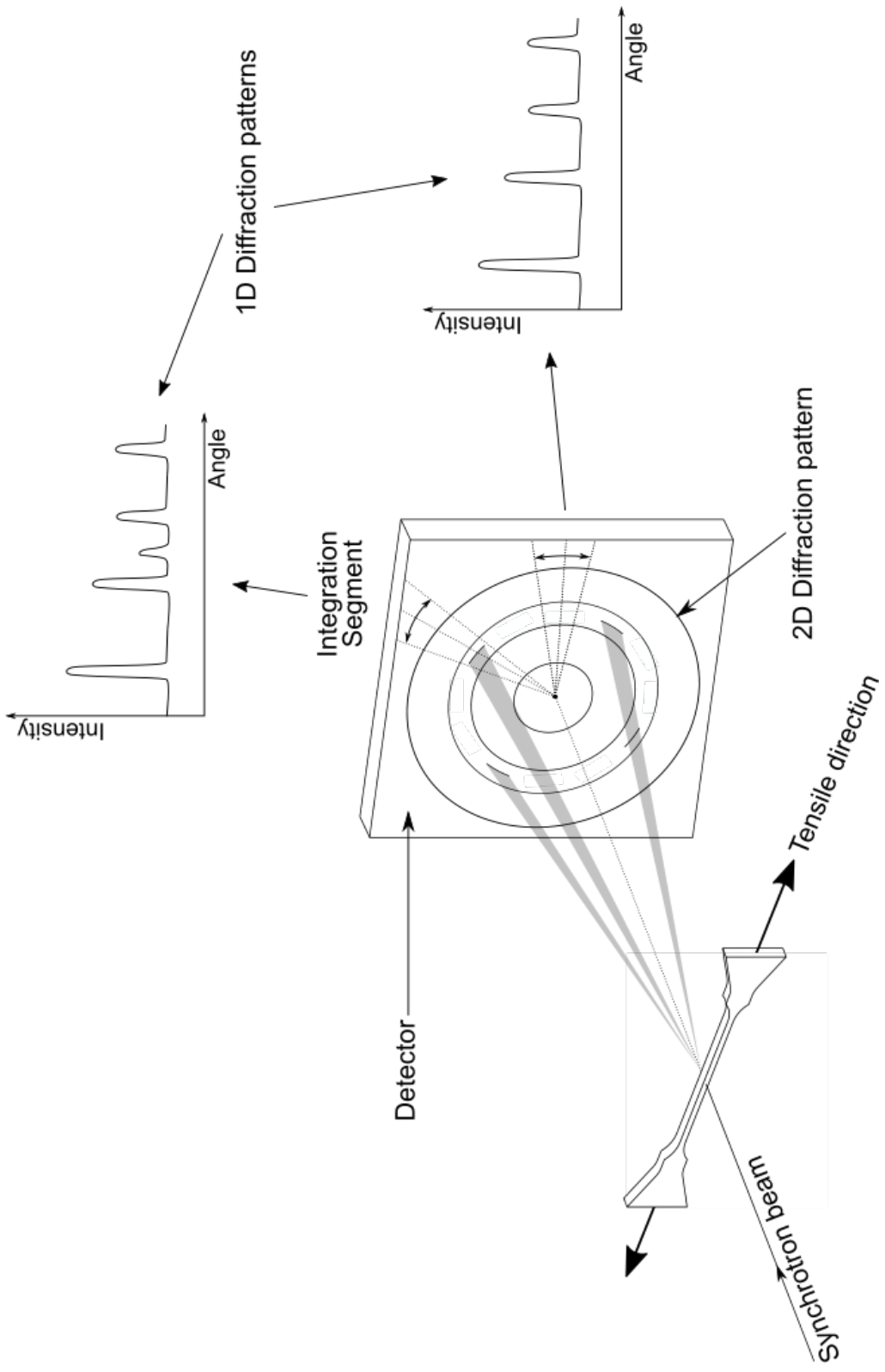

Fig. 2.2 A schematic drawing of the experimental set up during *in situ* synchrotron diffraction experiments. The tensile sample was subjected to changes in temperature and stress whilst being illuminated by the synchrotron beamline.

Gaussian function on a linear background. Peak positions were used to identify the phases present in the microstructure and the normalised peak areas were used as an indicative measure of the phase fraction.

2.1.3 Tensile testing

In situ tensile tests were conducted within the synchrotron beamline to a maximum stress of 300 MPa and *ex situ* tensile tests to failure were collected using a Tinius Olsen tensile testing rig with a 25 kN load cell. In both cases, a tensile stress was applied along the length of each sample, which was approximately parallel to the rolling direction in the cold rolling process.

In situ tensile testing

The tensile stress was applied in a direction perpendicular to the beamline using a Linkam TST350 tensile rig. An image of the Linkam TST350 rig set up in the beamline is shown in figure 2.3. Diffraction patterns were constantly recorded whilst the Linkam tensile rig was used to change the temperature and stress of the sample. All temperature changes were conducted at a rate of 30°C min^{-1}, and a constant stress of $\sim$ 5 MPa was applied to the specimen to ensure that any thermal expansions/contractions did not change the stress state of the sample. The application of a constant stress during heating and cooling regimes ensured that any temperature changes were isolated from the changes in stress. Thus, any effects on the sample could be directly attributed to a change in temperature or stress alone.

Tensile samples were cut from the cold rolled strip, as shown in figure 2.1, using electro discharge machining. The re-cast layer that formed where the wire had been in contact with the tensile sample was removed by mechanical grinding and polishing. Figure 2.1d shows a technical drawing of these tensile samples, with the key dimensions of the gauge labelled. The thickness and width of the gauge were dependent upon the depth of the re-cast layer that was ground from the sample surface. As a result, the quoted value of 0.6 mm is therefore an overestimate, and the width and thickness values were closer to 0.56 ± 0.04 mm.

The overall size of the tensile samples were limited by the space that was available inside the Linkam stage, and the size of the cold rolled strips that the specimens were cut from.

Whilst a small sample limited the number of grains that were sampled during the experiments, they minimised the potential of a thermal gradient forming across the gauge of the specimen.

Stress assumption Figure 2.4 shows an image of a sample that was loaded in the Linkam TST350 tensile rig. A uniaxial tensile stress was applied along the length of each sample and the value for the stress that is reported through out this work was calculated using the applied force and cross-sectional area of the sample. It should be noted that these stress values refer to the deviatoric (von Mises) component and assumes that the hydrostatic component is sufficiently small that it can be neglected. This assumption was required to simplify the experimental data to enable any trends between the stress and phase consitution to be identified. The aim of this work was to identify a simplified relationship between an applied uniaxial tensile stress and the martensitic phase transformation. Once this data has been collected and any trends identified, future investigations should focus on analysing the hydrostatic stress component as well. It is suggested that this could be achieved through the application of a compressive uniaxial stress. This work could not easily be conducted in this study because the cold rolled samples were too thin and surface effects would be too large.

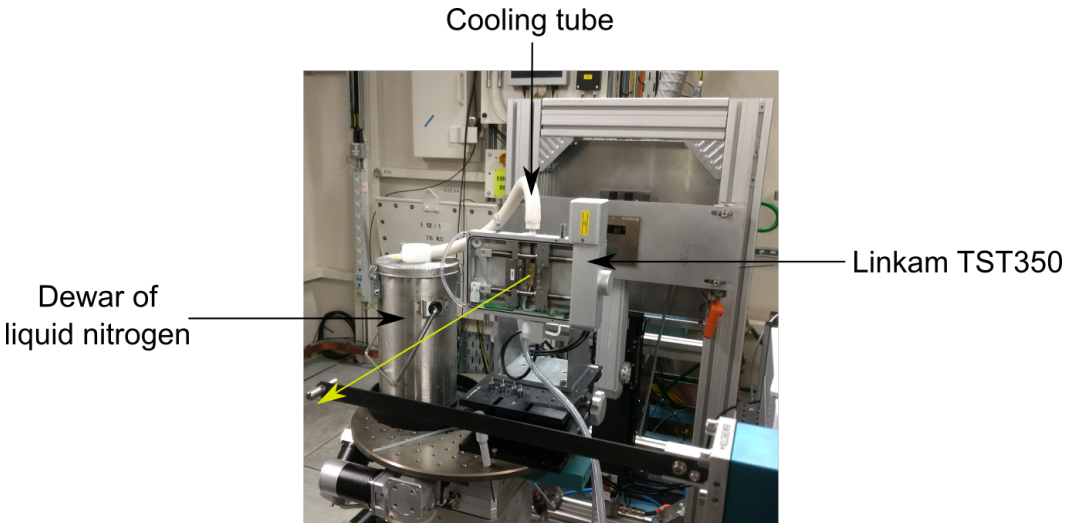

Fig. 2.3 An image of the Linkam TST350 tensile rig set up in the synchrotron beamline. The direction of the x-ray beam is shown using a yellow arrow.

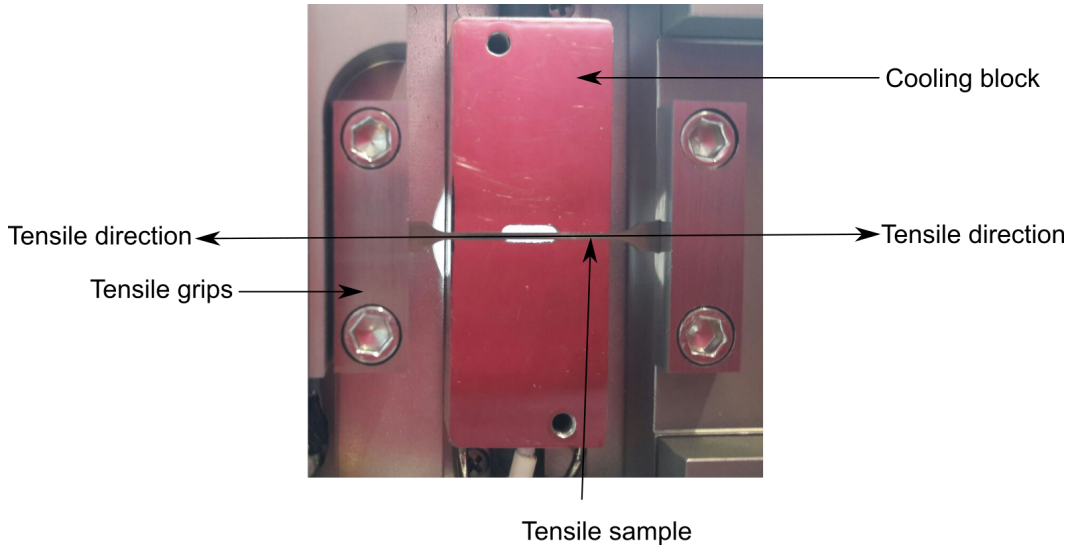

Fig. 2.4 Labelled image of the centre of the Linkam TST350 tensile rig showing the direction of the applied tensile stress.

Ex situ tensile testing

Tensile tests that were not conducted in a synchrotron beamline were obtained using a Tinius Olsen tensile testing rig with a 25 kN load cell. Figure 2.5 shows an image of the experimental set-up used during the *ex situ* tensile tests. All tensile tests were conducted under stress control at a rate of 4 MPa s^{-1}, which is equivalent to a strain rate of $\sim 66 \times 10^{-6}$ s^{-1} (using a Young's modulus of $\sim$ 65 GPa [18]. A slower strain rate to those that have been previously used which are generally of the order of 10^{-4} s^{-1} [13, 18, 58, 80] was chosen in order to enable the stabilisation of the system during incremental loading. For consistency across experiments, the size and shape of the tensile specimens were kept as similar as possible for these experiments.

Pre-loaded samples As a result of the cold rolling process, all of the tensile samples were slightly curved prior to loading in the tensile rig. This curvature could not be removed from the sample because during the subsequent heat treatments, the surface stresses that had resulted during processing relaxed and caused the sample to bend. Additionally, no post-heat treatment sample preparation could be conducted since any application of stress or temperature may have resulted in microscopic changes. Therefore, to reduce the artefacts that are introduced in a stress-strain curves when loading a curved sample, a preload of $\sim$ 10 MPa was added to

straighten out all samples prior to testing. Once a preload had been applied to each sample, a clip on extensometer was attached around the middle of the gauge to measure the strain during each test.

In some cases, the thickness of the sample was increased to 1 mm to avoid the sample bending as a result of the relaxation of surface stresses during heat treatment. However, this was an upper limit to how thick the samples could be rolled whilst maintaining a reduction ratio above 90%. Despite the sample size no longer being restricted by the space available in the Linkam testing rig, it was still restricted by the size of the cold rolled strip of material from which the tensile specimens were cut (figure 2.1).

Tests to failure and cyclic loading Firstly, a tensile test to failure was determined for all of the samples to obtain their yield stress values. After this, tensile load-unload cycles were conducted on a new sample, with a maximum stress value that was at least 100 MPa below the yield stress. This ensured that no plastic deformation occured during these load cycles, and that only the elastic deformation region was investigated.

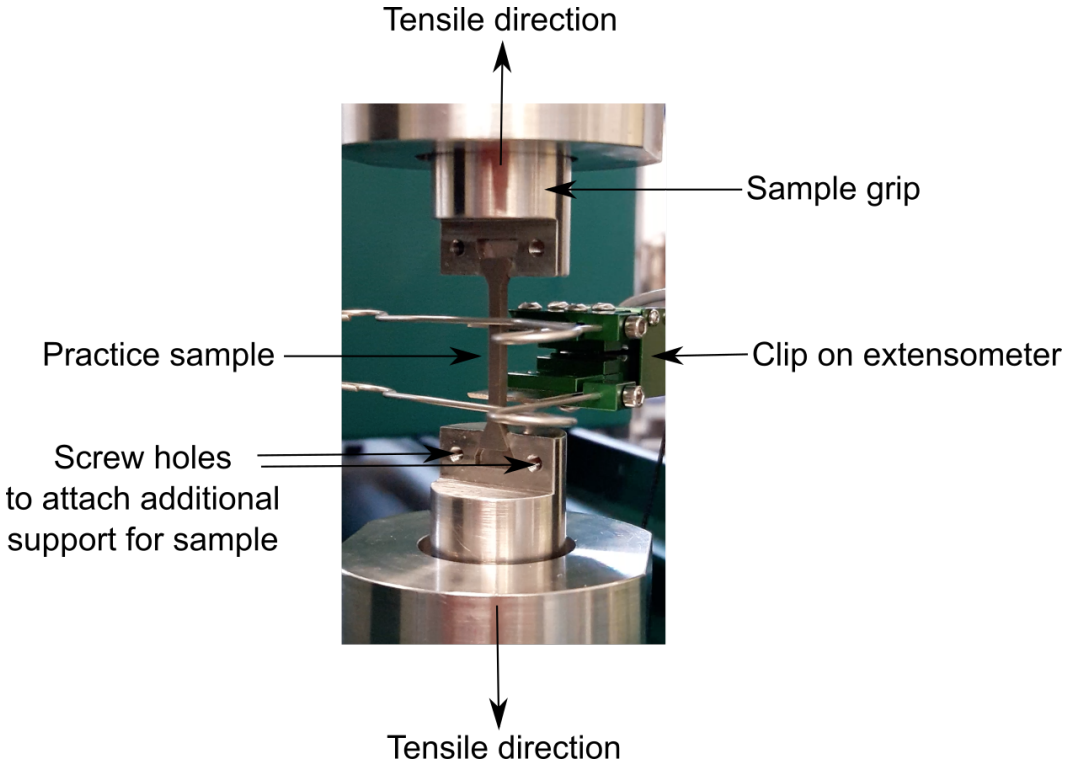

Fig. 2.5 *Ex situ* tensile test set up on the Tinius Olsen tensile rig using a practise sample and a clip on extensometer.

Optical and scanning electron microscopy

In the introduction it was discussed how important it is to characterise the initial microstructure of these alloys. Optical and scanning electron microscopy (SEM) were used to aid the identification of the phases present, and to identify the extent of any recrystallisation and grain growth that had occurred during the heat treatments used after cold rolling. Offcuts from the metallic strips, shown in figure 2.1 were glued to a bakelite stub and ground using silicon carbon grinding paper. The sample was glued rather than being hot or cold mounted to avoid the samples being exposed to any unnecessary heating or applied stresses (which could have resulted from the contraction of an epoxy resin). After grinding to 4000 grit, a suspension of colloidal silica which had been buffered to pH 7 using hydrogen peroxide, was used to polish the sample surface to a mirror finish. These cold rolled samples were then heat treated for the appropiate temperature and time. To expose the underlying grain structure, samples were etched in a solution of 8% HF and 15% HNO_3 in H_2O, and washed with ethanol.

Transmission electron microscopy

3 mm diameter discs were spark eroded from the sample, and hand ground to a thickness of $\sim$ 100 µm using silicon carbon grinding paper. Thin foils for study in the TEM produced via twin jet electro-polishing using a solution of 8% H_2SO_4 in CH_3OH at a temperature of -40°C and an applied potential of 20.5 V.

2.1.4 Determination of the chemical composition

The titanium and niobium composition of each alloy was determined by inductively coupled plasma-optical emission spectrometry (ICP-OES) using a Thermo Fisher iCAP 7400 Radial machine at University of Leeds. 0.45 g of each sample was dissolved in a solution of 7 ml hydrofluoric acid and 3 ml nitric acid using a CEM Mars microwave digestion system. The oxygen composition was determined at a certified external laboratory using a fusion-thermal conductivity method (LECO).

2.1.5 Laboratory based X-ray diffraction

Laboratory based X-ray diffraction (XRD) was obtained using a Bruker D8 ADVANCE diffractometer with Ni-filtered Cu Kα radiation. Samples were rotated within the X-ray beam to maximise the intensity of all peaks, and minimise the effect of texture on the relative peak heights. Samples were polished before any heat treatments were conducted to avoid any stress-induced artefacts that may have been produced during mechanical polishing. Peak positions were then used to identify the phase constitutions in the diffraction patterns.

Chapter 3

The influence of microstructure on the $\beta \rightarrow \alpha''$ transformation in Ti-24Nb (at.%)

3.1 Introduction

A marked difference between studies that have reported transformation temperatures for Ti-Nb alloys is the characterisation technique used to determine M_s. Early investigations used continuous cooling curves to identify temperatures at which phase transformations occurred [52, 53, 55]. More recently, DSC has been used [18–20, 57, 81] or samples have been thermally cycled over a range of applied stresses and the data extrapolated to predict a stress free M_s [12, 58]. Indirect measurement techniques, such as those mentioned above, measure changes in the sample that are thought to be associated with the transformation. However, their relative sensitivity to the transformation could introduce variations in values of M_s recorded. Critically, these techniques are also unable to unambiguously identify what is giving rise to the measured signal. This is of particular importance in the present case where other diffusionless phase transformations may occur, such as the formation of athermal omega (ω_{ath}). Consequently, to reduce such uncertainties and provide a better understanding of the $\beta \rightarrow \alpha''$ transformation, there is a need to perform *in situ* experiments that can provide a direct measurement of the phase constitution of a sample at specific temperatures and stresses.

To address this need, and to investigate the influence of microstructural features on the $\beta \rightarrow \alpha''$ transformation of binary Ti-Nb alloys, the behaviour of a Ti-24Nb (at.%) alloy has

been studied *in situ*, as a function of temperature using synchrotron radiation. Material was studied in both cold rolled and annealed states and these two conditions exhibited markedly different transformation behaviours. These results indicate that the occurrence of a thermally driven $\beta \rightarrow \alpha''$ transformation is highly dependent upon the microstructural condition of the material and this observation is used to rationalise the significant variations in M_s temperature reported in the existing literature.

3.2 Methods

Samples were arc melted and cold rolled to a reduction ratio of 90%, and rectilinear samples were cut from the rolled strip. Some of these samples were solution treated at 900°C for 5 minutes and water quenched. More details on these methods used to make the tensile samples are discussed in section 2.1. In this chapter, microstructural information from both CR and ST condition material was obtained using reflected light and TEM. *In situ* synchrotron XRD data were obtained using the I12 beamline at Diamond Light Source. Diffraction patterns were acquired as a function of temperature to provide direct evidence of the phases present in the sample. Each 2D diffraction dataset that was collected was azimuthally integrated around the full 360° to produce a 1D diffraction pattern using the Fit2D software [79]. A Linkam TST350 stage was used to vary the temperature of the specimens and maintain a constant holding stress of $\sim$ 4 MPa. To identify all of the key transformation temperatures, samples were subjected to a three step thermal cycle of (i) heating from 30 to 350°C, (ii) cooling from 350 to -196°C and (iii) heating from -196 to 350°C. All steps were conducted at a rate of 30°C min^{-1}.

3.3 Results

3.3.1 Composition of Ti-24Nb (at.%) in the CR and ST conditions

The measured Nb content of the alloy was 24.2 at.%, with O contents of 0.204 and 0.249 at% for the CR and ST condition samples respectively. These results indicated that minimal additional oxygen was picked up during the solution treatment. As mentioned in section 1.5.2,

previous studies have shown that an increase in oxygen concentration suppresses the M_s temperature on the order of 160°C per at.% of oxygen present [82]. As such, in the present work, a variation of only $\sim$ 7°C in M_s would be expected between samples in the two conditions based upon their measured compositional differences.

3.3.2 Initial condition of Ti-24Nb (at.%) in the CR condition

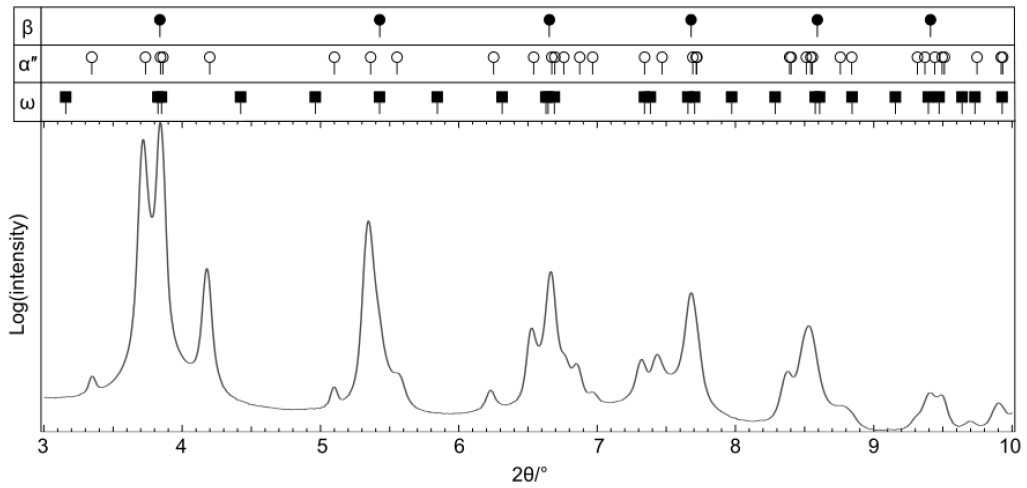

Fig. 3.1 Synchrotron XRD pattern of the Ti-24Nb (at.%) alloy in the initial cold rolled condition at room temperature.

A one-dimensional diffraction pattern from the initial CR state, obtained by integrating around the full two-dimensional Debye-Scherrer rings, is shown in figure 3.1. The diffraction pattern contained a number of well defined, albeit rather broad peaks, consistent with the deformed nature of the sample. Pawley analysis, performed in Topas Academic, indicated that the CR material contained both the β and α'' phases, with the corresponding peak positions indicated by the markers above the data. Metastable β Ti alloys are also well known to form the athermal ω phase during cooling [83, 84] and, therefore, the expected locations of the ω reflections have also been included. It should be noted that many of the ω and α'' reflections have very similar interplanar spacings and, as such, ascertaining whether or not a small fraction of the ω phase is also present in the CR material is challenging. Consequently, additional data was acquired from the initial CR condition material using transmission electron microscopy. A selected area diffraction pattern from this material, taken within a β region

along $[113]_\beta$, is shown in figure 3.2. Alongside the β reflections, additional signals were observed at $\frac{1}{3}$ and $\frac{2}{3}$ of the $< 112 >_\beta$, which is typical of the ω phase. For clarity, a key diagram with the $< 112 >_\beta$ demarked by dashed lines is inset to the diffraction pattern. The presence of these additional reflections provides direct evidence of the presence of the phase in the CR material, however, the intensity of these reflections was too weak to produce a satisfactory dark field image.

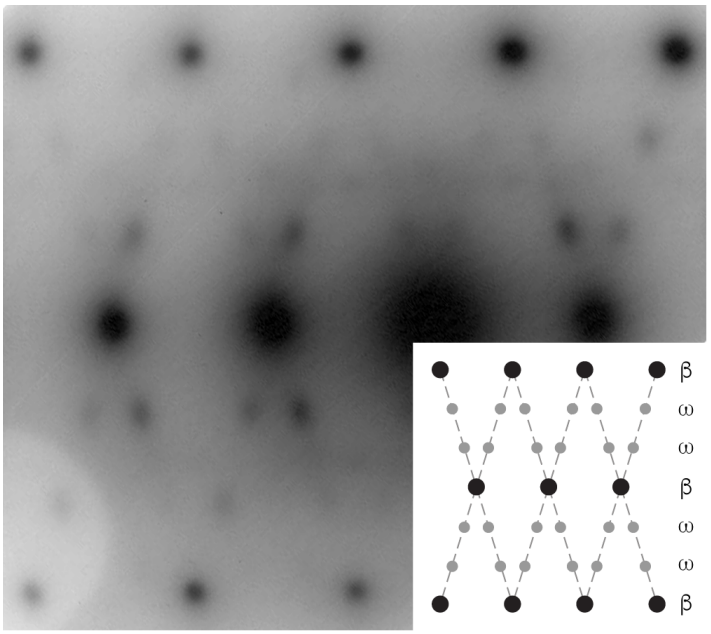

Fig. 3.2 Selected area electron diffraction pattern and associated key diagram of the cold rolled condition material prior to testing, taken from a region of β phase and showing clear evidence of the presence of the ω phase. The dashed lines indicate the $< 112 >_\beta$.

3.3.3 The influence of changes in temperature on the Ti-24Nb (at.%) in the CR condition

To study the influence of changes in temperature on the stability of the α'' phase, CR material was thermally cycled from room temperature to 350°C, cooled to -196°C and then reheated to 350°C at a rate of 30°C min^{-1} whilst diffraction data were recorded. Full ring integrated diffraction patterns from the key points in this thermal cycle are shown in figure 3.3. Upon heating to 350°C it can be seen that the α'' martensite had undergone a complete reverse transformation to the parent β phase. In addition to the β reflections, a few extremely small

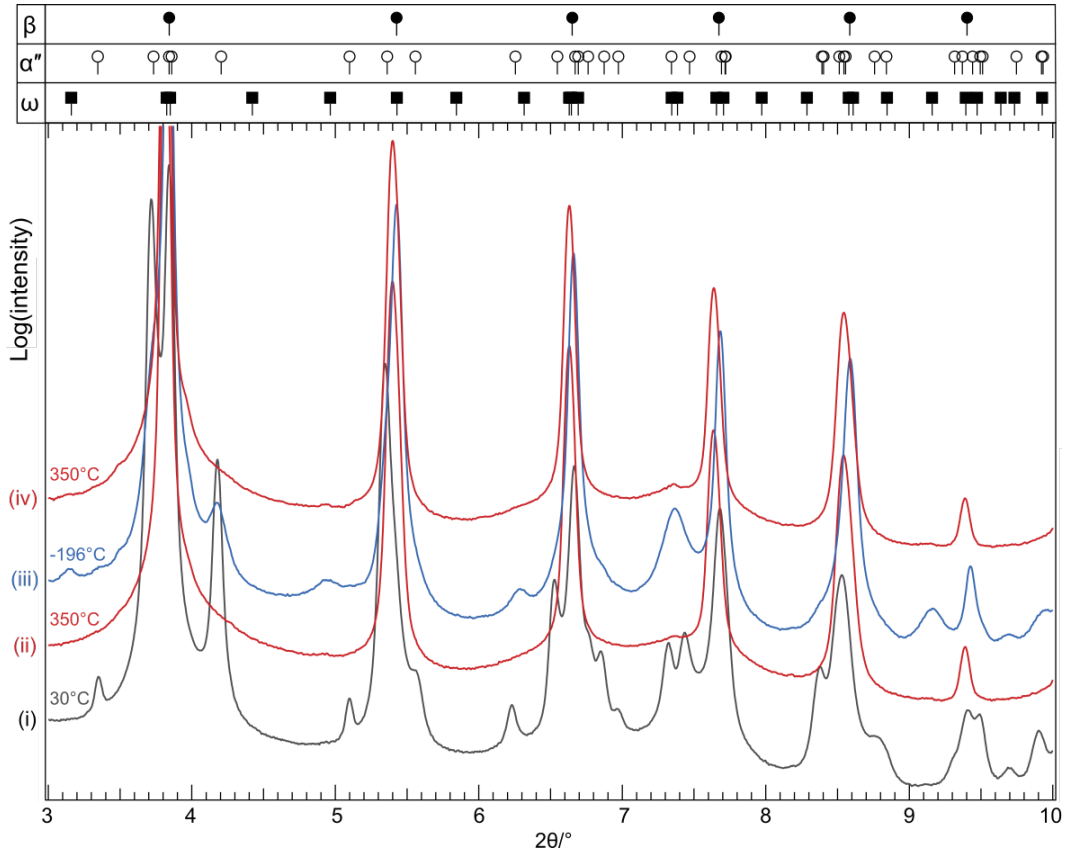

Fig. 3.3 Synchrotron XRD patterns for the Ti-24Nb (at.%) alloy in (i) the initial cold rolled condition at room temperature, and after subsequent (ii) heating to 350°C, (iii) cooling to -196°C, and (iv) reheating to 350°C. The initial broad α'' reflections are absent in both diffraction patterns that were collected at 350°C where sharper β and small ω reflections are present.

and broad peaks were observed in the diffraction pattern, some of which were in positions that uniquely corresponded to the ω phase (e.g. ~ 4.9 and $\sim 9.2^\circ$ 2θ), indicating that, at 350°C, the material consisted of β and ω phases only. Clear evidence of thermally induced transformations could be seen in the diffraction pattern acquired at -196°C, with a number of reflections corresponding to the α'' and ω phases exhibiting increased intensity. Upon reheating to 350°C all of the peaks corresponding to the α'' phase disappeared, consistent with the reverse α'' to β transformation observed during the initial heating. Again, as with the initial 350°C diffraction pattern, some additional small and broad peaks could be observed alongside the β reflections, which were consistent with the ω phase. The observation of these reversible transformations occurring during thermal cycling is in agreement with many literature studies [12, 62, 83, 84] but contradict the results of a more recent *in situ* diffraction study of an almost identical alloy, where no evidence of the β to transformation was observed upon cooling to approximately -170°C [78].

To provide a more detailed characterisation of the evolution of the α'' phase as a function of temperature, the changes in the $(021)_{\alpha''}$ peak, which is located at $\sim 4.2^\circ$ 2θ and is unique to the α'' phase, were assessed using a sequential fitting routine. The evolution of the fitted $(021)_{\alpha''}$ peak area, normalised to that obtained in the initial CR condition, is shown in figure 3.4 alongside the changes in temperature. For clarity both of these parameters have been plotted as a function of time. In addition, to aid comprehension, small inserts showing the diffraction signal in the range of 4.1 to 4.3° 2θ at key points in the thermal cycle have been included. Upon heating, the intensity of the $(021)_{\alpha''}$ was observed to monotonically decrease. However, this decrease in intensity was non-linear and the peak was indistinguishable above background at a temperature of $\sim$ 265°C. No other reflections, uniquely attributable to the α'' phase, were observed above this temperature and so it is believed that this temperature corresponds to the completion of the α'' to β transformation. This temperature is considerably higher, $\sim$ 120°C, than values previously reported in the literature [11, 19, 20, 41, 58].

Upon cooling, the $(021)_{\alpha''}$ became apparent at a temperature of $\sim$ 190°C and increased in intensity, again in a non-linear manner, as temperature decreased. As with the heating cycle, the onset of the β to α'' transformation observed here occurred at a considerably higher temperature, $\sim$ 100°C, than literature would suggest. It is interesting to note that the

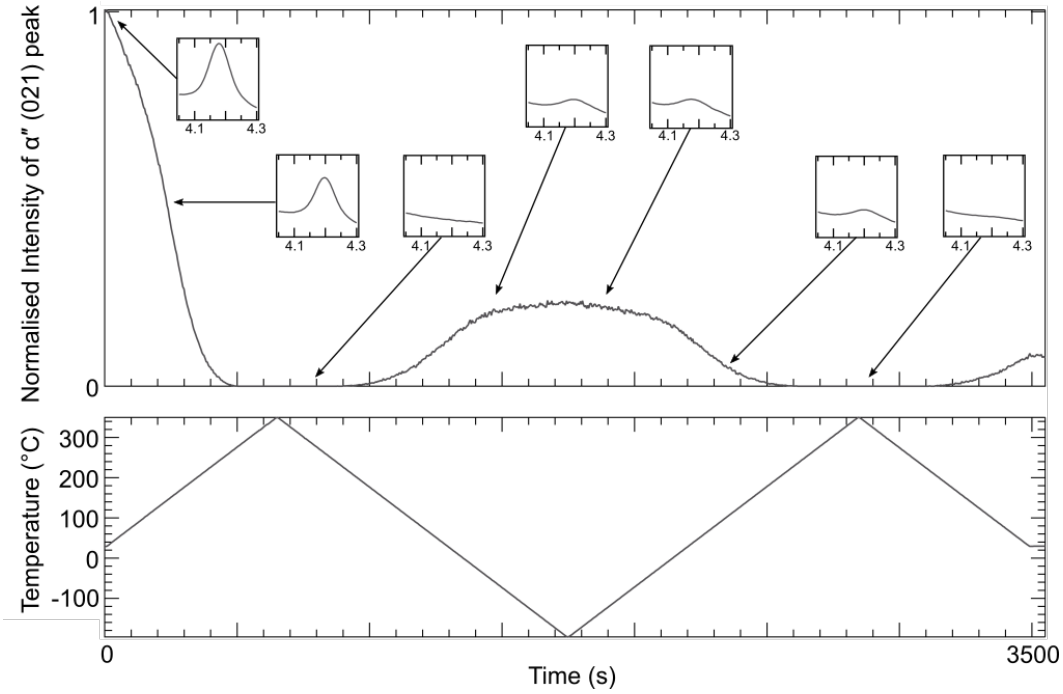

Fig. 3.4 Normalised peak area of the $(021)_{\alpha''}$ reflection as a function of time, plotted with respect to the accompanying temperature change for Ti-24Nb (at.%) in the cold rolled condition. The area beneath the peak reduces in intensity with increasing temperature until the peak becomes indistinguishable from the background above $\sim$ 265°C. Upon cooling, the peak area increases between $\sim$ 190°C and $\sim$ 60°C where the area curve plateaus upon further cooling. Upon reheating, the peak area decreases when the temperature increases above $\sim$ -40°C, becoming indistinguishable above the background above $\sim$ 200°C.

evolution of the $(021)_{\alpha''}$ intensity with temperature reached a plateau like region at -60°C. At temperatures below this point, the intensity of the $(021)_{\alpha''}$ did not change significantly and the magnitude of this intensity is significantly lower than that in initial CR condition. The observation of a plateau region is surprising, as this is not in line with conventional understanding of thermally driven martensite formation, where the transformation would be expected to proceed towards completion as temperature is reduced (see references [62, 85] for comparable *in situ* diffraction data). As such, the existence of a plateau in the cooling data would suggest that the driving force provided by lowering the temperature below -60°C was insufficient to further progress the β to α'' transformation.

When reheating to 350°C from -196°C, the intensity of the $(021)_{\alpha''}$ remained near constant, continuing the plateau region, until a temperature of $\sim$ -40°C was reached. At this point, the intensity of the $(021)_{\alpha''}$ began to decrease with increasing temperature, in a manner very similar to that of the increase observed during cooling. The temperature at which the $(021)_{\alpha''}$ reflection became indistinguishable from the background was found to be $\sim$ 200°C, which is lower than that observed on the initial heating and closer to corresponding values from the literature.

3.3.4 Initial condition of Ti-24Nb (at.%) in the ST condition

When working with metastable β Ti alloys, it is often common practice to subject cold-worked material to a brief solution heat treatment in the β phase field [29, 69, 70]. To examine whether such a thermal treatment has an effect on the β to α'' transformation some of the cold rolled material was heat treated at 900°C for 5 minutes, followed by a water quench inside a sealed tube. This exposure period is shorter than many of those used in previous studies but was chosen to limit grain growth and, therefore, maintain good diffraction counting statistics. A secondary electron image of the material following the solution heat treatment is shown in figure 3.5. An approximately equiaxed β grain structure was observed with an average grain size of $\sim$ 30 μm. Within all of the β grains parallel linear features could be seen, typical of a partial martensitic transformation. Since the solution heat treatment temperature is well above the observed thermal stability limit of the α'' phase, these features must have formed during

cooling. This would be consistent with the data presented in figure 3.4, which suggested that the β to α'' transformation began at a temperature of $\sim$ 190°C.

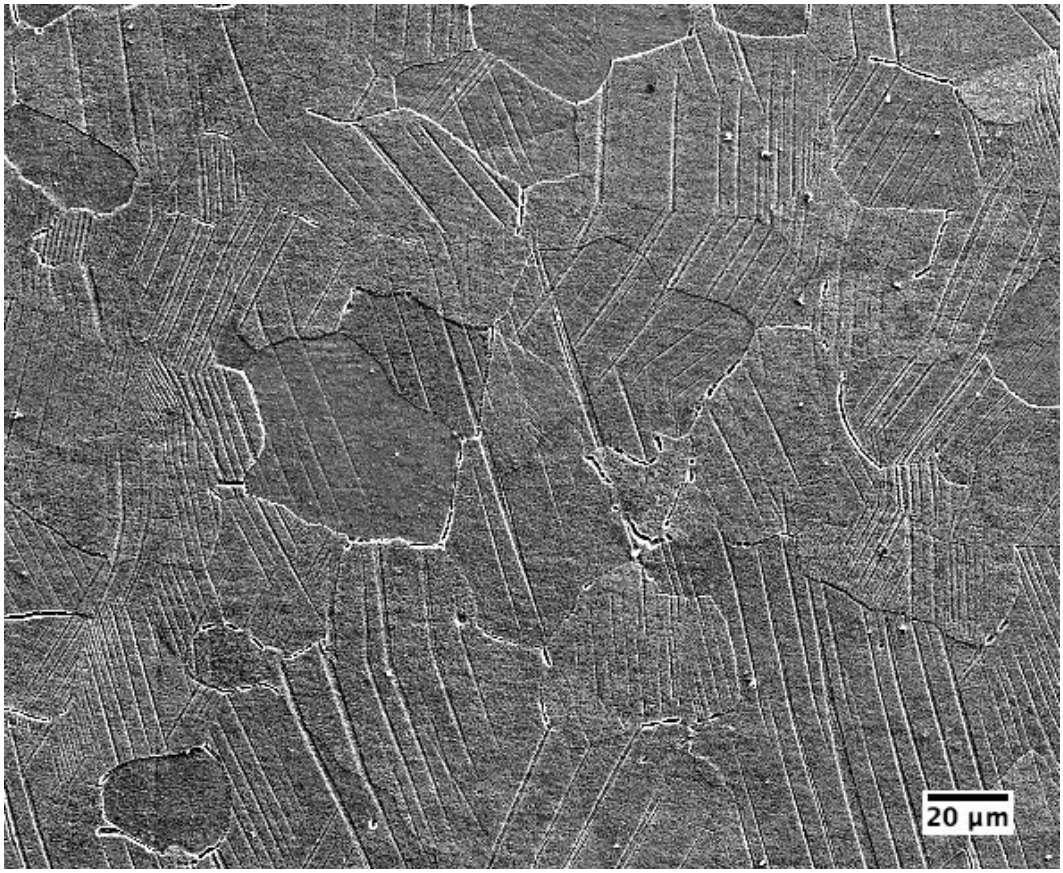

Fig. 3.5 Reflected light micrograph of as-quenched Ti-24Nb (at.%) in the solution treated condition, where α'' laths are visible within β grains.

A diffraction pattern obtained from the ST condition at room temperature is shown in figure 3.6. Strong peaks that corresponded to the β phase were clearly evident along with reflections that were consistent with α'' phase. Such an observation is in agreement with the microstructural features shown in figure 3.5. In addition, very small peaks could also be observed at positions unique to the ω phase, for example 3.1, 4.9 and 9.15° 2θ, suggesting that this phase was also present in the as-quenched ST condition. The presence of the ω phase was confirmed through transmission electron microscopy, where characteristic diffraction intensity was observed at $\frac{1}{3}$ and $\frac{2}{3} < 112 >_\beta$, for example in the $[110]_\beta$ diffraction pattern shown in figure 3.7.

To examine whether exposure to high temperature altered the transformation behaviour of the alloy, the ST material was subjected to the same thermal cycle as the CR condition material

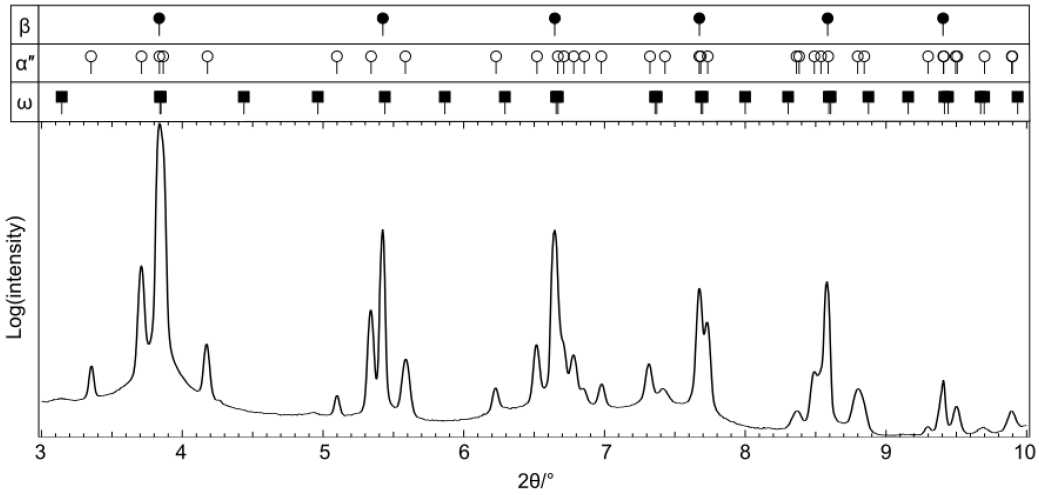

Fig. 3.6 Synchrotron XRD pattern of the Ti-24Nb (at.%) alloy in the initial solution treated condition at room temperature. Sharp β and α'' reflections and some broader peaks that could provide evidence for the ω phase.

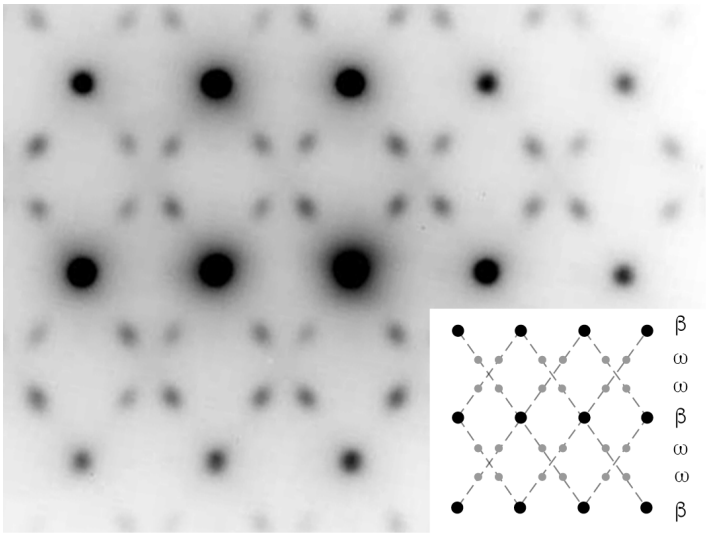

Fig. 3.7 Selected area electron diffraction pattern and associated key diagram of the solution heat treated condition material prior to testing, confirming the presence of the ω phase. The dashed lines indicate the $< 112 >_{\beta}$.

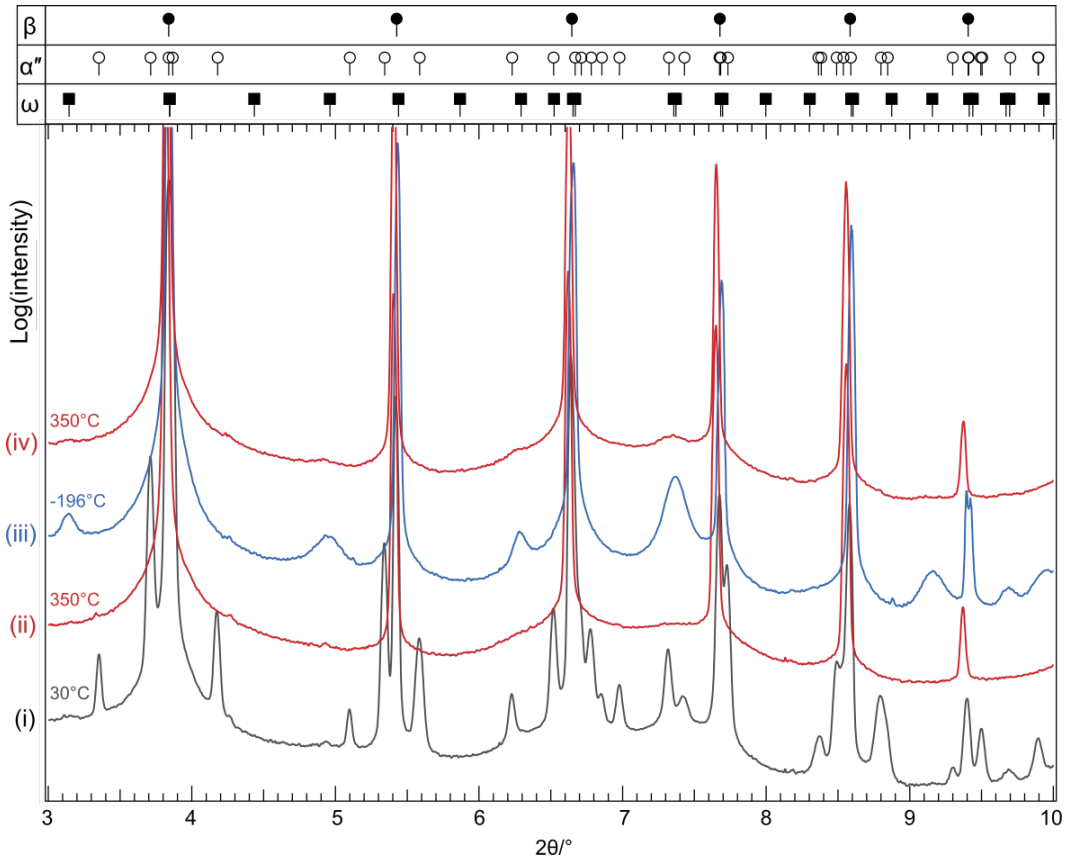

Fig. 3.8 Synchrotron XRD patterns for the Ti-24Nb (at.%) alloy in the solution treated condition in the (i) initial state at room temperature, and after subsequent (ii) heating to 350°C, (iii) cooling to -196°C, and (iv) reheating to 350°C. The initial sharp α'' reflections are absent in both diffraction patterns that were collected at 350°C where the sharp β and small ω reflections remain. Broad reflections corresponding to the ω phase are identified in the pattern at -196°C, whilst no evidence for the α'' is observed.

(30→350→-196→350°C with heating and cooling at rate of 30°C min^{-1}). Diffraction patterns, corresponding to the same key temperatures presented in figure 3.3, are shown for the ST condition in figure 3.8. As with the CR material, upon heating to 350°C, the peaks corresponding to the α'' phase were observed to disappear, which indicated that a complete reversion to the β phase had occurred, and, at 350°C, the material consisted of the β and ω phases only. When cooled to -196°C, broad reflections could be observed within the diffraction pattern, in locations consistent with the ω phase. However, no reflections were observed at locations that were unique to the α'' phase, suggesting that the β to α'' transformation had not occurred during cooling. This observation is in direct contrast to that observed above for the same material in the CR condition, where a β to α'' transformation did occur on cooling. However, it is consistent with the results recently presented in reference [37], where no thermally induced transformation to α'' was observed in a similar alloy following a heat treatment of 30 minutes at 900°C. Upon heating to 350°C, the ω peaks were observed to decrease in intensity but were still clearly visible above the background following heating.

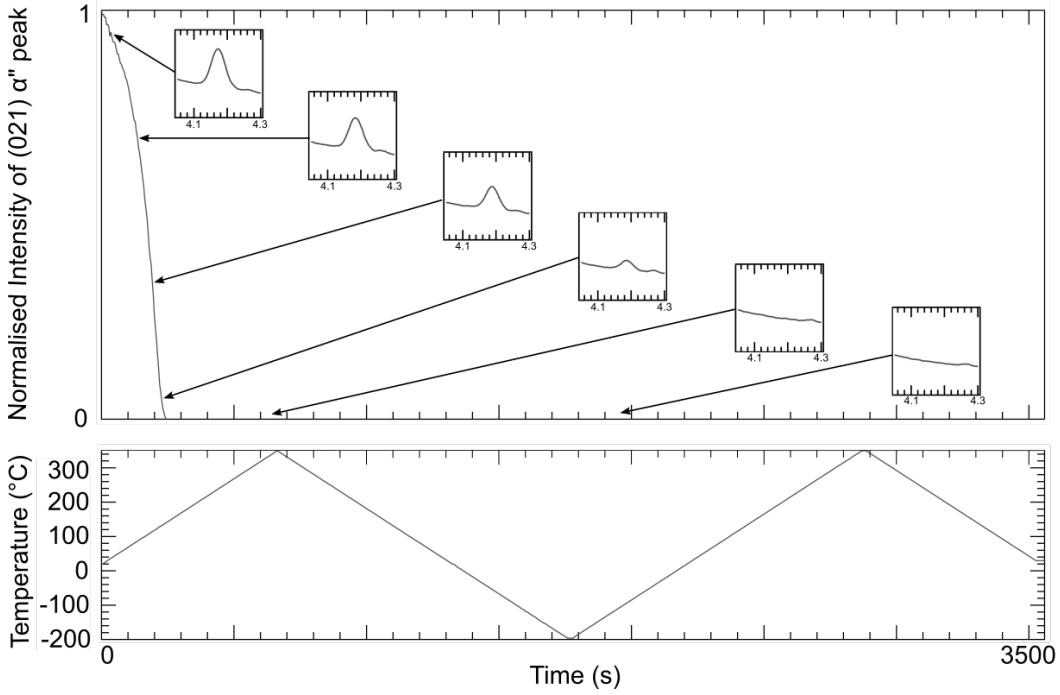

Fig. 3.9 Peak area beneath the $(021)_{\alpha''}$ reflection as a function of time, plotted with respect to the accompanying temperature change for Ti-24Nb (at.%) in the solution treated condition. The area beneath the peak is shown to reduce in intensity with increasing temperature until the peak becomes indistinguishable from the background level above $\sim$ 130°C. No further evidence of the $(021)_{\alpha''}$ was observed during this thermal cycle.

To provide a direct comparison with the CR condition data, the evolution of the $(021)_{\alpha''}$ peak was analysed throughout the entire thermal cycle. The change in normalised intensity of this peak, as a function of time is shown in figure 3.9, alongside the corresponding changes in temperature. Upon heating, the α'' present in the initial ST condition rapidly decreased and became indistinguishable above background levels at a temperature of ~ 130°C. Following this point in the thermal cycle, no evidence of the $(021)_{\alpha''}$ peak above background levels was observed again, nor was any other reflection observed that was consistent with the presence of the α'' phase.

3.4 Discussion

These results conclusively show that the microstructural condition can have a pronounced effect of the β to α'' transformation. In the present work, the α'' phase in the CR condition was found to persist to higher temperatures than the martensite present in the ST condition when heated under identical conditions. Similarly, when cooling at a constant rate from a martensite free condition, the CR material was found to form α'', whereas the ST condition material did not. Since, there is no appreciable compositional difference between the material in these two conditions, these differences in behaviour must be related to microstructural features. Potential differences between the two material conditions and, therefore, possible sources for this effect, include the size and texture of the parent β grains, the presence of the ω phase and the dislocation density in the material.

There have been a number of studies that have commented on the influence of β grain size on the stability of the martensite phase. However, no clear consensus on its effect has yet been reached, as opposing results have been reported from studies using different commercial metastable β alloys [86–89]. For example, work studying Ti-10V-2Fe-3Al (wt%) reported that a larger grain size increased the stability of the β phase with respect to the α'' martensite [87]. Conversely, smaller grains were found to suppress the martensitic transformation in Beta-Cez [86]. In the present work, the highly deformed nature of the CR condition made it very difficult to ascertain the initial grain size and so no further meaningful or conclusive comment can be made about its effect.

Additionally, it is noted that the texture of the β phase in the CR and ST samples is expected to have an effect on the amount of α'' phase. For example, if a given texture favours the formation of a martensitic lath, a higher amount of α'' might be expected. To investigate the effect of texture on the transformation behaviour in these alloys, both the CR and ST samples were prepared for electron back scattered detection (EBSD) analysis. For EBSD imaging the sample must be polished to a mirror finish and should be as flat as possible. This posed a significant problem because polishing Ti-24Nb samples to a sufficient level introduced significiant residual surface stresses. Upon subsequent heat treatment to 350°C, these residual stresses relaxed and the samples began to bend. The amount of curvature that was observed in the final sample was too large to obtain an EBSD image that would give the texture information of each sample. Hence, it was difficult to obtain information that enabled the effects of texture to be determined.

The ω phase has been reported to compete with the formation of the α'' phase in TiNb binary alloys [90]. As such, its presence would be expected to impede the $\beta \rightarrow \alpha''$ transformation, thereby suppressing the M_s temperature. Therefore, it is critical to characterise the initial microstructural condition of a material to a level sufficient to ascertain whether the ω phase is present or not. In the current study, the ω phase was observed in the initial conditions for both the CR and ST specimens. Furthermore, both microstructural conditions retained this phase during the first heating section heating of the thermal cycle (to 350°C), meaning that the subsequent cooling section of the thermal cycle started from material with identical phase constitutions, β+ω. As such, the variation in the occurrence of a $\beta \rightarrow \alpha''$ transformation cannot simply be attributed to the presence or lack of the ω phase.

Dislocation density is also known to influence the transformation behaviour of superelastic Ti alloys. For example, the Gum metals are reported to require cold work in order to exhibit their unique combination of properties [69, 70]. Cold work has been shown to produce local regions of significant misorientation within the microstructure as well as dislocations, which results in a considerable amount of residual strain in the material [70, 91]. It is believed that these defects and the residual strain aid the β to α'' transformation, rationalising the proposed requirement for cold work [92]. Similar results have been obtained through cyclic superelastic loading studies, which have shown that an increase in the concentration of lattice defects

increases the stability of the α'', enabling it to form at lower applied stresses [93, 94]. As such, these results suggest that materials with a greater density of dislocations would be more susceptible to the β to α'' transformation than those with fewer defects.

These previous findings give credence to the suggestion that microstructural condition influences transformation behaviour and, hence, the greater stability of the α'' phase in the CR material when compared to the ST material. However, there remain other features in the dataset that cannot be explained by existing transformation theories, which, therefore, necessitate further discussion. Following quenching from a solution heat treatment temperature in the β phase field, the ST condition material contained α''. This suggests that β to α'' transformation line lies above room temperature. Upon heating, the martensite was observed to revert back to the parent β phase at a temperature of $\sim$ 130°C. However, when subsequently cooled at a rate of 30°C min^{-1}, no α'' phase was observed. Similar behaviour has also been reported in references [77, 95, 96] but not discussed in detail. The major difference between the quenched and the heat and cooled state is the cooling rate experienced by the material. Consequently, it is believed that the formation of the α'' during quenching is a result of stresses relating to the cooling rate rather than intersecting a transformation temperature uniquely determined by composition.

The second key feature that requires discussion can be observed in the evolution of the $(021)_{\alpha''}$ in the CR material during cooling. The martensite phase was first observed at a temperature of $\sim$ 190°C and the intensity of the $(021)_{\alpha''}$ increased as the temperature was reduced. At a temperature of $\sim$ -40°C the increase in $(021)_{\alpha''}$ intensity began to slow, reaching an approximate constant magnitude at temperatures below $\sim$ -60°C. This might be expected if the β to α'' transformation was reaching completion, see references [97] and [98] for similar data in Ni-Ti based shape memory alloys. However, as can be seen in figure 3.3, β reflections were present throughout cooling and this phase remained dominant at all times. Therefore, the occurrence of the plateau region cannot be the result of the transformation reaching completion and the cessation of α'' evolution with decreasing temperature must be related to another factor, which is inconsistent with current descriptions of thermally driven martensitic transformations.

The absence of a thermally driven transformation in the ST material, despite cooling to -196°C, indicates that M_s must lie below this temperature and suggests that the Gibbs energy curves for β and α'' phases have not intersected. Consequently, the observation of the transformation at $\sim$ 190°C in the CR material indicates that microstructural factors must have a far greater influence on the relative positions of the Gibbs energy curves than temperature. One possibility, which could rationalise all of the results presented here and also explain the variations in transformation behaviour reported in the literature, would be that the β to α'' transformation occurs once a critical stress level, for a given temperature, has been reached. This critical stress is not simply associated with an applied load, but is the total stress within a material, which can have multiple contributions, both internal and external. These can include stresses that arise from thermal mismatches between grains or phases (type II stresses), as well as contributions from features within the microstructure, such as dislocations (type III stresses), in addition to any directly applied external stresses (type I stresses). If the sum of these contributions locally exceeds the critical transformation stress, then the Gibbs energy curve of the α'' phase falls below that of the β phase and the β to α'' martensitic transformation becomes favourable. The transformation will proceed until the stress reduction that results from the conversion of β to α'' is sufficient to decrease the total stress to a magnitude below the critical stress.

As such, when the CR material was cooled below $\sim$ 190°C the initial microstructural condition contained a sufficient contribution to the total stress to initiate the β to α'' transformation. Further cooling maintained the total stress level in the material above the critical stress for the given temperature, leading to continued transformation. However, at $\sim$ -60°C the total stress level must have fallen below the critical level, as no further increase in intensity was observed, and, as such, the total stress must have remained below the critical level despite further cooling.

Similarly, this hypothesis would also explain why material quenched from the solution heat treatment temperature could contain the α'' phase at room temperature, whilst not reforming this phase when cooled from 350°C at 30°C min^{-1}. Finally, the concept of the stress contribution to the Gibbs energy being responsible for the formation of the α'' phase is also able to rationalise the difference in behaviour between the CR and ST conditions. The

microstructural condition of the CR material, which is likely to have a significantly greater dislocation density, would be expected to result in significantly larger internal stresses (types II and III). Consequently, material in this condition would require a lower level of additional stress to trigger the β to α'' transformation than the ST condition material, consistent with the experimental observations. Thus the idea of the transformation being dependent upon total stress is able to explain the difference in behaviour between the CR and ST conditions, the occurrence of a plateau region in the evolution of the $(021)_{\alpha''}$ peak intensity in CR condition material and, the formation of martensite upon quenching in the ST condition material.

3.5 Conclusion and future work

Within the relevant literature, there are significant discrepancies in the martensite start temperature reported for Ti-Nb alloys, which have not yet been rationalised or explained. This study has explored the reasons for these variation through *in situ* diffraction studies of Ti-24Nb (at.%) in two microstructural conditions, cold rolled and solution heat treated, when subjected to a three step thermal cycle of (i) heating from 30 to 350°C, (ii) cooling from 350 to -196°C and (iii) heating from -196 to 350°C. In their initial states both microstructural conditions contained β, α'' and ω phases at room temperature. Upon heating to 350°C, the α'' phase in both material conditions reverted to the parent β phase, such that the phase constituents at 350°C were β and ω. Upon cooling from this temperature, the α'' phase was observed to reform in cold rolled condition material, starting at a temperature of $\sim$ 190°C. In contrast, no evidence of the β to α'' transformation was observed when the solution heat treated condition material was subjected to an identical cooling process, ending at -196°C. As such, it is clear from these results that M_s for this composition must lie below -196°C and that the microstructural condition of these materials has a significant influence over their transformation behaviour.

In addition to this marked contrast in transformation behaviour, there were additional features in the datasets of both material conditions that require further explanation. One example of this was the cessation of martensite formation in the cold rolled condition material prior to the completion of the cooling segment and whilst the microstructure still primarily consisted of the β phase. Another example was the observation of α'' in the initial microstructure

of the solution heat treated material, which had been quenched, but the subsequent lack of transformation in the same material upon cooling from 350°C. Neither of these observations fit with a conventional view of thermally driven martensite formation.

Instead, it is proposed that the martensitic transformation in this alloy occurs once a critical total stress has been reached at a given temperature. The total stress in a material will incorporate contributions from many different sources, including internal microstructurally related factors as well as any externally applied forces (e.g. type I, II and III stresses). This concept is able to rationalise all of the behaviours observed in the current study and is also likely to account for the variations observed in the previous literature. However, it is recognised that further studies are required to validate the hypothesis.

To further validate this hypothesis, the stress-strain behaviour of this material in both microstructural conditions must be investigated under the application of an external load, which would consider the additional effect of type I stresses on the transformation behaviour. Direct measurements for the phase constitution of the material that has been exposed to different thermal and stress conditions has been shown to be much more accurate in identifying a value for the transformation temperatures, when compared with the use of indirect techniques such as DSC or resistivity measurements. Furthermore, these datasets that show the phase evolutions as a function of temperature and an externally applied load can then be used to provide direct explanations for the stress-strain curves that have been recorded at room temperature here, and at additional testing temperatures previously reported in the literature.

Chapter 4

The effect of microstructural condition on the superelastic behaviour in Ti-24Nb (at.%)

4.1 Introduction

Previously, in Chapter 3, the effect of microstructural condition on the M_s temperature for a Ti-24Nb alloy was investigated and a marked difference in the transformation behaviour was observed. No thermally driven $\beta \rightarrow \alpha''$ transformation was observed on cooling a solution treated sample to -196°C, whilst the M_s temperature for the same alloy in the cold rolled condition was observed to be 190°C. This difference in behaviour, between two samples with the same Nb content and a difference in oxygen content of < 0.045 at.%, could not be accounted for using the known composition effects on M_s reported in chapter 3. Thus, the underlying reason for this variation in behaviour must have been a consequence of a microstructural difference. Previous studies have shown that the presence of the omega phase can interfere with the $\beta \rightarrow \alpha''$ transformation [90, 99, 100] and can have a detrimental effect upon the superelastic properties of Ti-Nb alloys [14, 101]. However, small quantities of athermal ω have been shown to have little effect upon the $\beta \rightarrow \alpha''$ transformation [46, 102], with one study reporting that the cold rolling ratio had a larger influence on the deformation behaviour [102]. In chapter 3, the initial microstructures of both microstructural conditions

were shown to contain similar amounts of the ω phase. Consequently, it was concluded that the higher dislocation density and thus, greater initial internal stress state of the cold rolled sample enabled the $\beta \rightarrow \alpha''$ transformation upon cooling. In contrast, the lower internal stresses of the solution treated material never reached a sufficient level to initiate the transformation despite cooling to -196°C. As such, it was proposed that the $\beta \rightarrow \alpha''$ transformation was driven by stress rather than reaching a single compositionally dependent temperature.

This theory is in its infancy, and requires further validation, especially with respect to the material's transformation behaviour when subjected to an externally applied load over a range of temperatures. Therefore, here we perform *in situ* synchrotron diffraction measurements on the same Ti-24Nb (at.%) alloy subjected to an elastic load-unload cycle at temperatures between 30 and -196°C. Material was studied in both the cold rolled and solution treated states in order to directly compare the effect of microstructural condition, and therefore, internal stress on the $\beta \rightarrow \alpha''$ transformation.

4.2 Methods

Tensile specimens, with gauge dimensions of $14 \times 0.56 \times 0.52$ mm, were cut aligned with the rolling direction using electro discharge machining and the resulting re-cast layer was removed by mechanical grinding and polishing. All mechanical polishing was conducted prior to any heat treatments being conducted to ensure that no α'' was induced through preparation techniques. As shown in chapter 3, stresses as low as a few MPa can induce the $\beta \rightarrow \alpha''$ transformation in the CR sample. As a result of this, all samples were heated to 350°C to remove any mechanically-induced α'' prior to further investigations into the effect of changes in temperature and stress on the transformation behaviour. Like in chapter 3, the CR sample was cut directly from the strip, heated to 350°C and then tested, and the ST sample was additionally subjected to a heat treatment at 900°C for 5 minutes followed by a water quench, and the same heat to 350°C. *In situ* synchrotron XRD data were obtained using the I11 beamline at the ESRF and diffraction patterns were acquired as a function of temperature and applied stress, to provide direct evidence of the phases present in the sample.

One dimensional diffraction patterns were generated by azimuthally integrating firstly around the full 360°20°, and then in segments using the Fit2D software [79] for further analysis. The Linkam TST350 stage was used to apply a sequence of thermomechanical cycles to the specimen, using a heating and cooling rate of 0.5°C s^{-1} (30°C min^{-1}) and a crosshead movement rate of 1 μm s^{-1}. The same slow heating/cooling rate was used in this study as in chapter 3 to avoid inducing the $\beta \rightarrow \alpha''$ transformation that had been observed in the samples cooled at higher quench rates. Each individual thermomechanical cycle involved the 4 steps of (i) cooling from 350°C to a target temperature, in the range -196 to 30°C (ii) loading the sample at the target temperature to 300 MPa, (iii) unloading the sample at the target temperature and (iv) a final reheat to 350°C. The samples in the CR and ST condition were subjected to this thermomechanical cycle initially at -196°C, followed by further cycles at temperatures -150°C, -100°C, -50°C and 30°C. The sample was then cooled to -175°C and subjected to the thermomechanical cycle at -125°C, -75°C, -25°C and 0°C. This order of temperatures was chosen to highlight any cycling effects that may have occurred in the sample during testing. Whilst the use of the same sample may have introduced effects from the cycling of the material, it was considered more important to sample the same set of grains in the same sample so that the transformation behaviour at different temperatures could be more accurately compared.

4.3 Results

4.3.1 Composition of Ti-24Nb (at.%) in the CR and ST conditions

Compositional analysis of material in the CR and ST conditions was reported in section and indicated a Nb content of 24.2 at.% and O contents of 0.204 and 0.249 at.% respectively. As such, only a minimal amount of additional oxygen was picked up during the solution treatment. Since previous studies have reported a suppression in M_s of 160°C for every at.% of oxygen present [45], the slight elevation in O content would be expected to result in only $\sim$ 7°C variation in M_s between the two conditions.

4.3.2 Initial condition of Ti-24Nb (at.%) in the CR condition

As mentioned in the introduction in section 1.6, it is critically important to characterise the initial phase constitution and microstructural condition of a superelastic alloy prior to testing. Figure 4.1a shows a one-dimensional diffraction pattern for the sample in the CR condition after being heated to 350°C, which was obtained by azimuthally integrating around the full 360° of the two dimensional diffraction pattern. Pawley analysis, performed in Topas Academic, indicated that the CR sample contained both the β and α'' phases. Peaks corresponding to the ω phase were not easy to distinguish in this dataset as a result of the broad peak profiles that were a consequence of the high level of plastic deformation. Consequently, ascertaining whether or not a small fraction of the ω phase was also present was challenging. However, in section 3.3 electron diffraction patterns acquired from the same material has conclusively shown its presence in the CR state. The macroscopic grain structure of the heated CR material following cooling to room temperature is shown in figure 4.1b and consisted of elongated β grains aligned to the rolling direction.

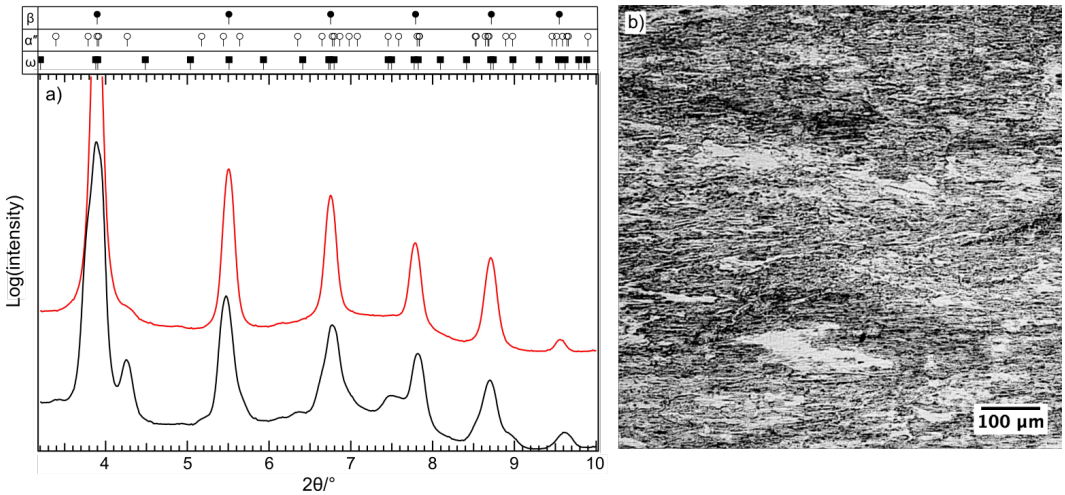

Fig. 4.1 Characterisation of Ti-24Nb (at.%) in the cold rolled condition using a) one dimensional synchrotron diffraction, and b) reflective light microscopy. In a), the initial condition of Ti-24Nb (at.%) directly after cold rolling is shown using the black trace. Diffraction peaks that correspond to the β and α'' are clearly visible. The peak positions that correspond to ω reflections are shown, since they are expected to be in the structure, but may have been masked by the broad β and α'' peaks. The red trace shows the one dimensional diffraction pattern for Ti-24Nb (at.%) in the CR condition at 350°C. The majority of the α'' reflections had disappeared, and a slight remnants of the $(021)_{\alpha''}$ peak at $\sim$ 4.2° 2θ remained. The corresponding optical microstructure for Ti-24Nb (at.%) after the heat and subsequent cool is shown in b), showing elongated grains.

4.3.3 The tensile behaviour of Ti-24Nb (at.%) in the CR condition

The tensile behaviour of Ti-24Nb in the heated CR during a test to failure is shown in figure 4.2. It is generally expected that when a load is applied to a superelastic alloy, the strain response at low stresses follow a linear elastic deformation [33]. However, the stress-strain curve shown in figure 4.2 did not exhibit a linear elastic response at any point. Instead, the gradient of the stress-strain curve changed as soon as an external load was applied. Since the initial microstructure contained both the β and α'' phases, this non-linear behaviour could either be attributed to the detwinning of the initial α'' variants, or the occurrence of a stress-induced $\beta \rightarrow \alpha''$ phase transformation.

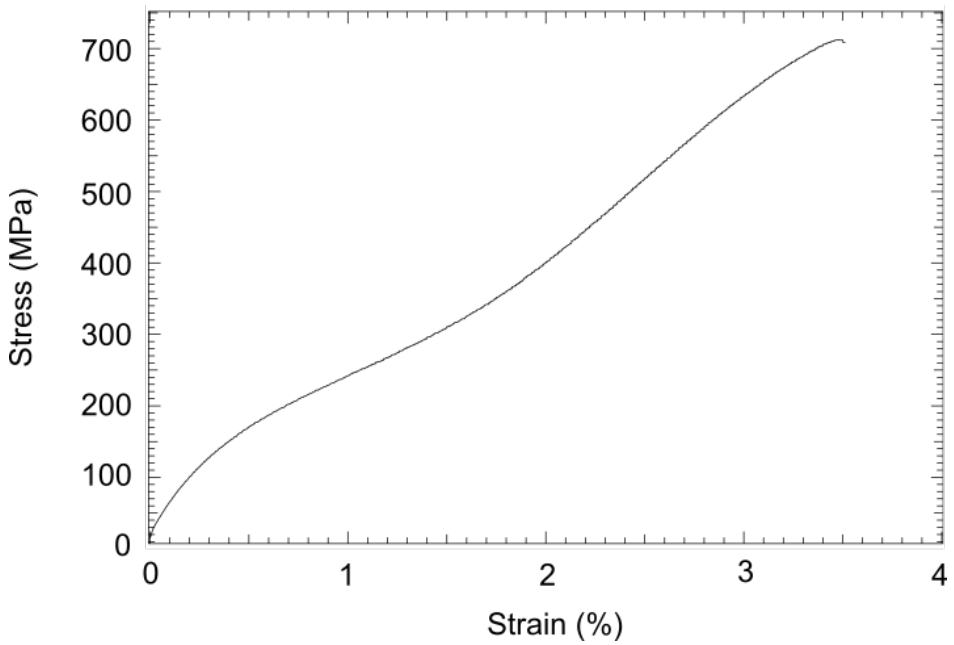

Fig. 4.2 Room temperature stress-strain curve for cold rolled Ti-24Nb (at.%) that had been heated to 350°C and subsequently cooled. No linear elastic region was observed, and the curve began to bend as soon as the load was applied. No ductile region was present for this sample.

To investigate this further, material in the heated CR condition was subjected to an *in situ* thermomechanical cycle with a target temperature of 30°C. One dimensional diffraction data was analysed from an integrated segment centred around an azimuthal angle 20° from the loading axis, as previous work, for example reference [94, 103], has shown that the α'' reflections form in distinct positions during loading experiments. The evolution of the α'' phase as a function of temperature and stress was tracked using the intensity of the

$(021)_{\alpha''}$ peak, which is unique to the α'' phase and located at $\sim 4.2°$ 2θ in figure 4.1a. One dimensional diffraction data that shows the $(110)_{\beta}$ and $(021)_{\alpha''}$ reflections at $\sim 3.9°$ and $\sim 4.2°$ 2θ is shown in figure 4.3 at 350°C both before and after the tensile cycle, and at the point of maximum applied stress of 300 MPa during this cycle. The intensity of the $(021)_{\alpha''}$ peak was observed to increase significantly at the point of peak load, and appeared to return to its initial state shown by the indistinguishable diffraction curves measured before and after the tensile cycle at 350°C. As observed in the tick marks at the top of the full diffraction patterns for the same alloy in the initial CR condition in figure 4.1a, the $(021)_{\alpha''}$ peak has a unique value of 2θ and stands alone in the one dimensional diffraction patterns. Hence, the intensity of this α'' peak was chosen, as it was previously shown in section 3.3, to be fitted with a Gaussian function, and then normalised to that of the initial CR condition, and traced as a function of temperature and stress during the thermomechanical cycles mentioned above. Data corresponding to the normalised peak area for the thermomechanical cycle run to a target temperature of 30°C, is shown in figure 4.4, alongside the applied changes to the temperature and stress.

At 350°C, the sample contained a very small amount of the α'' phase and, when cooled, the increase in the intensity of the $(021)_{\alpha''}$ indicated that the material had dropped below M_s and the $\beta \rightarrow \alpha''$ transformation had begun. The area beneath the $(021)_{\alpha''}$ was observed to increase gradually as the temperature was reduced from 350 to 30°C. During a short pause between the end of the cool, and the application of the load, the area appeared to settle at a constant value, indicating that the transformation had not lagged, and had reached an equilibrium with the cooling rate used. Upon the application of a load, which is indicated by the dotted guidelines in figure 4.4, the peak area was observed to increase at a faster rate as soon as the loading began. As such, these data indicate that the critical stress required to drive the $\beta \rightarrow \alpha''$ transformation is < 4 MPa, thus providing an explanation for the lack of a linear elastic region in figure 4.2. In addition, the rate of change of the $(021)_{\alpha''}$ peak area with respect to time was observed to increase with the applied load. Since the stress increased at an approximately constant rate, as can be seen from the lower part of figure 4.4, an increasing fraction of α'' was formed with each additional increment of stress.

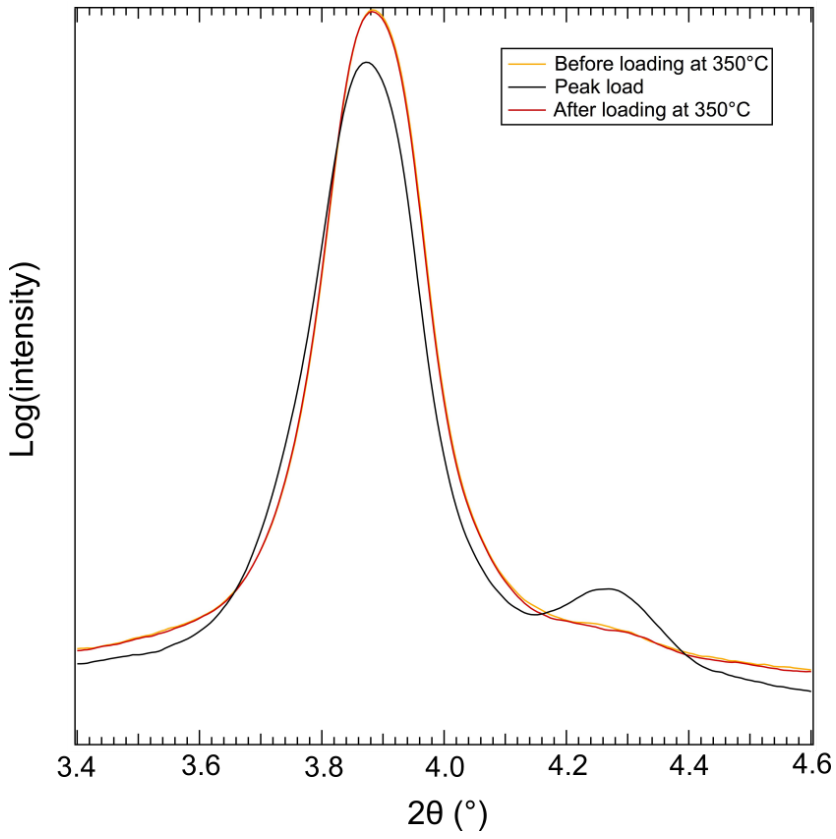

Fig. 4.3 Comparison of the one dimensional diffraction data for Ti-24Nb in the cold rolled condition at 350°C before and after the thermomechanical cycle. No change in the $(110)_{\beta}$ and $(021)_{\alpha''}$ peaks were noticeable.

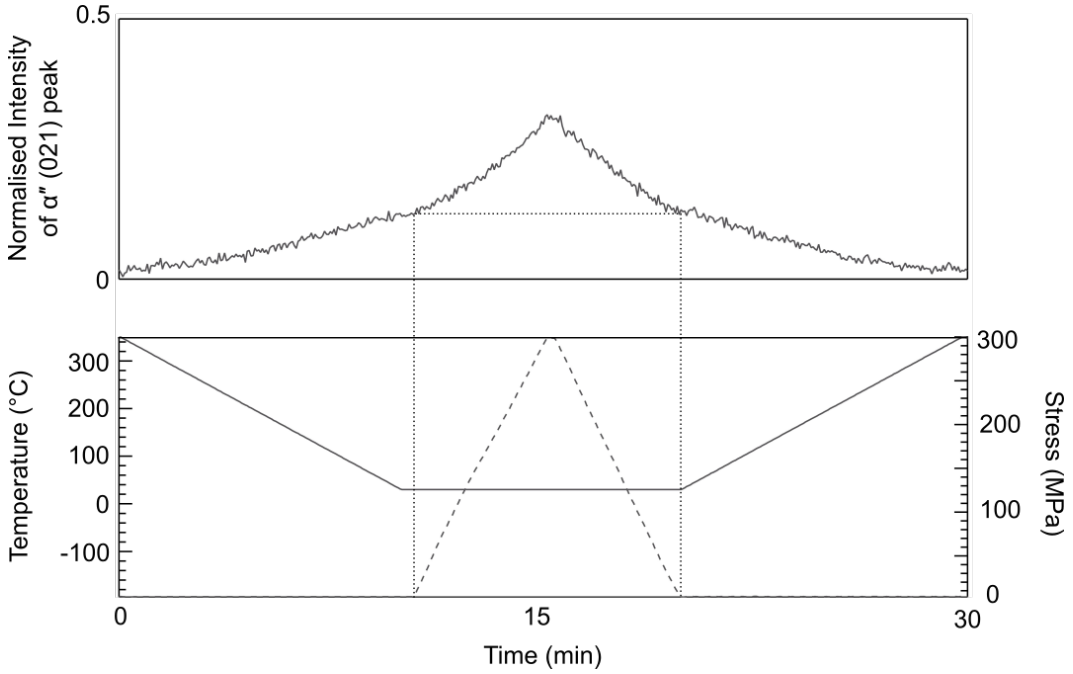

Fig. 4.4 Peak area beneath the $(021)_{\alpha''}$ reflection as a function of time, plotted with respect to the accompanying temperature and applied stress changes for Ti-24Nb (at.%) in the cold rolled condition. The area beneath the peak is shown to increase in intensity with decreasing temperature below $\sim$ 312°C. At 30°C, when the load was applied, the $(021)_{\alpha''}$ peak area began to increase at a faster rate, reaching a maximum at the maximum stress. Upon unloading, the intensity of the $(021)_{\alpha''}$ peak decreased to its original value above $\sim$ 320°C.

More significantly, the reverse behaviour occurred upon the removal of the applied load which is shown by the intensity of the $(021)_{\alpha''}$ peak decreasing as the magnitude of the applied stress was reduced. This indicated that a reverse transformation was occurring with the α'' phase reverting to the parent β phase. Furthermore, upon removal of all of the applied stress, the intensity of the $(021)_{\alpha''}$ peak was found to have the same magnitude as it did prior to loading. This observation suggested that all of the α'' phase, which formed as a result of the macroscopically applied stress, was fully reversible. Such behaviour was intriguing, as it cannot be rationalised by current critical temperature based transformation theories, which imply that when unloaded below M_s, no change in the α'' variants are expected [1, 2]. Upon reheating to 350°C, the $(021)_{\alpha''}$ peak area decreased to a value that was indistinguishable from the background, indicating that the stability limit of the α'' phase had been surpassed.

The data presented in figure 4.4 indicated that a reversible transformation between the β and α'' phases occurred in response to loading and unloading. However, this figure does not provide unambiguous information as to the potential variant reorientation of the α'' phase present prior to loading. And despite the initial amount of the α'' phase present in the sample being small, the potential of a reorientation of these variants contributing to this unusual behaviour should not be assumed not to occur. Had a variant reorientation occurred then it would be expected to be non-reversible and, therefore, would likely lead to change in the $(021)_{\alpha''}$ intensity following unloading in addition to a residual lattice strain. To elucidate this point, the applied macroscopic stress as a function of lattice strain (equation 4.1) for the $(110)_{\beta}$ reflection, analysed from an azimuthal segment centred on the tensile axis is shown in figure 4.5.

$$\text{Lattice strain} = \frac{\left[\frac{1}{\sin\theta} - \frac{1}{\sin\theta_0}\right]}{\frac{1}{\sin\theta_0}} \tag{4.1}$$

Again, there was no evidence of a linear elastic region in this dataset, rather a curved response typical of a stress induced transformation [92, 104, 105]. Critically, upon unloading, the lattice strain followed the same path as on loading, returning to the same condition as prior to testing. Consequently, no residual lattice strain was observed, indicating that reorientation of the initial α'' variants had not occurred and that the non-linear stress strain behaviour was entirely related to the reversible $\beta \leftrightarrow \alpha''$ transformation.

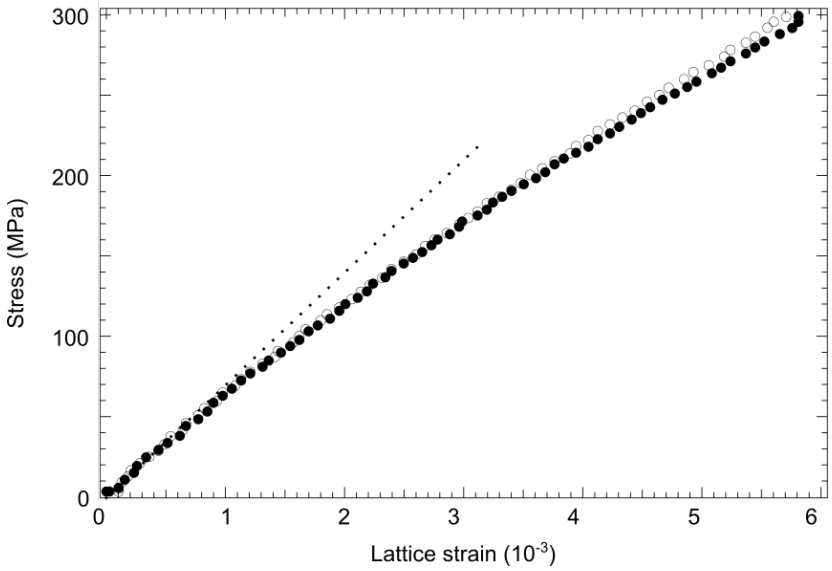

Fig. 4.5 Plot of the applied stress versus the β lattice strain of the $\{110\}_\beta$ interplanar spacings for Ti-24Nb (at.%) in the CR condition that had been heated to 350°C. A non-linear elastic deformation behaviour was seen.

4.3.4 The effect of temperature on the $\beta \rightarrow \alpha''$ transformation

To provide more insight into the stress-induced transformation behaviour of Ti-24Nb in the CR condition over a range of temperatures, the same sample was subjected to the same stress cycle between -196°C and -50°C. The corresponding data is presented in figure 4.6, which shows the changes in the fitted $(021)_{\alpha''}$ peak area, normalised to that of the initial CR condition. In all cases, the martensite peak increases in intensity as the temperature is reduced. However, as observed in section 3.3 in figure 3.4, the intensity of this reflection reached a maximum value prior to the cooling segment being complated. This suggested that the transformation had ceased prior to reaching completion, despite further reductions in temperature. The temperature at which the cessation occurred was found to be the same for all of the cooling segments with a magnitude $\sim$ -30°C, as shown in figure 4.7. Upon the application of external load, the area of the $(021)_{\alpha''}$ reflection was observed to instantly and rapidly increase at all temperatures, to a maximum that corresponded to the maximum applied load. As the applied load was removed, the area of the $(021)_{\alpha''}$ reflection decreased indicating a reversion of the α'' phase to the parent β had occurred. The reversion of the α'' phase formed under applied load was found to be complete at temperatures above and including -150°C, where the intensity of the $(021)_{\alpha''}$ reflection at the end of the unload segment was

identical to that prior to loading. At -196°C the intensity of $(021)_{\alpha''}$ reflection following unloading was slightly elevated compared to its magnitude prior to loading. In all cases, upon reheating to 350°C, the martensite phase reverts back to its former level. These observations indicate that superelastic behaviour, i.e. the spontaneous formation and reversion of α'' under the application and removal of an applied load, occurred at all of the temperatures studied, a range of 220°C. They also conclusively show that such behaviour can occur even in the presence of a pre-existing martensite formed by cooling, inconsistent with current thermally dominated martensite theory.

4.3.5 Effect of cycling

To identify any cycling effects that may have resulted from the use of the same sample in each thermomechanical cycle, the one dimensional diffraction patterns at 350°C before the cooling segment of all thermomechanical cycles were compared, as shown in figure 4.8. The diffraction patterns are labelled with the target temperature for the cycle that was about to be applied to the sample, for example, the pattern that is labelled with -196°C shows the diffraction pattern for the sample at 350°C before the thermomechanical cycle at -196°C. The four high intensity peaks that are not labelled in figure 4.8 can be attributed to the β phase. The remaining peaks, that corresponded to the α'' and ω phases, are labelled with the sets of planes that contribute to the associated reflection.

As discussed above, the only diffraction peak that could be attributed to the α'' phase alone was observed at $\sim 4.2°$ 2θ. The intensity of this peak was not observed to noticeably change after each thermomechanical cycle, and suggested that the amount of the α'' phase was not significantly effected during the cycles. Similarly, the peaks at $\sim 4.9°$ and $\sim 6.1°$ 2θ, which were indexed as the $(111)_{\omega}$ and $(002)_{\omega}$ peaks, did not noticably change between cycles. However, the peak at $\sim 7.4°$ 2θ, which could correspond to either the $(031)_{\omega}$ and $(132)_{\alpha''}$ peaks, was observed to increase by a significant amount after every cycle. Whilst it is difficult to identify whether this increase occurred as a result of the ω or α'' phase, the different shapes of the equivalent peaks that have been previously observed can be used to postulate. In section 3.3, diffraction patterns for Ti-24Nb in the solution treated condition that had been quenched from 900°C, heated to 350°C, and subsequently cooled to -196°C were

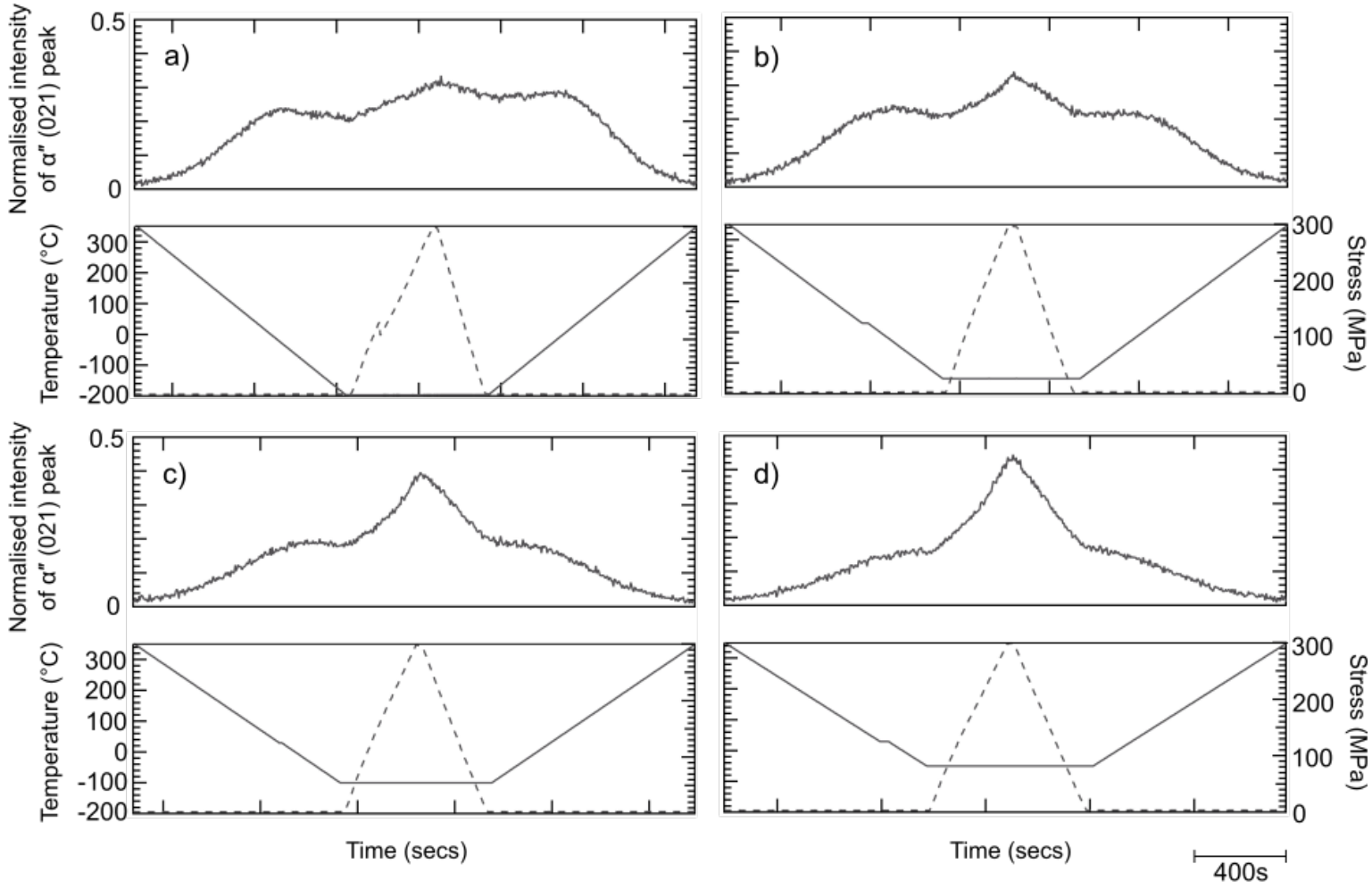

Fig. 4.6 Peak area beneath the $(021)_{\alpha''}$ reflection as a function of time, plotted with respect to the accompanying temperature and applied stress changes for CR Ti-24Nb (at.%) that was subjected to the four step thermomechanical cycle at a) -196°C, b) -150°C, c) -100°C and d) -50°C. In all cases, the peak area increased during cooling, and increased at a faster rate as soon as the external load was applied. Full superelastic recovery was seen at all temperatures, apart from -196°C, where a residual amount of α'' was retained.

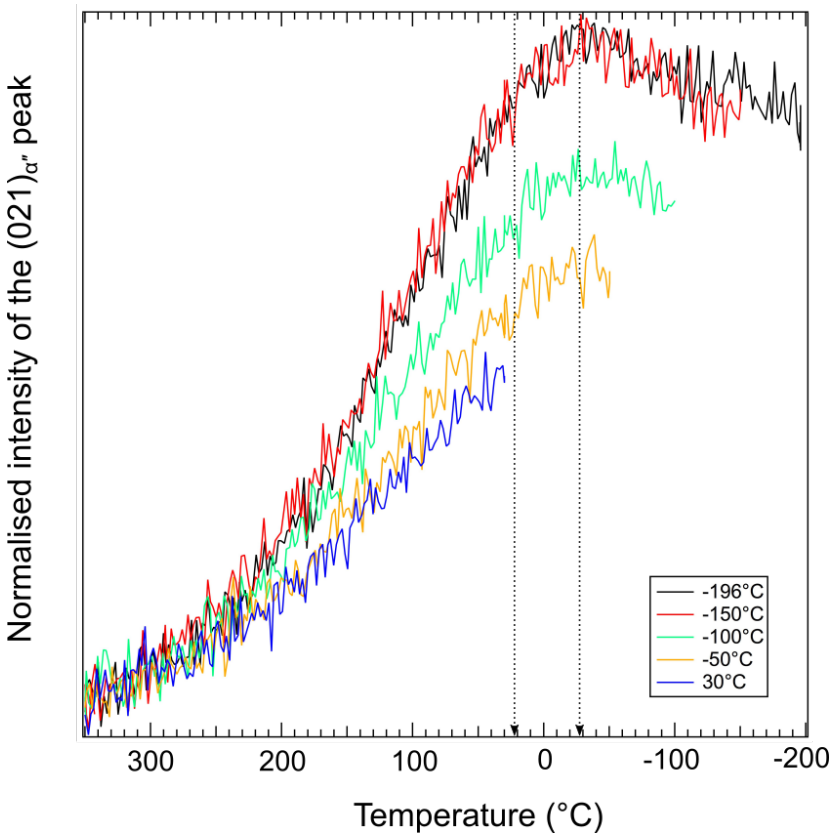

Fig. 4.7 Overlay of the normalised $(021)_{\alpha''}$ peak area for the cooling stages of all of the thermomechanical cycles. The rate of increase in peak area with the reduction of temperature decreased when the temperature was reduced below $\sim$ 20°C, and subsequently stopped increasing when the temperature was reduced below $\sim$ 30°C.

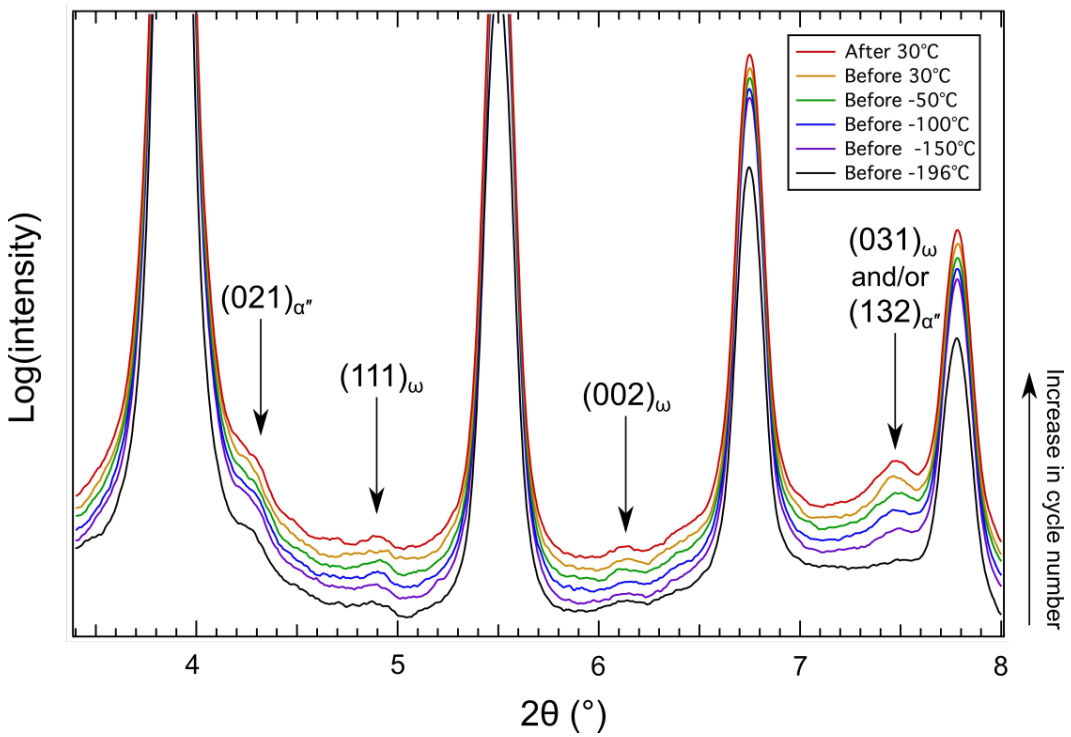

Fig. 4.8 One dimensional diffraction patterns for Ti-24Nb in the CR condition at 350°C before all thermomechanical cycles that were conducted on the same sample. Each trace is labelled with the temperature that corresponded to the target temperature of the test that was about to be run. No change in the peaks that corresponded to the α'' phase were seen, and peaks that corresponded to the ω phase increased in intensity after each cycle, but, particularly, after the 4th cycle (yellow trace).

shown in figure 3.8. In the quenched state, two clear α'' peaks were observed at $\sim 7.4°$ that were sharp and eassily distinguishable from each other. In contrast, in the pattern for Ti-24Nb at -196°C, a much broader peak that corresponded to the ω phase was observed at the same value of 2θ. Since the peak in figure 4.8 was also observed to be fairly broad, it was suggested that the increase in the peak intensity had resulted from the formation of the ω phase during the thermal cycling. However, due to the low intensity of this peak, the progressive fitting of the peak area as a function of cycling could not be used to verify this.

4.3.6 Initial condition of Ti-24Nb (at.%) in the ST condition

To investigate the role of microstructure on the transformation behaviour of Ti-24Nb under an applied load, material in a solution heat treated condition was also considered. To be consistent, the solution heat treated material was also heated and cooled between room temperature and 350°C under identical conditions to the heated CR material in the previous sections. Laboratory XRD data and the associated microstructure from this initial condition of the material (preheated ST condition) is shown in figure 4.9. A relatively small, equiaxed grain structure was observed, with no evidence of any lenticular features, which might indicate the presence of a martensitic phase. Laboratory XRD data confirmed this, with the corresponding pattern containing the β phase only and no reflections in positions associated with the α'' phase.

4.3.7 The tensile behaviour of Ti-24Nb (at.%) in the ST condition

The stress-strain response of the heated ST condition material is shown in figure 4.10. In contrast to the tensile behaviour of the heated CR, an initial linear elastic response was observed up to a stress $\sim$ 150 MPa. As shown in the insert, above this applied stress level, the stress-strain response began to curve, indicating that the stress-induced $\beta \rightarrow \alpha''$ transformation had initiated. The transformation region continued with increasing stress until the macroscopic yield point was reached, at a stress of $\sim$ 400 MPa.

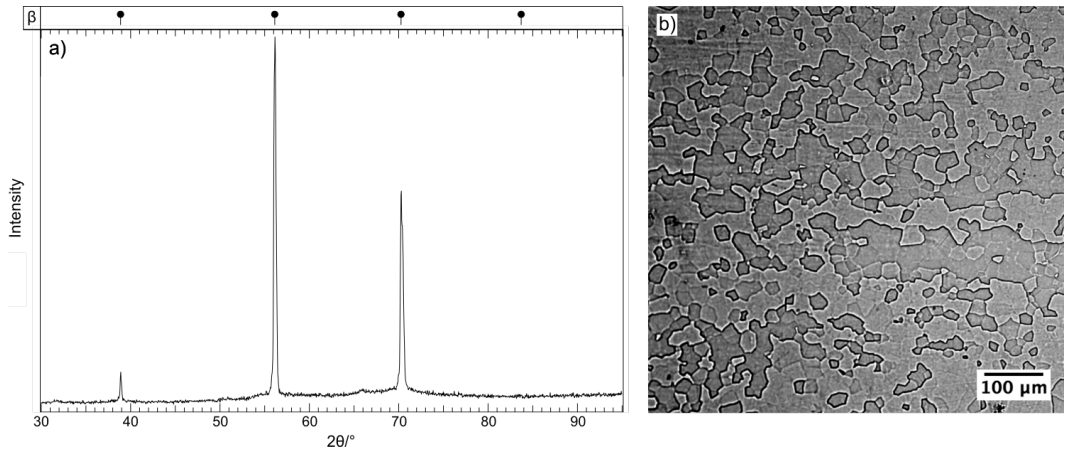

Fig. 4.9 a) XRD pattern for Ti-24Nb (at.%) in the ST condition after a preheat to 350°C obtained using a laboratory source. Sharp β reflections were seen, and no peaks corresponding to the α'' or the ω phases were evident. b) The corresponding microstructure obtained using reflective light microscopy, which showed an equiaxed β grain structure.

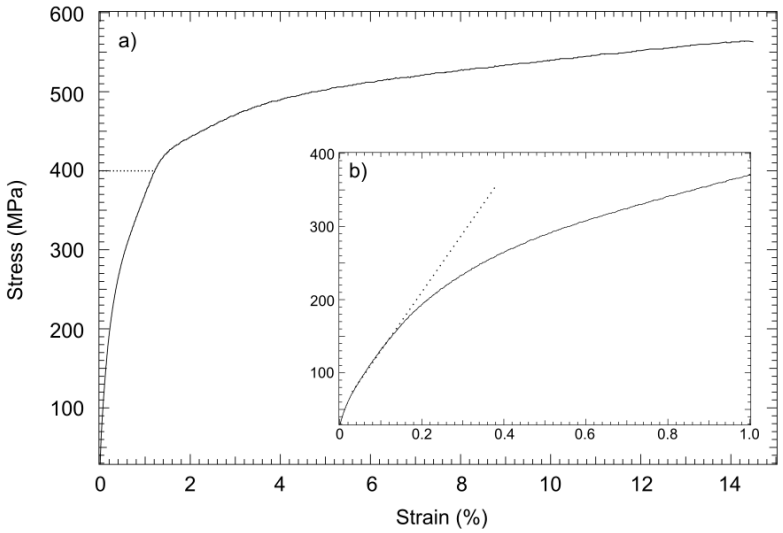

Fig. 4.10 a) Room temperature stress-strain curve for solution treated Ti-24Nb that had been heated to 350°C and subsequently cooled. The linear elastic region of the curve, shown in b), occurred to a stress value of 150 MPa. Above 150 MPa, the curve changed in gradient, typical of the occurrence of the $\beta \rightarrow \alpha''$ transformation. At 400 MPa, the material began to yield, and failed after a ductile region.

4.4 Discussion

4.4.1 The total stress based argument

Current temperature based transformation theories imply that alloys deformed below their M_s temperature cannot undergo the reverse $\alpha'' \rightarrow \beta$ transformation upon unloading as there is no thermodynamic driving force [1, 2, 33]. As such, the evidence presented here, showing that the reverse transformation occurred when CR Ti-24Nb was loaded at -196°C, indicates that the sample must have an M_s temperature below -196°C.

As such, the increase in the intensity of the $(021)_{\alpha''}$ peak when the material was cooled from 350°C must be the result of an additional driving force. Recently, this behaviour has been rationalised through a total stress argument based on the same material that was introduced in the previous chapter. If the M_s temperature for this alloy composition lies below -196°C, then the value of Gibbs energy for the α'' phase must lie above the value for the β phase at all temperatures above -196°C. Therefore, the difference between these values at a given temperature can be associated with the critical stress required to induce the $\beta \rightarrow \alpha''$ transformation. If the material contains sufficient internal stresses, such that the critical stress is reached, then the transformation can occur in the absence of an externally applied load. The internal stress will be a combination of Type II and Type III stress and, therefore, relates to the microstructural condition of the material. Since the $\beta \rightarrow \alpha''$ transformation acts to reduce the total stress level, a consequence of this proposed mechanism is that the internal stress level will not exceed the critical stress for the current temperature.

Further evidence as to the accuracy of this hypothesis can be seen by comparing the effect of an applied stress on the transformation behaviour in Ti-24Nb in the heated CR and ST conditions. As the material in the heated CR condition had undergone the $\beta \rightarrow \alpha''$ transformation during cooling, the total stress level at room temperature was expected to lie just below the critical stress. Consequently, when subjected to an externally applied load the critical stress at this temperature would immediately be reached leading to further $\beta \rightarrow \alpha''$ transformation. As such, the immediate increase in intensity of the $(021)_{\alpha''}$ peak and the absence of a linear elastic response can be explained.

During unloading, the magnitude of the applied stress decreased, which, in turn, reduced the total stress level in the material. This new lower stress level must be below the critical stress for parts of the material and, hence, leads to the reverse $\alpha'' \rightarrow \beta$ transformation in these regions. This behaviour continues as the externally applied load is progressively reduced until completely removed, at which point the material will have returned to its original, pre-load, condition with the fraction of α'' associated with the internal stress level.

When Ti-24Nb in the heated CR condition was subjected to the thermomechanical cycle at -196°C, the intensity of the $(021)_{\alpha''}$ peak did not revert back to its value prior to loading, indicating a residual strain was present in the sample. Whilst not shown here, the stress-lattice strain data for this load cycle resulted in a residual compressive lattice strain for the $(110)_{\beta}$, $(200)_{\beta}$, $(220)_{\beta}$ and $(310)_{\beta}$ planes, consistent with either the occurrence of detwinning of the α'' that was present prior to loading, or an incomplete $\alpha'' \rightarrow \beta$ transformation upon unloading.

In heated ST condition material, the critical stress required to induce the $\beta \rightarrow \alpha''$ transformation at 30°C was $\sim$ 150 MPa. Since, the heated CR material contained the α'' phase at the same temperature, the magnitude of the internal stress would be expected to be similar to the total stress in the heated ST condition at 150 MPa. If this were to be the case, then the stress-strain curve for the CR material should follow the same form as that of the heated ST material when offset by $\sim$ +150 MPa, thereby accounting for the proposed difference in internal stress levels. As shown in figure 4.11. When this offset is applied, the two stress-strain curves map directly over one another, until the onset of macroscopic yielding, at $\sim$ 400 MPa. The successful application of this simple concept adds further credence to the proposed total stress description of the $\beta \rightarrow \alpha''$ transformation in Ti-24Nb.

4.4.2 The Gibbs energy curves for β and α'' in Ti-24Nb (at.%)

The Gibbs energy curves as a function of temperature were discussed with respect to the current temperature based transformation theories in section 1.4 and the transformation temperatures for a given alloy composition were shown in figure 1.9 relative to the temperature where the Gibbs energy curves for the β and the α'' phases were shown to cross. Since the work that was conducted in this study, and in the previous chapter, have concluded that the

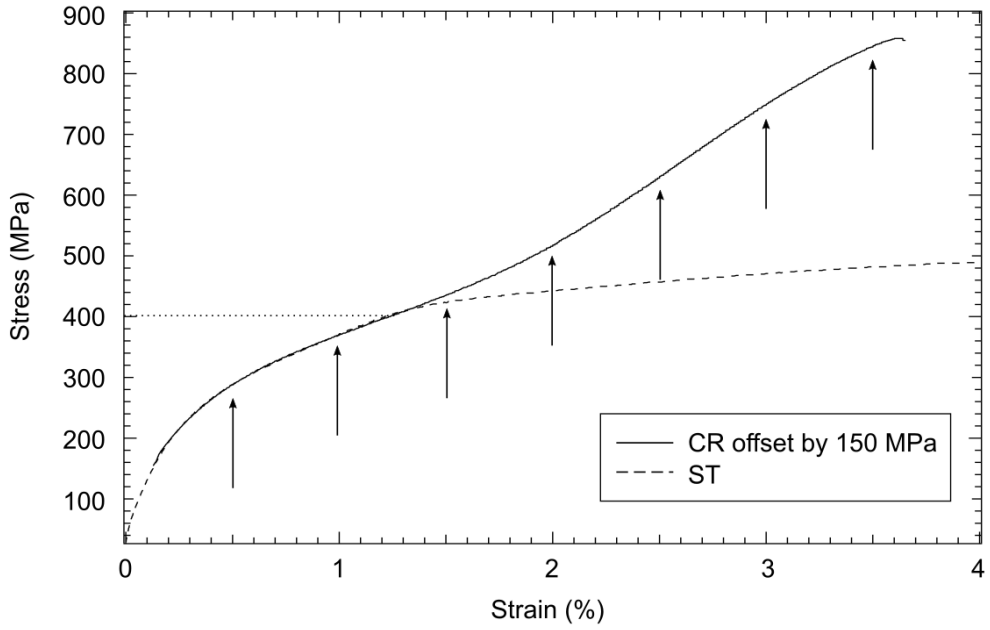

Fig. 4.11 Overlay of the stress-strain curves for Ti-24Nb in the cold rolled and solution treated conditions. The curve for the CR material has been offset by +150 MPa and the curves followed the same shape until the onset of yield in the solution treated Ti-24Nb material.

current temperature based transformation theories cannot be applied to Ti-24Nb, the Gibbs energy curves shown in figure 1.9 also need to be reconsidered. Figure 4.12 shows a newly revised schematic diagram for the Gibbs energy versus temperature plot for Ti-24Nb, which have been drawn using the conclusions from the datasets above. To clarify this, it has been assumed that the activation energy for the $\beta \rightarrow \alpha''$ transformation is small relative to the difference in the Gibbs energies.

Firstly, the lack of thermally activated $\beta \rightarrow \alpha''$ transformation in Ti-24Nb in the ST condition indicated that the Gibbs energy curves for the β and α'' phases may not cross at temperatures above -196°C. Therefore, the two Gibbs energy curves for the Ti-24Nb alloy has been generated with no overlap above -196°C, as shown in figure 4.12. However, in contrast to this, Ti-24Nb that was in the CR condition was observed to undergo a thermally driven $\beta \rightarrow \alpha''$ transformation when the temperature was reduced below 190°C and, therefore, it was concluded that the internal stress level of the alloy in this condition must have contributed to the total stress level of the material. With reference to figure 4.12, this conclusion indicated that when the temperature was decreased below 190°C, the total stress, which included contributions from Type II and III stresses in the microstructure, had exceeded the critical

stress at 190°C to induce the $\beta \rightarrow \alpha''$ transformation. Upon cooling below 190°C, the $\beta \rightarrow \alpha''$ transformation was observed to continue until -60°C, where it was observed to cease. This suggested that the total stress level of the CR Ti-24Nb at temperatures between 190°C and -60°C was sufficient to exceed the critical transformation stress over all of these temperatures. Finally, when the material was cooled below -60°C, the $\beta \rightarrow \alpha''$ transformation did not occur, suggesting that additional cooling was insufficient to drive the transformation any further.

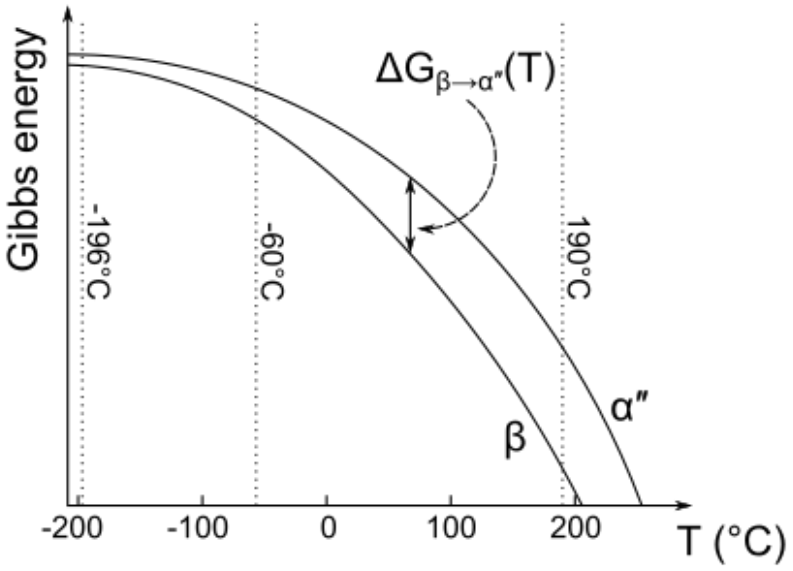

Fig. 4.12 A schematic plot of the newly proposed Gibbs energy curves for the β and α'' phases as a function of temperature for Ti-24Nb. These schematic curves do not represent the true shape of the Gibbs energy curves as a function of temperature, and are shown to demonstrate that they do not cross. For simplicity, the effect of increasing enthalpy with an increase in temperature has not been considered in this plot.

4.5 Conclusion and future work

In situ diffraction experiments and tensile tests were conducted on Ti-24Nb in the CR and ST conditions. These, alongside additional characterisation techniques, were used to show a marked difference in the conditions required for the $\beta \rightarrow \alpha''$ transformation to occur between these sample conditions. Thermomechanical cycles to a maximum stress of 300 MPa were conducted over a wide range of temperatures to investigate the influence of temperature and applied stress upon the forward and reverse transformations. The consequential influence

upon the stress-strain behaviour through the measurement of tensile tests to failure at room temperature were investigated. The observations within the datasets could not be explained using current temperature based transformation theories alone, which led to the proposal of a new stress based theory. Most of the literature surrounding the martensitic transformation in Ti-24Nb alloys has been focused around the key transformation temperatures [11, 12, 19, 54, 57, 58, 106–108]. These characteristic temperatures for general martensitic transformations have been related to the chemical free energies of the β and α'' phases as a function of temperature [9, 35, 37, 38]. In particular, the M_s and A_s temperatures have been related to the metastable equilibrium temperature where the chemical free energy lines cross [37, 38]. However, the lack of a thermally driven $\beta \rightarrow \alpha''$ transformation in Ti-24Nb in the ST condition during cooling indicated that the free energy lines of the β and α'' did not cross at temperatures above -196°C. Therefore, a new stress based argument was proposed to speculatively explain the transformation behaviour in Ti-24Nb. In the datasets, the critical stress required to induce the $\beta \rightarrow \alpha''$ transformation in the ST material was $\sim$ 150 MPa higher than that in the CR condition, for which *in situ* diffraction experiments showed evidence of the transformation as soon as an external load was applied. Therefore, it was suggested that the additional internal stresses that were expected to be present in the CR material (when compared with the ST condition) that contributed towards an overall critical stress required to drive the β to α'' transformation in this Ti-24Nb alloy. A revised schematic diagram for the Gibbs energy versus temperature plot for this Ti-24Nb alloy was drawn, and explained in terms of the total stress based mechanism. The Gibbs energy curves for the β and α'' phases were concluded to not cross for this alloy, which is in contrast to similar diagrams that have been drawn in previous literature that have been proposed to explain all martensitic transformations. Further work is required to identify potential features in the microstructure that have influenced the differences in transformation behaviour for Ti-24Nb in the CR and ST conditions. The clear differences in the initial microstructures for these alloys include the grain size and shape, and the dislocation density.

Chapter 5

The effect of dislocation density and grain size on Ti-24Nb-4Zr-8Sn (wt.%)

5.1 Introduction

In chapters 3 and 4, the effect of a 5 minute heat treatment at 900°C on Ti-24Nb (at.%) was shown to have a significant effect on the $\beta \rightarrow \alpha''$ transformation, which resulted in the proposal of a new stress-based mechanism for this transformation. The microstructures that corresponded to the cold rolled and solution treated conditions indicated a change in dislocation density and grain size as a result of rapid recrystallisation, suggesting that these changes may have directly impacted the difference in the deformation behaviour. In section 3.4 it was also noted that the difference in texture may have resulted in the observed change in transformation behaviour. However, residual surface stresses resulted in significant sample curvature, which made texture analysis of these samples challenging. It is also noted that the effect of texture is difficult to isolate from the effect of high dislocation density and grain size. Therefore, in this section, the individual effects of the grain size and dislocation density on the superelastic behaviour in a similar alloy (Ti-24Nb-4Zr-8Sn (wt.%)) were investigated.

The general concensus from current literature suggests that high levels of cold work, followed by rapid heat treatments can improve the superelastic behaviour in Ti-Nb alloys [12, 14, 58, 65–68, 74, 77]. Often, alloys that can reach large superelastic strains are considered to exhibit good superelastic properties. Therefore, the aim of these studies has focused around

optimising the superelastic strain that is achievable for a given alloy composition, which has been achieved by changing the amount of cold work, and the subsequent heat treatments that have been used to produce the samples [14, 65, 66, 68].

To determine the maximum recoverable strain that is achievable in a specific alloy, cyclic stress-strain curves are often evaluated for a specimen that has been loaded to a stress that lies just below the value of the yield stress, that is then completely removed. These experiments enable the elastic deformation behaviour of different alloys to be directly compared, however, many of these studies do not identify or discuss the source of any differences that arise between stress-strain curves. For example, stress-strain hysteresis loops for Ti–20Nb–6Zr [65], Ti-26Nb [66] and Ti-24Nb [58] that were loaded directly after being cold rolled to reduction ratios of 99%, 90% and 95% respectively, were observed to show almost full superelastic recovery after unloading. The full reversibility of the $\beta \rightarrow \alpha''$ transformation that was observed directly after cold rolling was surprising, since other reports had suggested that a high dislocation density acts to stabilise the α'' phase [69, 70, 92, 109]. Therefore, the α'' variants that were formed during loading would have been predicted to remain stable during the subsequent unloading if the dislocations were stabilising the α''. In all of these studies, this unusual transformation behaviour was not drawn to attention in the discussions, and are thought to have been overlooked.

Generally, alloys are cold rolled to high reduction ratios, often in excess of > 90% [12, 14, 58, 65, 66], to refine the grain size and increase both the yield stress and strength of the alloy. This is often attractive for industrial applications because a higher yield stress allows superelastic alloys to achieve larger strains before the onset of macroscopic yield. However, reasons why such high reduction ratios have been used are unclear in the literature. Therefore, to elucidate the effect of the reduction ratio, and, in turn, the dislocation density, the tensile behaviour of a well-understood commercial Ti-24Nb-4Zr-8Sn (wt.%) alloy was measured for samples that were cold rolled to reduction ratios between 50 and 90%.

After initial cold working, subsequent heat treatments are often applied to reduce the dislocation density, and encourage recrystallisation to produce a more ductile material. Recent studies have used short heating periods at lower temperatures that favour smaller grain sizes to maximise the value of the yield stress [58, 65, 74] because a higher yield stress maximises

the extent of the $\beta \rightarrow \alpha''$ transformation that can occur before the onset of macroscopic yield. However, the effect of the grain size on the critical transformation stresses are rarely discussed. Consequently, here, a systematic study investigating the tensile behaviour of the same Ti-24Nb-4Zr-8Sn (wt.%) alloy, cold rolled to 90% and heated at 900°C for periods between 5 and 60 minutes to vary the grain size is presented.

The stress-based mechanism that was proposed in the previous two chapters stated that the internal stress level of Ti-24Nb (at.%) contributed to the total stress level in the sample, in turn, reducing the amount of additional external stress that was required to induce the $\beta \rightarrow \alpha''$ transformation. Therefore, it is predicted that an increase in the dislocation density would result in the reduction of the minimum amount of applied stress that is required to induce the $\beta \rightarrow \alpha''$ transformation, since the magnitude of the internal type III stresses are expected to increase with an increasing dislocation density.

The stresses that are associated with the grain structure in a material commonly arise from the mismatches between neighbouring grains (type II stresses). As a result, these stresses are heavily localised in the microstructure at the grain boundaries between grains, and are highly dependent upon their relative orientations. Therefore, it is believed that the grain size will not have a significant effect upon the magnitude of the localised stresses, but may influence the overall stress distribution in the microstructure. This is because smaller grain sizes will increase the surface area of the grain boundaries in the material, and will, in turn, increase the number of sites that will be the focus of the mismatch stress. The effect of the grain size upon the localised internal stresses is expected to be very sample-dependent, and, therefore, the effect of grain size on the macroscopic stress-strain behaviour is studied here.

5.2 Methods

Due to the availability of the arc melted samples that were used in chapters 3 and 4, a commerically produced Ti-2448 (wt.%) alloy was used in this investigation of dislocation density and grain size. In contrast to the previous alloys, which contained titanium and niobium, this alloy also contained tin and zirconium. These additional elements are known

as neutral alloying additions in titanium alloys and do not significantly change the β-transus temperature (see section 1.1.1).

Sections were cut from the commercially produced Ti-2448 (wt.%) bar using electro discharge machining and cold rolled to reduction ratios of 50, 60, 70, 80 and 90%, all with a final thickness of ~ 0.7 mm. Tensile specimens, with gauge dimensions of $14 \times 0.56 \times 0.7$ mm were cut along the rolling direction of the cold rolled strips also using electro discharge machining. The re-cast layer was gently removed by hand grinding and polishing, and the samples were cleaned using ethanol and acetone, wrapped in a Ta foil getter and encapsulated in an evactuated quartz tube. To remove the plastically induced α'' that had formed during this cold working process, the samples were subsequently heated to 300°C, which was $\sim$ 340°C above the reported A_f temperature [110]. The encapsulated sample was held at 300°C for 1 minute before being air cooled to room temperature, which allowed a sufficient amount of time for the sample to reach the desired temperature, whilst limiting the formation of the ω_{iso} phase.

Samples for the grain size investigation were cold rolled to 90%, and were also cleaned and encapsulated in an evacuated quartz tube. The samples were then heated at 900°C for 5, 15, 30 and 60 minute periods before being air cooled. Offcuts from the cold rolled strip were used to prepare samples for reflective light microscopy and laboratory based XRD to investigate the initial phase constitution and grain sizes of material in each condition.

Stress-strain curves for each sample were determined using a Tinius Olsen tensile testing frame with a 25 kN load cell to ensure consistency across studies. Initially, tensile tests to failure were conducted at a constant loading rate of 4 MPa s^{-1} to identify the onset of macroscopic yield in the samples for both the dislocation density and grain size investigations. Cyclic load-unload stress-strain curves were then obtained, with a maximum stress value of 700 MPa for the dislocation density tests and 500 MPa for the grain size samples, which had been determined to be sufficiently below the yield stress for all material. XRD was used to identify the phase constitution before and after these loading cycles. More details on how these techniques were used to obtain data are highlighted in chapter 2.

5.3 Results

5.3.1 Dislocation density

Initial characterisation

XRD and reflective light microscopy were used to characterise the initial microstructure of Ti-2448 (wt.%) that had been cold rolled to different reduction ratios. Figure 5.1 shows microstructures for the samples that were cold rolled to a reduction ratio of 60, 70, 80 and 90%. Elongated features that were aligned parallel to the rolling direction were observed, indicating that the high levels of plastic deformation had stretched the original grain structure. Wavy lines were observed in the images corresponding to the 60 and 80% samples, which were thought to be related to the typical marbled structure that has commonly been observed in β-Ti alloys that have been heavily deformed [69, 71, 111–113]. Closer examination of the microstructures using scanning electron, or even, transmission electron microscopy is generally required to understand these features in more detail, and have been studied in previous work [70]. As a result of the high levels of defects that were still present in these microstructures, the images that corresponded to different reduction ratios could not easily be compared.

Figure 5.2 shows the diffraction patterns for the samples that were cold rolled to 50, 60, 70, 80 and 90% after being heated to 300°C. The black lines show the patterns that were recorded before the tensile tests, which showed peaks that were broad and had a low intensity. These peak shapes were characteristic of an alloy that had undergone a high level of plastic deformation [74]. The positions of all of the peaks were used to identify the β and α'' phases in all of the samples prior to loading, which were most identifiable by the $(112)_{\beta}$ and the $(202)_{\alpha''}$ reflections at $\sim 69.7°$ and $\sim 72.6°$ 2θ respectively.

Comparisons between the samples that were cold rolled to different reduction ratios was difficult due to the broad nature and low intensity of the diffraction peaks. However, comparisons between the same sample tested before and after the tensile cycle was still possible. The patterns that correspond to Ti-2448 (wt.%) cold rolled to 70, 80 and 90% showed an indiscernible difference between the sample prior to and after loading, suggesting that either (i) no detwinning or $\beta \rightarrow \alpha''$ transformation occurred during loading, or (ii) a fully

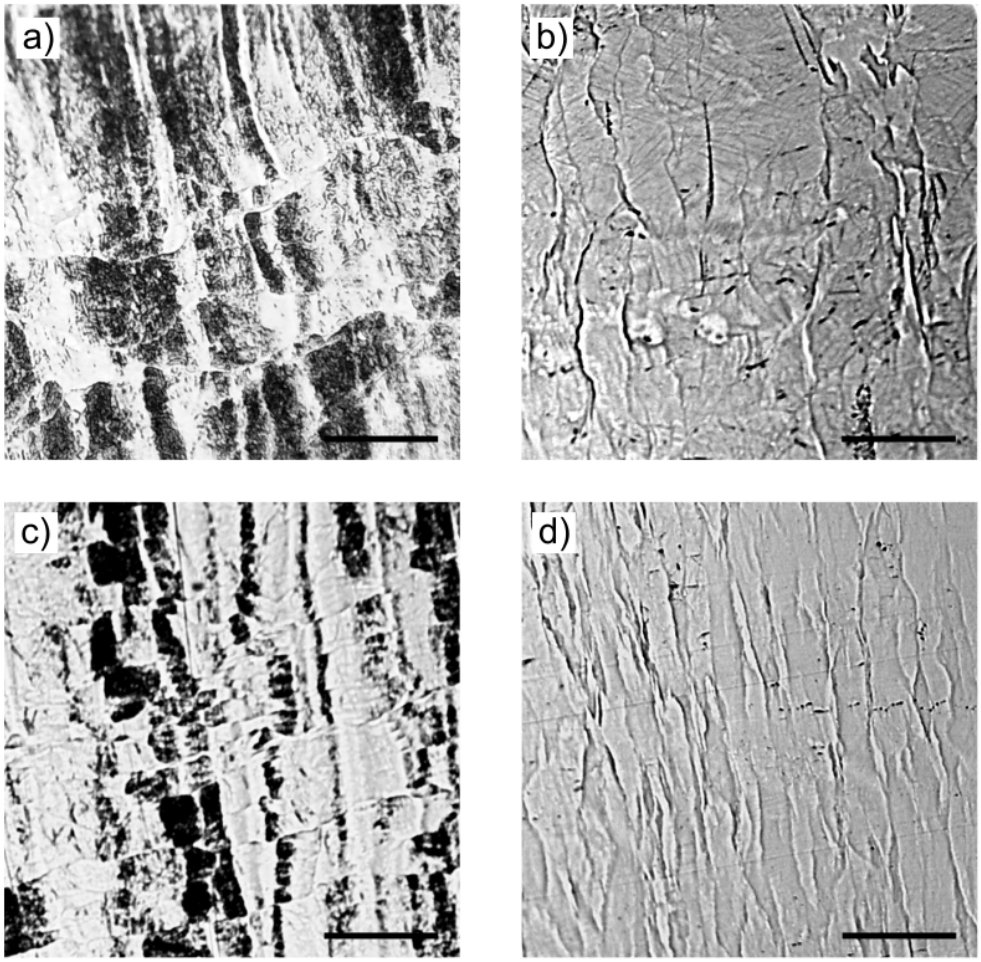

Fig. 5.1 Reflective light microscopy images for Ti-2448 (wt.%) that was cold rolled to reduction ratios of a) 60, b) 70, c) 80 and d) 90% followed by an initial heat to 300°C and a subsequent cool to room temperature. The scale bar in each image represents 50 μm. All images show a broken grain structure with elongated features aligned along the rolling direction, which is approximately vertical in all of the images.

reversible $\beta \leftrightarrow \alpha''$ transformation had occurred. The sample that was cold rolled to 60% showed a slight increase in the $(200)_{\alpha''}$ peak at $\sim 59.6°$ 2θ and the $(130)_{\alpha''}$ peak at $\sim 63.7°$ 2θ after the tensile cycle. Similarly, the sample that was cold rolled to a reduction ratio of 50% showed a significant increase in the intensity of the $(200)_{\alpha''}$ reflection. It was difficult to identify whether these peaks had increased as a result of the initial α'' variants reorienting, or whether the $\beta \rightarrow \alpha''$ transformation had occurred. Additionally, these increases may have resulted from the grains that had been selected during the measurement of these patterns. It is likely that the differences in the diffraction patterns that were recorded before and after loading had resulted from a different number of grains being sampled. For example, if a grain that was favourably oriented to form α'' was sampled, a higher volume fraction may have been recorded compared with a grain that was less favourably oriented. This effect is a limitation of the use of small samples, in addition to material that can exhibit a significant amount of texture. As a result of this, it is likely that the material post load may not have contained more α'' than it did prior to loading. Therefore, the XRD patterns must be used with caution when drawing conclusions that relate to any differences in the phase constitution of these materials before and after the tensile loops.

Tensile behaviour

Tensile tests to failure for all of the cold rolled samples are shown in figure 5.3. As a result of an initiation artefact from the load frame, the strain values for the curves have been offset to a value of zero at 200 MPa to allow the direct comparison between the stress-strain behaviour in the cold rolled material. The stress-strain behaviour for all of the reduction ratios were very similar and showed a non-linear elastic reponse above 200 MPa, which curved with a decreasing gradient as the applied stress was gradually increased. These results are unsurprising since all of the cold rolled samples had been shown to contain a significant amount of the α'' phase. The variants of α'' that were present were expected to be preferentially aligned with the rolling direction since a considerable amount of deformation was still present in the samples after being heated to 300°C. Therefore, when the cold rolled samples were subjected to a tensile load, along the rolling direction, further reorientation of the α'' variants seemed unlikely. Hence, upon loading, any non-linear behaviour that occurred,

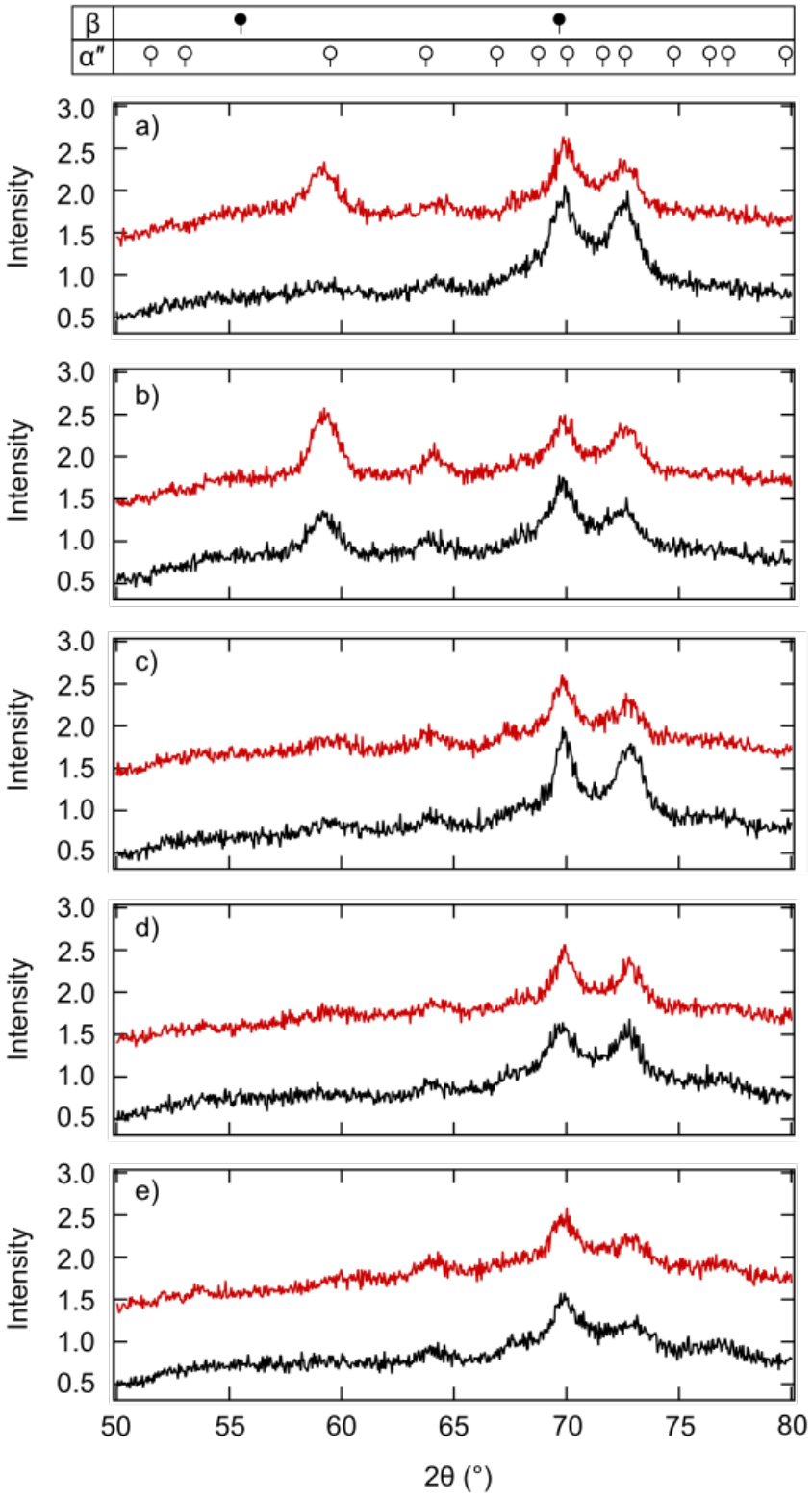

Fig. 5.2 The XRD patterns corresponding to Ti-2448 (wt.%) that was cold rolled to reduction ratios of a) 50, b) 60, c) 70, d) 80 and e) 90% followed by an initial heat to 300°C and a subsequent cool to room temperature. The black lines at the bottom of each figure represent the patterns for the samples prior to loading, and the red lines that are offset above this line correspond to the sample after the tensile cycle. Broad and low intensity peaks corresponding to the β and α'' phases are present in all cases.

would be expected to be as a result of small amounts of detwinning, or, the occurrence of the $\beta \rightarrow \alpha''$ transformation, which was also expected to be limited, since a lot of α'' was already present.

The length of the ductile region was observed to decrease with a increasing reduction ratio, however, since the amount of plastic deformation is heavily dependent upon the sample being tested, this effect could not be concluded without repeatable data for additional samples in each condition being obtained.

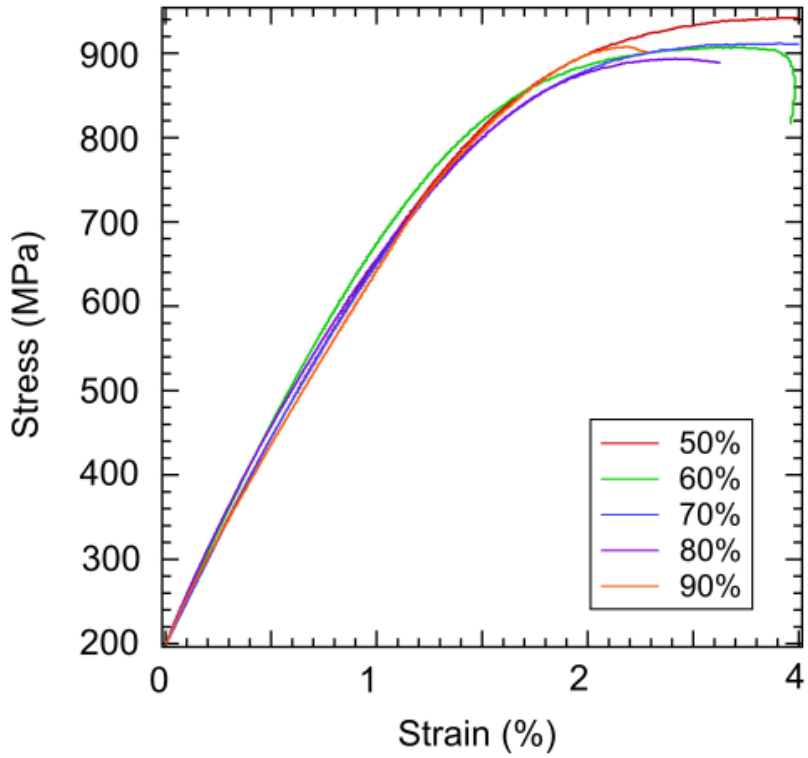

Fig. 5.3 Stress-strain curves to failure for Ti-2448 (wt.%) cold rolled to reduction ratios from 50 to 90%. Non-linear behaviour was observed in all tensile curves above a stress value that appeared to decrease with an increasing reduction ratio.

To investigate any more subtle differences between the tensile behaviour, the strain response of Ti-2448 (wt.%) in each cold rolled condition was measured during a load-unload cycle to a maximum stress of 700 MPa, and the resultant stress-strain hysteresis loops are shown in figure 5.4. In all cases, a very thin hysteresis loop showing full superelastic recovery was observed, suggesing that the the cause of the non-linear elastic region was the occurrence of the $\beta \rightarrow \alpha''$ transformation, since detwinning would not reverse when the applied stress

was removed. Additionally, the size of the hysteresis loop was observed to decrease slightly with an increase in the reduction ratio, suggesting that samples that had been subjected to higher levels of plastic deformation showed poorer damping behaviour, since the area within the curve can be correlated to the energy absorbed during the test. The amount of strain that was achieved when the samples were loaded to a stress of 700 MPa is plotted in figure 5.5 as a function of the reduction ratio. Since full superelastic recovery was observed in all cases, this value of strain is also equal to the magnitude of the recovered strain after the load was completely removed. A clear decrease in the achieved strain values was observed as the reduction ratio was increased, suggesting that the increase in the extent of deformation resulted lower transformation strains.

5.3.2 Grain size

Initial characterisation

To investigate the effect of grain size on the transformation behaviour of Ti-2448 (wt.%), samples were cold rolled to a reduction ratio of 90% and subsequently heat treated at 900°C for 5, 15, 30 and 60 minutes. To demonstrate that the all of the samples had undergone recrystallisation, a microstructure for Ti-2448 (wt.%) heated for the shortest amount of time, 5 minutes, is shown in figure 5.6. An equiaxed grain structure with an average β grain size $\sim$ 29 μm was observed, confirming that 5 minutes was sufficient to induce recrystallisation. Additional images were obtained for the samples that were heated for longer time periods. From these, the diameters for 50 grains in each sample were measured, and used to obtain a grain size distribution for each heat treatment length, which are shown in figure 5.7. The average grain size increased with longer heat treatment periods, indicating that grain growth had continued to occur after the initial recrystallisation. The range of values for the grain diameter appeared similar in the samples that were heated for 5 and 15 minutes, but increased significantly in the samples that were heated for 30 and 60 minutes, with the smallest and largest grains in the 60 minute sample being measured as 49 μm and 161 μm respectively.

XRD patterns for all heat treated material before the tensile tests are shown in figure 5.8. In all cases, sharp peaks that corresponded to the β phase were observed, and no reflections for the α'' phase were seen. The additional step that appeared on the left hand side of the

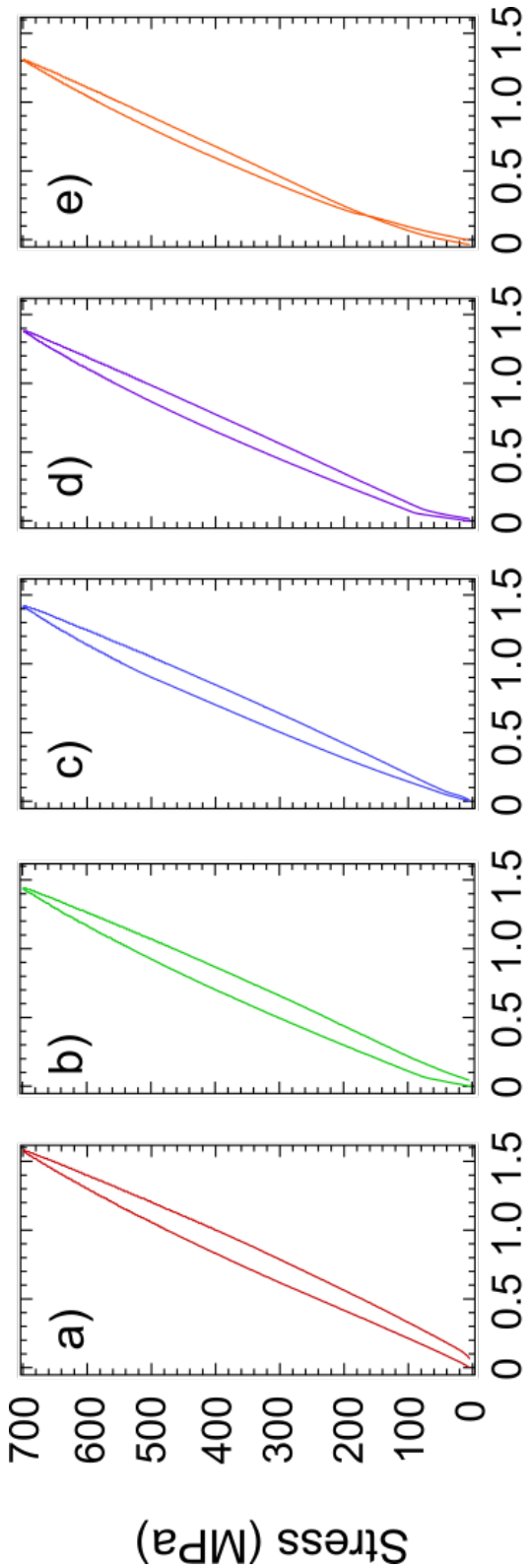

Fig. 5.4 Stress-strain hysteresis curves to a maximum stress of 500 MPa for Ti-2448 (wt.%) cold rolled to reduction ratios from 50 to 90%.

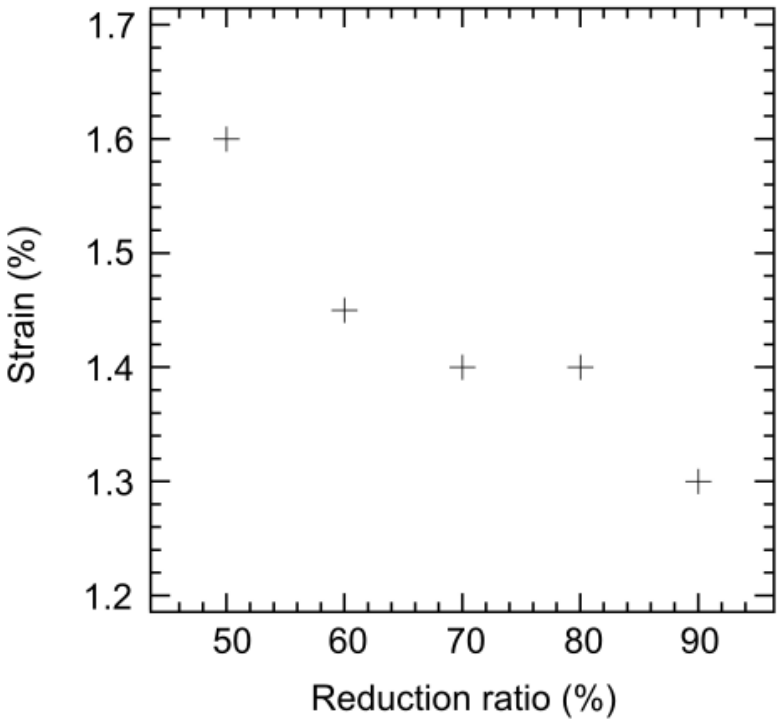

Fig. 5.5 The recovered superelastic strain as a function of reduction ratio in cold rolled Ti-2448 (wt.%) . The amount of strain that was both achieved, and recovered decreased with an increase in reduction ratio.

$(110)_\beta$ reflection, at a value of $\sim 38^\circ$ 2θ was thought to be an artefact of the diffractometer, and was not thought to relate to the sample. This is because the peak had appeared randomly in patterns that were recorded for the exact same sample, in the same loading orientation during previous experiments. However, the source of this artefact remains unknown.

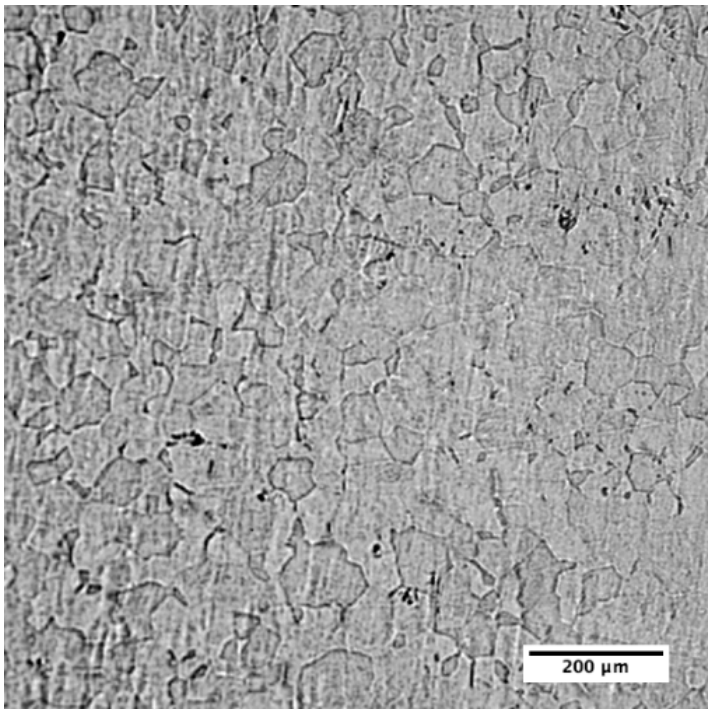

Fig. 5.6 An image of the Ti-2448 (wt.%) sample heated for 5 minutes at 900°C using reflective light microscopy. A β grain structure with an average grain size of $\sim$ 29 µm is seen.

Tensile behaviour

Tensile curves to the point of yield for each heat treatment condition are shown in figure 5.9. The strain values were offset to zero for an applied stress value of 200 MPa due to an artefact that had resulted from the load cell settling into movement. Above 200 MPa, non-linear elastic deformation was seen for all conditions, which could be attributed to the occurrence of the stress-induced $\beta \rightarrow \alpha''$ transformation since no α'' was observed in the initial XRD patterns in figure 5.8. The stress that corresponded to the onset of yield were measured from these curves and are plotted in figure 5.10 as a function of $\frac{1}{\sqrt{d}}$ to investigate if the Hall-Petch relation [75, 76] applied to these samples. The onset of yield was observed to increase with an increased heat treatment period, however, a linear trend with the inverse square root of the

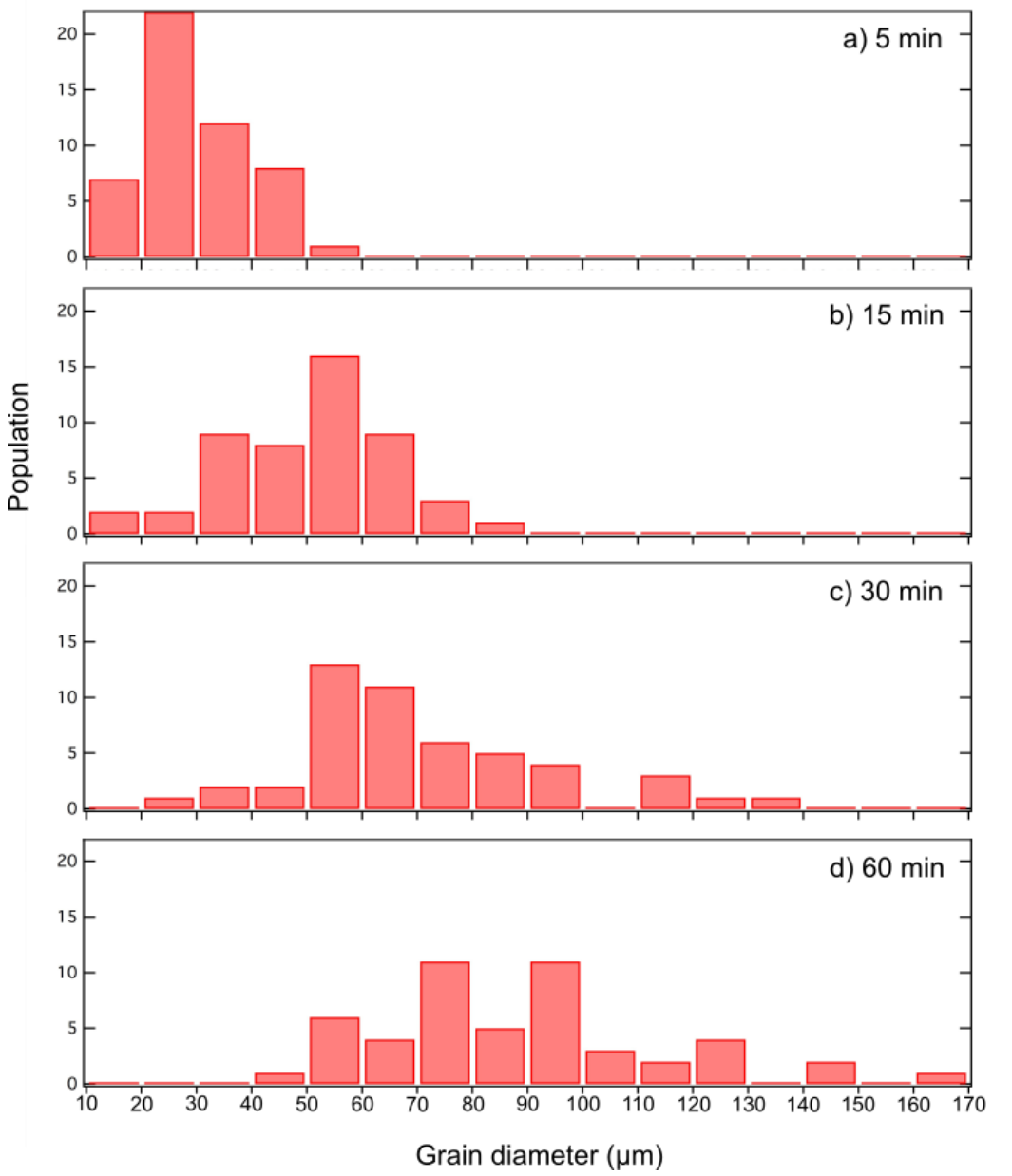

Fig. 5.7 Grain size distribution plots for Ti-2448 (wt.%) cold rolled to 90% and heat treated at 900°C for a) 5, b) 15, c) 30 and d) 60 minutes and air cooled.

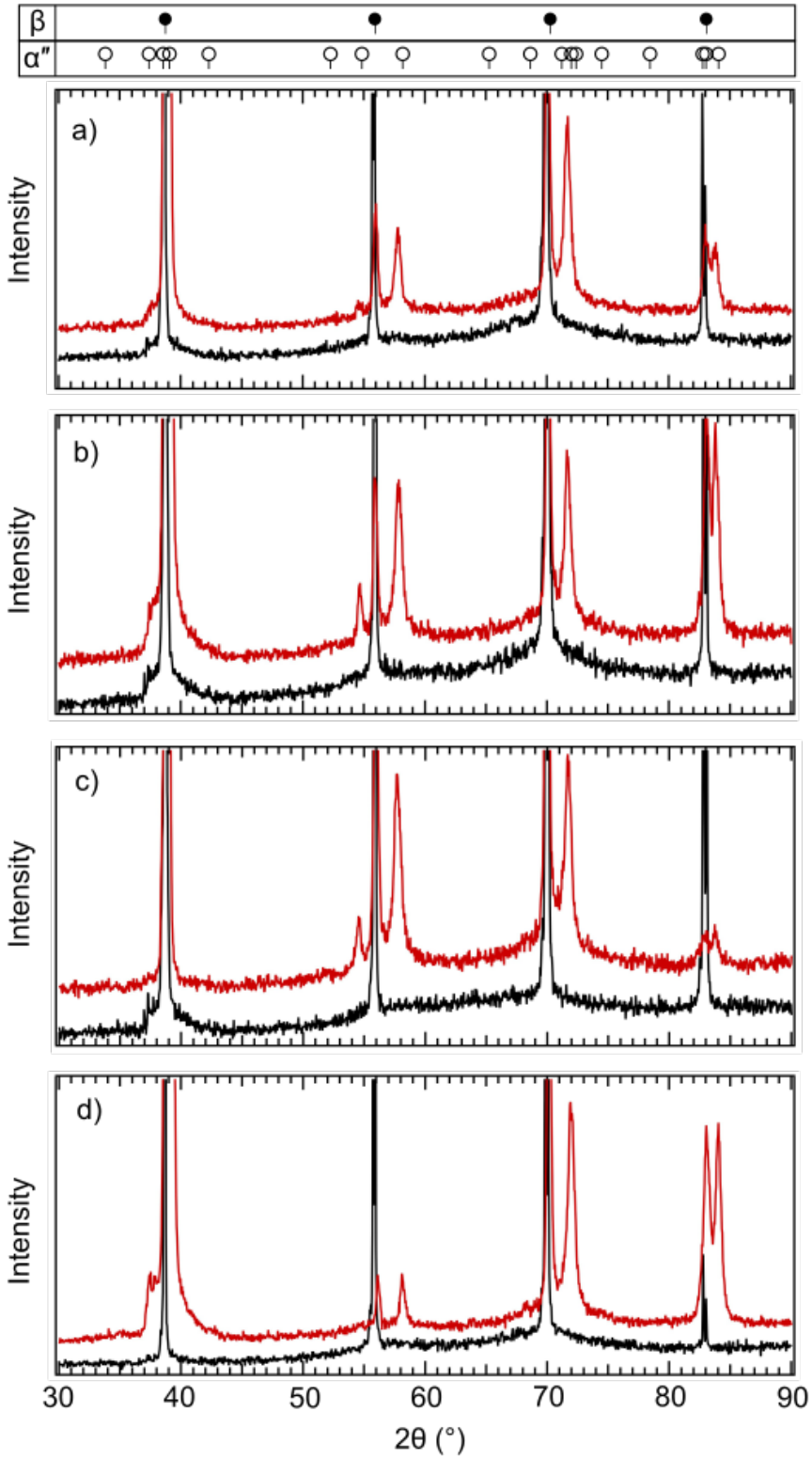

Fig. 5.8 XRD patterns for Ti-2448 (wt.%) cold rolled to a reduction ratio of 90%, and subsequently heat treated at 900°C for a) 5, b) 15, c) 30 and d) 60 minutes both before and after the load-unload tensile cycle to a maximum stress of 500 MPa. The black line at the bottom of each figure corresponds to the sample prior to loading, and the red line that lies at an offset represents the pattern for the sample after the tensile cycle. All of the samples prior to loading contain peaks that correspond to the β phase alone, and additional α'' peaks are seen in all of the patterns after the cyclic test.

grain diameter was not clear from the four points considered. It is thought that this may have resulted from the small number of grains that were used to obtain the average grain size, or the use of an individual tensile test to obtain a value for the yield stress. However, due to the limited amount of sample available, and the difficulties obtaining micrographs for these samples, additional tensile tests and micrographs could not be obtained in the available time frame, and should therefore be considered in future work.

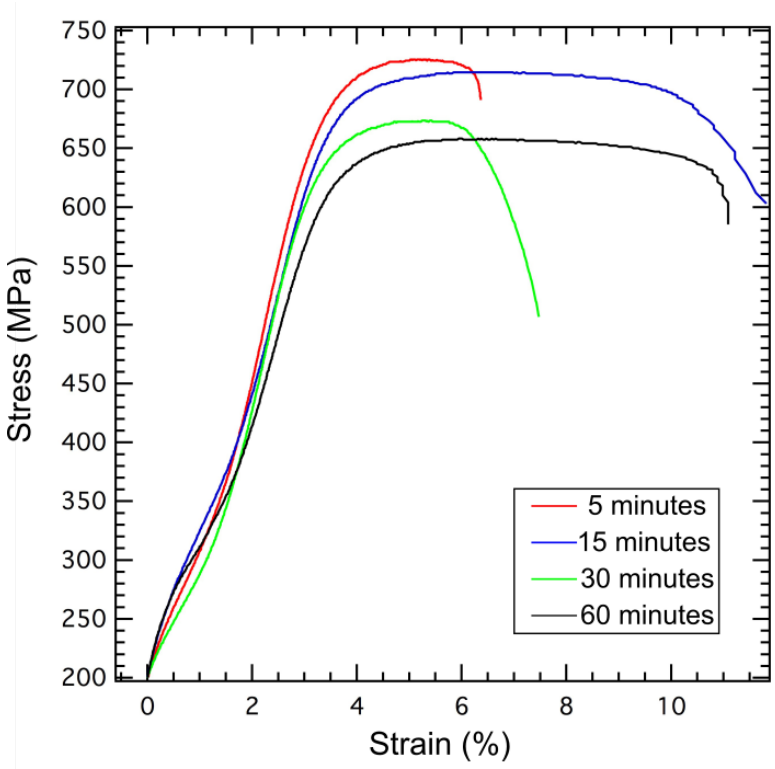

Fig. 5.9 Tensile curves to failure for Ti-2448 (wt.%) cold rolled to 90% and heat treated at 900°C for 5, 15, 30 and 60 minutes and air cooled. Strain values are offset to zero at a stress of 200 MPa.

The stresses that are reported in figure 5.10 were used to ensure that the maximum stress of the stress-strain hysteresis loops, were considerably below the yield point of each condition. Samples in each heat treated condition were subjected to an externally applied stress to a maximum value of 500 MPa, and the strain response during loading and unloading was recorded. The resulting stress-strain hysteresis loops are shown in figure 5.11a. The loading segment of the tensile curves for the samples heated for 5, 15 and 30 minutes exhibited very similar behaviour, showing non-linear elastic behaviour above 100 MPa. The curve that corresponded to the sample that was heat treated for 60 minutes followed a shape that was

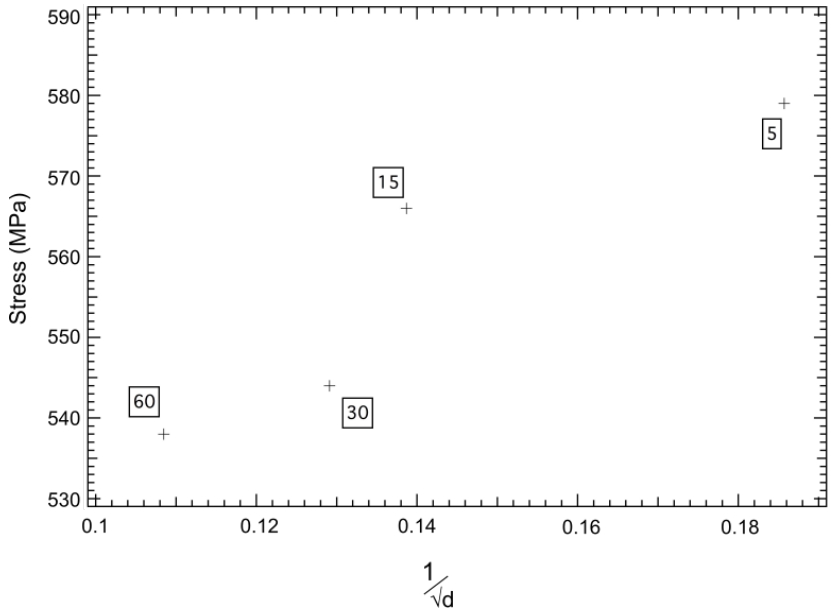

Fig. 5.10 A plot of the yield stress as a function of $\frac{1}{\sqrt{d}}$, where d is the average grain size for samples of cold rolled Ti-2448 (wt.%) heated to 900°C for 5, 15, 30 and 60 minutes. Each point is labelled with the corresponding heat treatment time period.

very similar as observed for the samples heated for shorter time periods, however, the σ_{SIM} for this condition took a higher value of $\sim$ 150 MPa. Since this difference was not observed in the tensile tests in figure 5.9, it is suggested that this observation may not be due to the larger grain size, but the result of an individual sample being tested. However, due to the restricted amount of sample remaining, these tests were not repeated. Above $\sim$ 300 MPa, all four curves were observed to increase in gradient, a characteristic which can be attributed to the $\beta \rightarrow \alpha''$ transformation requiring more stress to achieve the same amount of transformation strain. Since the increase in grain size reduced the number of grains that were present in the tensile sample, the effect of texture and orientation of the grains is expected to have had a more pronounced effect on the recorded tensile curves in the samples heated for 60 minutes. Consequently, the effect of the grain size on the strains achieved in each sample cannot be isolated from the effects of texture and grain orientation, and, therefore, a direct comparison of the strains between these samples cannot be reliably connected to the change in grain size. Despite this, it is still interesting to note that upon unloading, the sample that was solution treated for 60 minutes was observed to curve back towards the stress axis at a faster rate than the shorter heat treatments, which has been highlighted in figure 5.11b. This result suggested

that amount of the transformation strain that could be recovered during the unloading segment of the stress-strain cycle, may be able to be influenced by changing the heat treatment period of a sample.

The most notable observation in the stress-strain curves that are shown in figure 5.11 was that none of the samples completely recovered the strain once the applied stress had been removed, which suggested that some residual martensite was retained in the samples. This was in contrast with reports in previous studies, which have all shown full superelastic recovery in Ti-2448 that was subjected to different thermomechanical processes, including hot rolling [114], hot forging, warm rolling to 75% and 88% [115], and a range of thermomechanical heat treatments [99]. To investigate potential explanations for this residual strain, XRD patterns were recorded after each load-unload cycle, and were compared with those that were recorded prior to loading. The corresponding patterns are shown in figure 5.8, with the black and red lines showing the phase constitution before and after the tensile tests respectively. Prior to loading, Ti-2448 (wt.%) in all of the heated conditions showed evidence for the β phase alone, and no peaks that corresponded to the α'' phase were observed. After loading, additional intense peaks that correponded to the α'' phase were observed in all of the samples, which confirmed that the residual strain must have resulted from retained α'' in the microstructures.

5.4 Discussion

5.4.1 General form of stress-strain curves for superelastic materials

To aid the explaination for the datasets that were reported in this study, the general stress-strain response of a superelastic alloy must be considered. The schematic diagram in figure 5.12 shows the stress-strain curve that is commonly expected to be seen for a superelastic material that is loaded from a microstructure that initially contains no α''. The first segment, labelled (i), shows the initial elastic deformation of the β phase. This is followed by the second segment, labelled (ii), which refers to the part of the loading curve when the $\beta \rightarrow \alpha''$ transformation initially begins to occur. The gradient of this line is generally shallow, and is often shown as a flat plateau [2], suggesting that the first martensite variants to form require

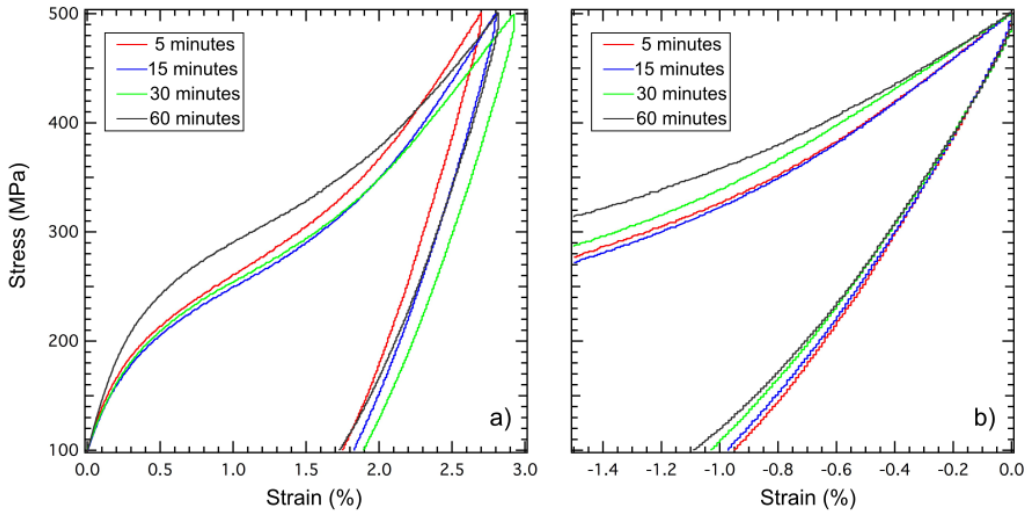

Fig. 5.11 a) The stress-strain hysteresis loop recorded for cold rolled Ti-2448 (wt.%) heated at 900°C for 5, 15, 30 and 60 minutes when loaded, and subsequently unloaded to a maximum stress of 500 MPa. Strain values are offset to zero at a stress of 100 MPa. b) An insert of the same plot with the maximum achieved strain offset to zero.

fairly small changes in the applied stress. The final section that is labelled (iii) shows the gradient of the stress-strain curve to increase again, indicating that to obtain the same amount of transformation strain as in segment two, a larger stress must be applied. These changes in gradient suggest that as the $\beta \rightarrow \alpha''$ transformation proceeds, the new martensite variants become increasingly more difficult to form. Considering this, the difference in transformation behaviour of the cold rolled and solution treated conditions can now be explained.

5.4.2 Cold rolled Ti-2448 (wt.%)

Initial condition of the CR Ti-2448 (wt.%) samples

Current thermally driven theories use key transformation temperatures to predict the phase constitution and transformation behaviour of an alloy at a specific temperature and stress. In chapter 1, the schematic diagram that was shown in figure 1.6 was used to demonstrate this concept. The transformation temperatures that have been reported in the literature for Ti-24Nb-4Zr-7.5Sn have been quoted as -42°C (A_f), -44°C (A_s), -50°C (M_s) and -53°C (M_f) [110]. Therefore, these temperatures would predict that a sample of Ti-2448 (wt.%) that had been heated above 300°C and slowly cooled to room temperature should contain no α'',

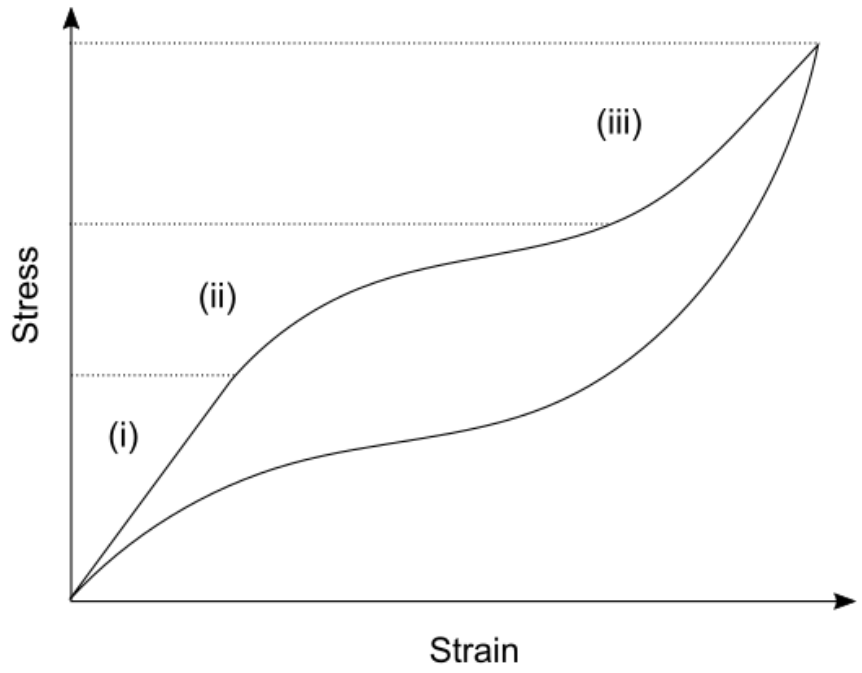

Fig. 5.12 Schematic diagram of the stress-strain response for a superelastic material that shows full superelastic recovery. The loading segment has been separated into segments that show (i) the linear elastic region, (ii) the initial occurrence of the $\beta \rightarrow \alpha''$ transformation, and (iii) the continued $\beta \rightarrow \alpha''$ transformation that requires a higher amount of stress initiate.

since the sample had been heated more than 340°C above the reported A_f temperature. In addition to this, if a Ti-2448 (wt.%) sample was subjected to a load-unload cycle at room temperature, full superelastic recovery would be expected, since room temperature lies above A_f, and, consequently, M_s.

The datasets that were presented here show multiple discrepencies from these predictions, and can be used to further validate the stress based mechanism that was proposed in chapters 3 and 4 for Ti-24Nb. The first discrepancy was observed when all of the cold rolled Ti-2448 (wt.%) samples showed evidence for both the β and α'' phases after the initial heat to 300°C, when the transformation temperatures suggested that no α'' should be present. The new stress-based mechanism can explain this observation in terms of the residual stress level that is expected to be present in the microstructure as a result of the high dislocation density that formed during plastic deformation. It is possible that the M_s temperature for the alloy studied in this work differed from those previously reported due to slight differences in alloy composition, and consequently, it is suggested that the M_s temperature for the alloy used here lies above room temperature, offering an explanation why some α'' was initially present.

Tensile behaviour of the CR Ti-2448 (wt.%) samples

When an alloy that is subjected to a tensile cycle at a temperature between M_s and M_f, upon loading, a non-linear elastic deformation is expected, as a result of detwinning of the initial α'' variants, the occurrence of the $\beta \rightarrow \alpha''$ transformation, or a combination of both. During unloading, only the elastic deformation of the initial phases is expected to be recovered since the testing temperature lies below A_s and there is no driving force for the $\alpha'' \rightarrow \beta$ transformation. Therefore, if the M_s and M_f temperatures for this Ti-2448 (wt.%) alloy lay either side of room temperature, as was indicated by the phase constitution of the XRD patterns, an open hysteresis loop would be predicted. Critically, full superelastic recovery was observed upon unloading Ti-2448 (wt.%) in all of the cold rolled conditions, contradicting all of the predictions using current thermally driven transformation theories. Again, the stress based approach can explain these observations through the consideration of the total stress level of the sample, which included both the internal and external stresses. At room temperature, the internal stress level in the cold rolled samples was sufficient to have formed

some α''. As an additional load was then applied to the CR samples, the total stress level was sufficient to continue the $\beta \rightarrow \alpha''$ transformation, forming more martensite. This was further validated by the occurrence of the non-linear deformation at applied stresses as low as 200 MPa, which suggested that by the time that this value for the applied stress had been reached, a sufficient amount of the $\beta \rightarrow \alpha''$ transformation had occurred to see the change in gradient on a macroscopic scale. Once this external stress was removed, the total stress level of the sample decreased, and no longer exceeded the critical transformation stress. Consequently, as the applied stress was removed, the reverse transformation was observed to occur, resulting in the complete recovery of the transformation strain that was achieved during loading. It is important to note that the absolute start transformation temperature, which may be defined by the temperature where the Gibbs energy curves for the β and α'' phases cross, could not be determined in these experiments since all of the samples contained a significant amount of internal stress.

Since a negligible amount of residual strain was observed in any of the cold rolled samples, it is concluded that the $\beta \rightarrow \alpha''$ transformation was responsible for the deviation from the linear elastic behaviour upon loading, as opposed to detwinning which would not show any recovery during unloading. This conclusion was supported by the XRD patterns that were recorded for the samples rolled to 70, 80 and 90%, but seemed contradicted by the samples rolled to 50 and 60%, which indicated an increase in α'' content after the cycle. However, it is thought that the difference in peak intensities in these XRD patterns resulted from different grain sampling between tests, and the α'' observed was present both before and after the tensile cycles.

Figure 5.12 showed the commonly reported schematic diagram for the typical stress-strain curve for a superelastic material. It is clear that the hysteresis loops that were recorded for all of the CR samples did not show a region that was consistent with segment two of this diagram, which showed a shallow gradient as the $\beta \rightarrow \alpha''$ transformation occurred. Instead, a steep gradient was observed, with a slight non-linearity as the applied stress was increased. In chapter 4, the stress-strain response of Ti-24Nb in the CR condition was compared with the ST condition by offsetting the stress-strain curve by a value that corresponded to the differences in the internal stress levels of both materials. The application of the same analysis to the

results here, suggested that the internal stress level in all of the CR Ti-2448 (wt.%) samples was sufficient to offset the stress-strain curve to start at a stress value that lies in segment three, offering an explanation for the lack of a plateau-like region and the steep gradient. It important to note that the obtainable strains are expected to vary with the samples orientation relative to the rolling direction, but, since all of the samples were cut long the length of the cold rolled strip of material, that the effects this are thought to be small.

The effect of dislocation density

The size of the superelastic hysteresis loops that were recorded for the CR Ti-2448 (wt.%) samples was observed to decrease as the reduction ratio increased. Similar behaviour has been observed in previous studies which reported a decrease in the hysteresis loop size with cycling, which was attributed to the build up of dislocations after each cycle [93]. Therefore, it is suggested that both the thin shape of the hysteresis loops, and the decrease in loop size with higher reduction ratios had resulted from an increase in dislocation density with cold rolling. However, this relation of the increased reduction ratio with a greater dislocation density could not be directly verified using the peak widths of the diffraction peaks, as initially thought, since the peak intensity that was achievable using a laboratory based X-ray source was too small to allow a comparison between samples.

The total strain that was achieved in the CR samples was observed to decrease with an increase in reduction ratio. Previous studies have reported that grain orientation relative to the loading direction can heavily influence the amount of the transformation strain [39]. Hence, it is suggested that the increase in the elongation of the grains, which resulted from greater amounts of cold work, had caused this decrease in the total strain at maximum load. This can be understood in terms of the length of the martensite lath that can grow in a β grain, which is suggested to be limited by the dimension of the grain perpendicular to the rolling direction. Additionally, it is also suggested that an increase in the dislocation density may have acted as a barrier to the size of martensite variants that were able to form, thus, also reducing the strain that was achieved.

5.4.3 Solution treated Ti-2448 (wt.%)

Initial condition of the ST Ti-2448 (wt.%) samples

To investigate the effect of the solution treatment time on the same Ti-2448 (wt.%) alloy, samples were cold rolled to 90% and heated at 900°C for different periods of time ranging from 5 to 60 minutes. All of these samples contained no α'' in the initial condition prior to loading, suggesting that the internal stress level of all of the samples was below the critical transformation stress that was required to drive the $\beta \rightarrow \alpha''$ transformation. These results were consistent with the observations in the datasets for Ti-24Nb in chapters 3 and 4. Consequently, it was predicted that the shape of the stress-strain curves for the solution treated samples should follow a much shallower curve than observed in the CR samples.

Tensile behaviour of the ST Ti-2448 (wt.%) samples

The yield stress of the heat treated samples was observed to decrease with an increasing average grain diameter, following a trend similar to that predicted using the Hall-Petch relation [75, 76]. However, the use of four datapoints, that were obtained from a dataset of 50 grains, was insufficient to draw a more solid conclusion with respect to these values. To elucidate this relationship further, solution treatment time periods that fill the gaps between these data points should be considered in future work.

The loading segments of the superelastic hysteresis loops that were recorded for the solution treated samples showed a much more evident non-linear trend than observed in the CR alloys, which was consistent with the common shape of the stress-strain curve, shown by the schematic diagram in figure 5.12. The initial linear elastic response was small in these samples, suggesting that their internal stress level did not lie too much below the critical stress required to drive the transformation.

All of the results so far have indicated that in the solution treated samples, the β phase was more thermodynamically stable than the α'' phase. Therefore, it seemed surprising that upon unloading, the superelastic recovery that was observed in these samples was only partial and that some α'' has been retained. This unusual behaviour suggested that the internal stress state of the solution treated material after the load-unload cycle must have been higher than it

was prior to loading, and, that the change in the stress level was sufficient to retain some of the α''. The source of this additional stress is suggested to be associated with the build up of dislocations during the cyclic tensile test [93]. Similar work that has considered the effect of the build up of dislocations whilst subjecting a GUM metal to a similar tensile cycle [94] has shown the stress-strain behaviour to stabilise after $\sim$ 15 cycles. Therefore, it is suggested that the high dislocation density that must be present in the cold rolled samples must have reached a similar stability, and any changes in the dislocation density during the cycle here was negligible, offering an explanation why the martensite was not retained after the load was removed.

The amount of strain that was acheived when the solution treated samples were loaded was considerably higher than the values that were obtained in the cold rolled specimens. Since the grain structure of the solution treated samples was much more equiaxed and contained fewer dislocations and grain boundaries than the cold rolled samples, it is suggested that the achievable strain was much higher because the growth of the martensite laths was considerably less restricted than it was in the cold rolled samples.

The effect of grain size

The period of time that Ti-2448 (wt.%) that had been heated at 900°C did not appear to have a significant effect upon the amount of externally applied stress that was required to initiate the occurrence of the $\beta \rightarrow \alpha''$ transformation, suggesting that the increase in the average grain size from $\sim$ 29 μm to $\sim$ 89 μm did not significantly change σ_{SIM}. Since the critical transformation stress for the samples heated for 60 minutes did not show a significant difference in the tensile test to failure, it was concluded that the increased value observed for the tensile loop was as a result of sample variation. Since the 60 minute sample had grown larger grains, the total number of grains that were sampled was reduced, and, therefore, the amount of variation between samples is expected to be more significant than for material where a larger number of grains were considered.

5.5 Conclusion and future work

Superelastic hysteresis loops were conducted on samples of Ti-2448 (wt.%) that had been cold rolled to different reduction ratios to vary the dislocation density. In all cases, full superelastic recovery was observed at room temperature, which was explained using the total stress based approach. These data suggested that current thermal theories cannot be used to explain the transformation behaviour in metastable-titanium alloys. The hysteresis loops were very thin, and the area within the curve decreased as the reduction ratio was increased. This was attributed to the increase in the dislocation density, which was consistent with reports in previous literature.

The total superelastic strain that was achieved in the cold rolled samples reduced with higher reduction ratios. This was attributed to the smaller transformation strains that were associated with the more elongated grains in samples that had been cold rolled to higher reduction ratios. Additionally, the presence of more dislocations was thought to limit the size of the martensite laths, but evidence to support this was not obtained. Considerably higher superelastic strains were recorded for the solution treated samples, which indicated that the contribution of the transformation strains to the total strain in the tensile direction was larger for recrystallised grains than the elongated ones.

To investigate the effect of the grain size on the superelastic behaviour, Ti-2448 (wt.%) was solution treated for various time periods, and the corresponding stress-strain curves were determined. Despite the β phase being the more thermodynamically stable phase before loading, an incomplete superelastic response was observed in the stress-strain loop, which was confirmed to have resulted from retained martensite in the final unloaded microstructure. The build up of dislocations during the cyclic test was suggested to have increased the internal stress level of the solution treated samples, offering an explanation for the presence of the retained martensite in the unloaded state.

The grain size did not appear to have had a significant effect upon the superelastic behaviour in the solution treated alloys. However, the reduction in the number of grains that were sampled in each case had decreased as the grain size was increased, which was thought to have resulted in slight differences in the achieved strains.

Whilst this study provided an initial insight into the effect of dislocations and grain size on the superelastic behaviour of metastable-titanium alloys, there were many aspects of the experimental work that could be improved upon in future work. Initially, the sensitivity of a laboratory based XRD experiment did not allow the comparison between cold rolled samples due to the low intensity and broad nature of the diffraction peaks. In future work, a monochromatic source should be considered to reduce the effect of different wavelengths on the peak width. It is thought that this may allow the direct comparison between samples that have been cold rolled to different reduction ratios. The tensile tests that were collected for all of the samples in this study were obtained using individual samples. Whilst the tensile tests to failure could be compared with the tensile hysteresis loops, the measurement of the superelastic behaviour of these samples with individual samples could not solely be relied upon. Therefore, in future investigations, it is suggested that the stress-strain curves for multiple samples are recoreded to ensure that the reported behaviour was repeatable. This is particularly important for the future use of these alloys in engineering applications, since the repeatibility of mechanical properties is crucial.

The effect of the grain size on the superelastic properties was difficult to isolate from the effect of grain orientation and sampling, since the number of grains reduced as the average grain size of the sample increased. Future work should consider the use of bigger samples, which would reduce the effect of the number of grains on the differences between stress-strain curves, and would also reduce the influence of other microstructural features such as cracks. Additionally, more than four different solution treatment times should be considered. This would allow more insight into any trends that may occur as the grain size is changed.

Chapter 6

Effect of Nb contents on the transformation behaviour in Ti-Nb alloys

6.1 Introduction

To date, the literature that has investigated the superelastic properties in Ti-Nb alloys have focused on the effect of niobium content on the transformation temperatures [11, 12, 18–20, 84, 106, 107]. The datasets that have been presented in the previous chapters have provided convincing evidence that current thermally driven theories used to describe other superelastic systems, such as NiTi, cannot be applied to Ti-Nb-based alloys. Instead, a total stress based approach has been proposed, which can rationalise both the datasets here, and those that remain unexplained in the literature. In this final chapter, the niobium content in the binary Ti-Nb system has been investigated using *in situ* experiments to enable further comparisons with the current datasets that have been presented in the literature.

It is the general concensus that the M_s temperature of Ti-Nb alloys decreases with higher niobium contents. Commonly, it is suggested that the depression of the M_s temperature is linearly dependent upon the niobium content, with a gradient on the order of 40°C per at.% [11–13, 18, 19]. However, within the associated literature there are also reports of Ms temperatures that deviate significantly from this trend line, which are often in excess of 30°C from the temperature predicted by the trend line. More significantly, some studies did not observe a thermally driven $\beta \rightarrow \alpha''$ transformation at all when a Ti-Nb alloy with an M_s

significantly above room temperature was reheated from the quenched state, and subsequently re-cooled at a slower rate [20, 77, 95, 96]. The new stress based argument that was proposed in chapters 3 and 4 has been able to justify the discrepencies in M_s within the literature for alloys of the same, or similar, nominal composition. However, there still remains a discrepency in the gradient of the trendline that has been reported in the literature, which varies from -28°C [19] to -44°C [12], as shown in figure 1.12. If it is assumed that in each separate study, the samples with different concentrations of niobium were produced in the same way, and had a similar oxygen contents, the internal stress level should be similar. Therefore, the values for the gradient of the trendlines should represent the effect of niobium on the start transformation temperature, and are not expected to depend on the internal stress state of the material.

This study aims to investigate the true relationship between niobium content and the start transformation temperature for an alloy set that has been produced using the exact same methods to minimise the difference in internal stress level as a result of processing. Three alloys that contained 22, 26 and 28 at.% Nb were subjected to a four step thermomechanical cycle. Data for Ti-24Nb for the same thermomechanical cycle was collected, and reported in chapter 4 and is compared with these additional datasets in the discussion. To compliment these datasets, *ex situ* tensile curves to failure, and superelastic hysteresis loops were collected for each alloy composition. These curves enabled comparisons between the M_s temperatures and the stress-strain behaviour recorded here, with the datasets that were reported in previous literature.

6.2 Methods

Ti-Nb alloys with target compositions of 22, 26 and 28 at.% Nb were arc melted using the same method as was used in chapters 3 and 4. Samples were cold rolled to > 90% reduction ratios, with a final sample thickness of $\sim 0.56 \pm 0.02$ mm. Tensile specimens with gauge dimensions of $14 \times 0.56 \times 0.7$ mm were cut using electro discharge machining, and the re-cast layer was removed by gently hand grinding. All cold rolled samples were subjected to a four step thermomechanical cycle, which involved (i) cooling from 350°C to a target temperature, in the range -150 to 30°C (ii) loading the sample at the target temperature to 300 MPa, (iii)

unloading the sample at the target temperature and (iv) a final reheat to 350°C. As in chapters 3 and 4, a Linkam TST350 stage was used to apply a sequence of thermomechanical cycles to the specimen, using a heating and cooling rate of 0.5°C s^{-1} and a crosshead movement rate of 1 μm s^{-1}. Each individual thermomechanical cycle involved the four steps of (i) cooling from 350°C to a target temperature, in the range -150 to 30°C (ii) loading the sample at the target temperature to 300 MPa, (iii) unloading the sample at the target temperature and (iv) a final reheat to 350°C. Diffraction images, with an exposure time of 0.5 s, were recorded every 4 s, giving a temperature resolution of 2°C for the dataset. *In situ* synchrotron data was obtained using the ID11 beamline at the European Synchrotron Radiation Facility (ESRF). Further details on these experiments are discussed in chapter 2. All of the one dimensional diffraction patterns in this study were extracted using an azimuthal integration of a 20° segment centred around an angle in the two-dimensional diffraction ring that showed a high intensity of the α'' reflections. The intensity beneath the $(021)_{\alpha''}$ peak was determined using the same method as was used in the previous work for Ti-24Nb in chapters 3 and 4, by sequentially fitting each peak with a Gaussian function and a linear background.

The range of values that the M_s temperature could take were identified for each alloy composition using the point where the intensity of the $(021)_{\alpha''}$ peak began to increase above the background level in the peak area plots. The one dimensional diffraction patterns that corresponded to the temperatures within this range were used to more accurately determine the temperature where the first diffraction peak that correponded to the α'' phase was observed. In all cases, the first peak to be identified was the $(021)_{\alpha''}$ peak, and, as a result, data corresponding to the intensity of the $(021)_{\alpha''}$ reflection is reported. A similar method was also used to identify additional key temperatures in the transformation.

The concentration of titanium and niobium for the alloy in both conditions were determined by inductively coupled plasma-optical emission spectrometry (ICP-OES) using a Thermo Fisher iCAP 7400 Radial machine. The oxygen composition was determined at a certified external laboratory using a fusion-thermal conductivity method (LECO).

6.3 Results

6.3.1 Chemical compositions

The chemical composition was determined for all Ti-(22-28)Nb alloys, in at.%, after cold rolling and are shown in table 6.1. These results indicated that the target compositions were very close to the actual niobium contents, and that a minimal amount of oxygen was picked up during the arc melting process in all alloys, which contained similar quantities of oxygen. Trace amounts of other minority elements, such as carbon and nitrogen, were expected in these alloys, and, therefore, were not measured.

Table 6.1 The measured chemical compositions (in at.%) for the arc melted Ti-(22-28)Nb alloys. The actual chemical compositions were well represented by the target compositions.

	Ti	Nb	O
Ti-22Nb	77.8	22.0	0.20
Ti-24Nb	75.7	24.1	0.19
Ti-26Nb	73.7	26.1	0.22
Ti-28Nb	71.6	28.2	0.22

6.3.2 Progress of the $(021)_{\alpha''}$ peak intensity during the thermomechanical cycle

Start temperatures of the martensitic transformation during cooling

To directly measure the start temperatures for these Ti-Nb alloys, the intensity of the $(021)_{\alpha''}$ peak was tracked during the thermomechanical cycle. The start temperature was determined to be the value where the intensity of the $(021)_{\alpha''}$ peak began to increase above its initial level.

Figure 6.1a shows the change in intensity of the $(021)_{\alpha''}$ peak during the thermomechanical cycle. At 350°C, the non-zero value of the peak area showed that prior to cooling, some of the α'' phase remained in the sample. To confirm this was the case, and not an error in the fitting, the one dimensional diffraction patterns for the range of 2θ values were the $(021)_{\alpha''}$ peak is expected are shown in figure 6.1. The progress of the peak during cooling and loading (figure 6.1b) and unloading and heating (figure 6.1c) are shown. The initial one dimensional

diffraction pattern, shown in figure 6.1b, shows the small $(021)_{\alpha''}$ peak that was observed at 350°C, demonstrating the peak area plots were an accurate way to determine transformation progress during the thermomechanical cycles. Upon cooling, the intensity of the $(021)_{\alpha''}$ peak immediately began to increase, indicating that the M_s temperature for Ti-22Nb in the CR condition was above 350°C, thus, confirming why α'' was present at 350°C.

The change in intensity of the $(021)_{\alpha''}$ peak in Ti-26Nb is shown in figure 6.2. The diffraction patterns in figure 6.2b confirmed that no α'' was present in the sample at 350°, suggesting that the M_s temperature for Ti-26Nb was below 350°C. Upon cooling, the intensity of the $(021)_{\alpha''}$ peak was observed to increase above zero at a temperature value of $\sim$ 274°C.

Figure 6.3 shows the equivalent plot for the $(021)_{\alpha''}$ peak area for Ti-28Nb. Since this alloy contained the highest amount of Nb, it was surprising that the sample contained a fraction of α'' at 350°C, which was confirmed in the diffraction patterns shown in figure 6.3b. Upon cooling, the intensity of the $(021)_{\alpha''}$ peak remained constant until the temperature was decreased below $\sim$ 235°C, which suggested that the small amount of α'' that was initially present was not an indication of the transformation temperature being above 350°C, but may have been a result of some high areas of localised stress in the sample.

The M_s temperatures for all of the alloy compositions, including those that were recorded for Ti-24Nb in chapters 3 and 4 are summarised in table 6.2. Since the amount of α'' in the initial condition of Ti-22Nb at 350°C was very small, the M_s temperature has been approximated as 350°C.

Plateau temperatures of the $(021)_{\alpha''}$ peak area during cooling

When all three alloys were cooled below their M_s temperatures, the intensity of the $(021)_{\alpha''}$ peak continued to gradually increase until a critical temperature was reached, where the intensity appeared to reach a constant value. This plateau-like region had previously been observed in chapters 3 and 4 when Ti-24Nb in the CR condition was cooled to -196°C. The plateau could not be explained using current thermally driven transformation theories, but could, however, be rationalised using the new stress based approach, which suggested that below the plateau temperature, the total stress level in the sample was insufficient to exceed the critical transformation stress at the given temperature. Hence, these results for alloys that

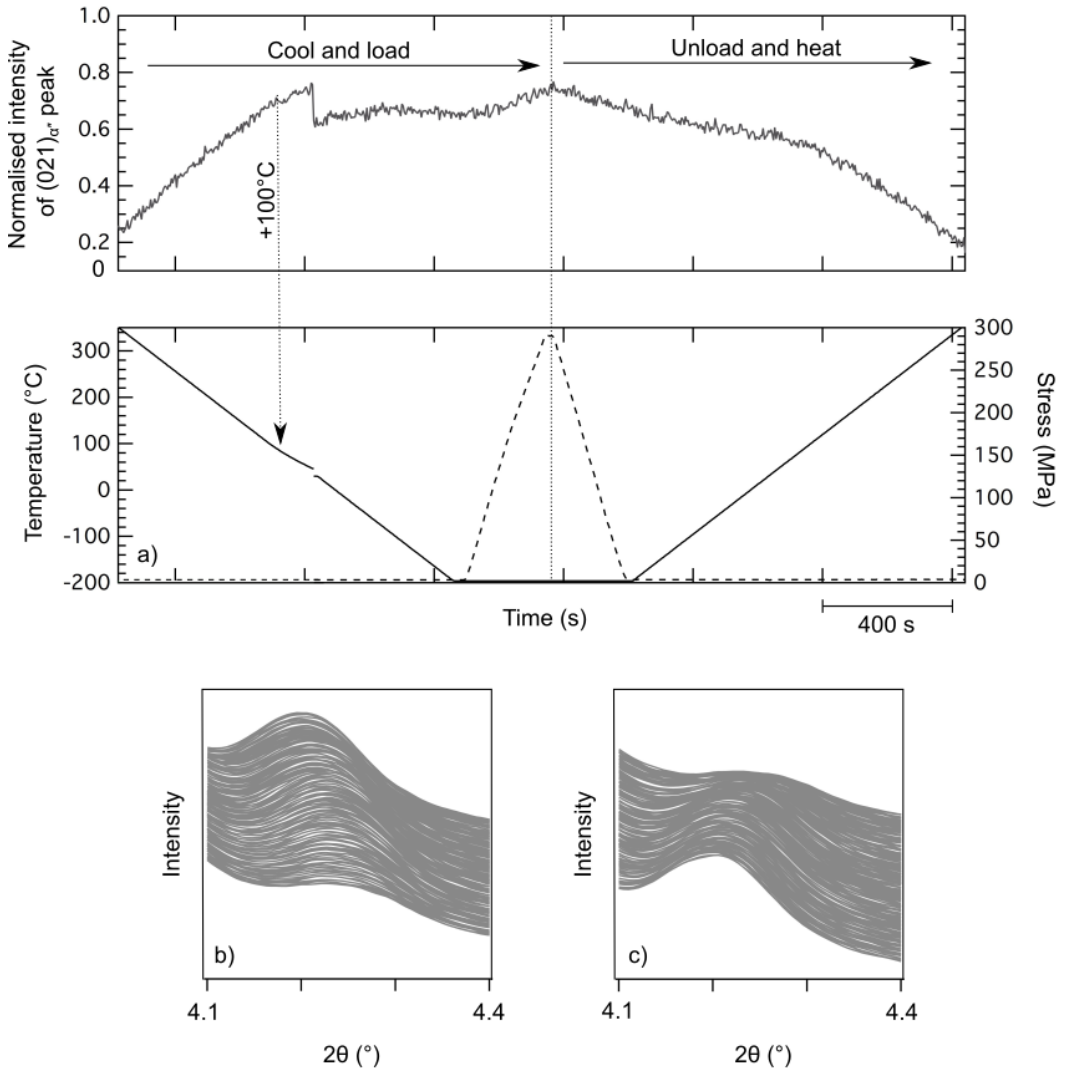

Fig. 6.1 a) Normalised peak area of the $(021)_{\alpha''}$ reflection as a function of time, plotted with respect to the accompanying temperature change for Ti-22Nb (at.%) in the cold rolled condition. Initially, at 350°C, the intensity of the $(021)_{\alpha''}$ peak is non-zero. Upon cooling, the peak area increases between $\sim$ 350°C and $\sim$ 100°C where the area curve plateaus upon further cooling. The peak intensity increased as soon as the load was applied. Upon reheating, the peak area decreased when the temperature was increased, becoming indistinguishable above the background above $\sim$ 290°C. The progress of the one-dimensional diffraction pattern between 4.1° and 4.4° 2θ is shown during a) the cool and load, and b) the unload and reheat.

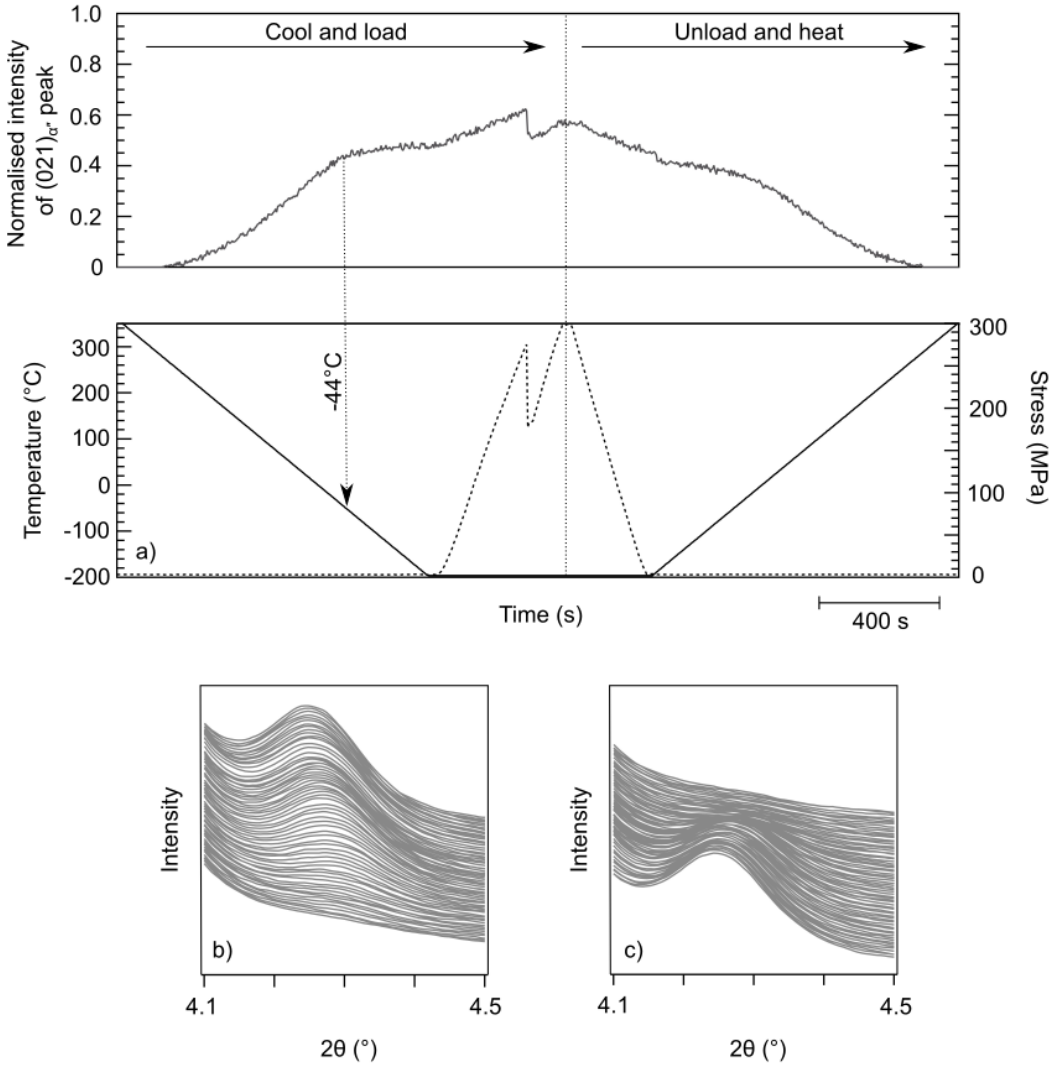

Fig. 6.2 a) Normalised peak area of the $(021)_{\alpha''}$ reflection as a function of time, plotted with respect to the accompanying temperature change for Ti-26Nb (at.%) in the cold rolled condition. Upon cooling, the peak area increases between $\sim$ 274°C and $\sim$ -44°C where the area curve plateaus upon further cooling. The peak intensity increased as soon as the load was applied. Upon reheating, the peak area decreased when the temperature was increased, becoming indistinguishable above the background above $\sim$ 290°C. The progress of the one-dimensional diffraction pattern between 4.1° and 4.5° 2θ is shown during a) the cool and load, and b) the unload and reheat.

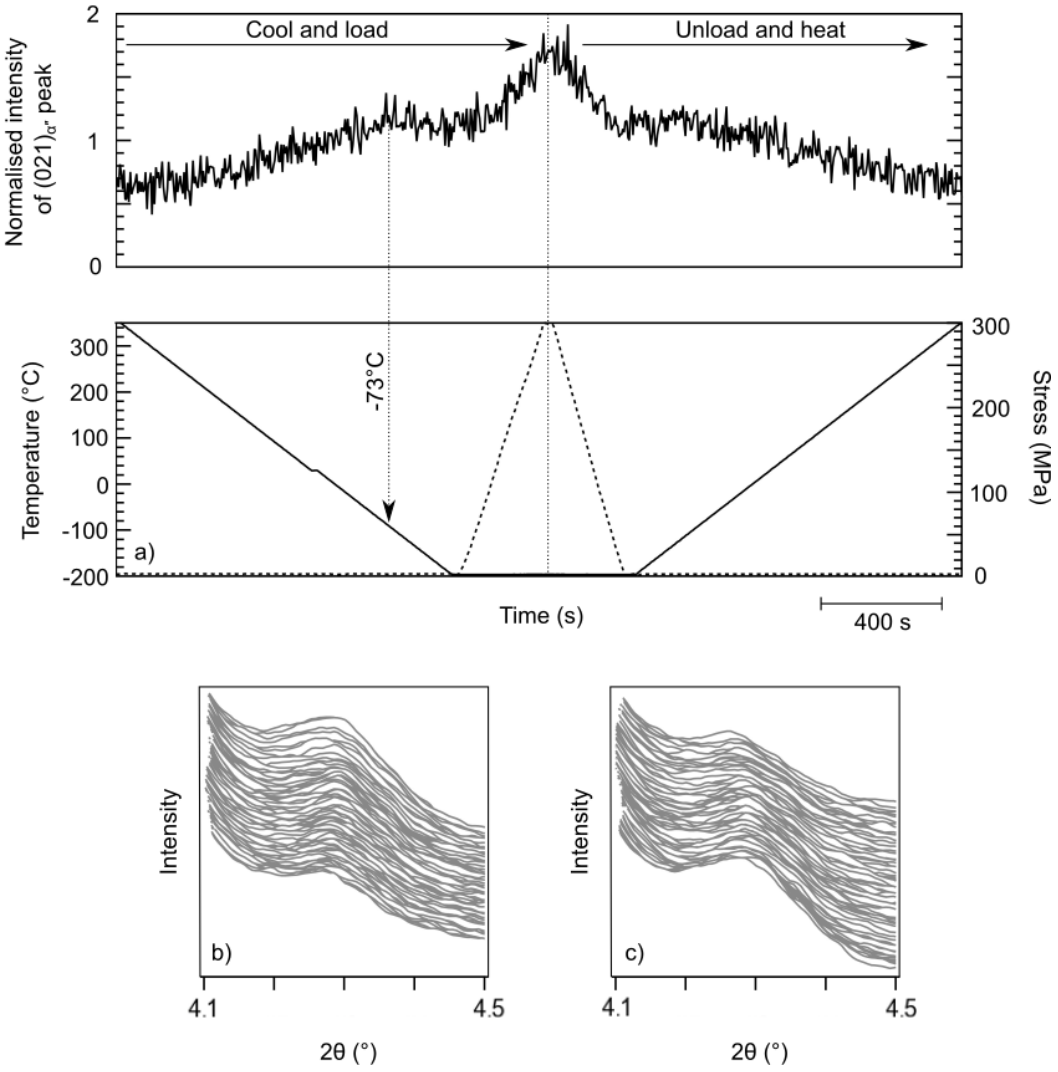

Fig. 6.3 a) Normalised peak area of the $(021)_{\alpha''}$ reflection as a function of time, plotted with respect to the accompanying temperature change for Ti-28Nb (at.%) in the cold rolled condition. Upon cooling, the peak area increases between $\sim$ 235°C and $\sim$ -73°C where the area curve plateaus upon further cooling. The peak intensity increased as soon as the load was applied. The peak intensity increased as soon as the load was applied, and the value prior to loading was reobtained when the load was completely removed. Upon reheating, the peak area decreased when the temperature was increased, returning to its value prior to the initial cooling step. The progress of the one-dimensional diffraction pattern between 4.1° and 4.5° 2θ is shown during a) the cool and load, and b) the unload and reheat.

contained 22, 26 and 28 at.% Nb also showed this plateau region, suggesting that this may be the case for all Ti-Nb alloys that form the α'' martensite phase. The temperatures when this plateau was reached in each alloy, are summarised in table 6.2. and the values for Ti-24Nb were determined from figure 4.7 and added to this table for reference.

The plateau-like region in Ti-22Nb was particularly noticeable, since it formed at the highest temperature, and, therefore, formed the longest plateau. It is clear from the data in figure 6.1a that the area beneath the $(021)_{\alpha''}$ peak negligibly changed below the plateau temperature, shown by the flat nature of the peak area curve. This suggested that as the temperature was cooled below $\sim$ 100°C, the total stress level in the sample was insufficient to exceed the temperature dependent critical transformation stress. However, the closeness of these two values could only be determined by applying an external load to the sample to see how much additional stress was required to contine the $\beta \rightarrow \alpha''$ transformation.

The plateau temperature was observed to decrease in value for Ti-26Nb and Ti-28Nb, indicating alloys that contained a higher niobium content continued to transform to lower temperatures. Additionally, the decrease in plateau temperature could be related to the increase in the total internal stress level of the sample that was required to induce the $\beta \rightarrow \alpha''$ transformation. If it was assumed that the internal stresses in these samples at 350°C, before loading, was solely based on the manufacturing processes used to make the samples, the magnitude of the internal stress in all cases at room temperature can be assumed to be similar. Therefore, as the samples were cooled, the additional stresses that arose from thermal mismatches between grains or phases may also be assumed to be independent of niobium content. Consequently, lower plateau temperatures could be related to a higher value of stress required to induce the $\beta \rightarrow \alpha''$ transformation. Hence, it is suggested that an increase in niobium content results in a higher total critical stress that is required for the $\beta \rightarrow \alpha''$ transformation to occur.

Load-unload cycles

In section 6.3.2 it was suggested that at temperatures between the plateau temperature and -196°C, the total stress level in the sample did not exceed the critical stress for transformation within this temperature range. However, the difference between these values remained unclear.

Table 6.2 A summary of the start transformation temperature and plateau temperature for Ti-(22-28)Nb alloys.

	M_s (°C)	Plateau temperature (°C)
Ti-22Nb	350	100
Ti-24Nb	312	30
Ti-26Nb	274	-44
Ti-28Nb	235	-73

To elucidate this, a load was subsequently applied to all of the alloys at -196°C to determine the value of the critically applied stress that was required to induce further transformation. In all cases, as soon as the external load was applied to the sample, the $(021)_{\alpha''}$ peak area was observed to immediately increase, suggesting that for all alloys, the internal stress level lay just below the critical transformation stress at -196°C.

During the unloading segment of the thermomechanical cycles for Ti-22Nb and Ti-28Nb (figures 6.1 and 6.3), the intensity of the $(021)_{\alpha''}$ peak was observed to decrease back to its original value prior to loading. Hence, full superelastic recovery was observed in both alloys that were loaded > 430°C below their recorded M_s temperature. This exact behaviour had previously been observed in chapter 4 for Ti-24Nb in the same microstructural condition, suggesting that the stress based argument was applicable in Ti-22Nb and Ti-28Nb also. Unfortunately, a load drop, which was thought to have resulted from the tensile sample slipping in the grips, caused a rapid decrease in the peak area value for Ti-26Nb, and this conclusion could not be made for Ti-26Nb. However, examination of the evolution of the $(021)_{\alpha''}$ peak area value during loading and unloading, in figure 6.2, indicated that this could also have been the case in Ti-26Nb.

Finally, the relative changes in the peak area during cooling and loading in the same alloy could be compared enabling the relative amounts of α'' to be approximated. The increase in the $(021)_{\alpha''}$ peak intensity in Ti-22Nb during loading was observed to be much smaller than the change that was observed during cooling, indicating that the extent of the $\beta \rightarrow \alpha''$ transformation had majoritively occurred during the cooling segment. In contrast, when the Ti-28Nb sample was loaded, the change in the $(021)_{\alpha''}$ peak intensity was observed to be similar to the change that had occurred during cooling, indicating that the application of the external stress was required to progress the $\beta \rightarrow \alpha''$ transformation further in this alloy. It

appeared that in Ti-Nb alloys that contained a smaller amount of Nb, a significant amount of the $\beta \rightarrow \alpha''$ transformation occurred during the cooling segment, and when the load was applied, the transformation did not progress much further. In contrast, in alloys that contained more Nb, a smaller fraction of the $\beta \rightarrow \alpha''$ transformation occurred during cooling, and the external load was required to significantly progress the transformation further. These observations provide additional evidence to suggest that the value of the critical transformation stress at -196°C had increased with an increase in niobium content.

Additional features of the $(021)_{\alpha''}$ peak area plots during the thermomechanical cycles

Two drops in the peak area data were observed in the thermomechanical cycles for Ti-22Nb and Ti-26Nb. Figure 6.1 showed a sudden decrease in the peak area during the cooling segement of the cycle, which had occurred as a result of the temperature reduction halting at $\sim$ 40°C. Consequently, the run had to be paused and restarted from room temperature without the beamline recording data. This change in $\sim$ 10°C resulted in an immediate reduction in the amount of α'' that was measured in the sample.

Similarly, in figure 6.1, a drop in the $(021)_{\alpha''}$ peak area was observed during the loading segment for the thermomechanical cycle for Ti-26Nb. This decrease in peak area had resulted from a sudden drop in the applied load, which was thought to have occurred due to the tensile sample slipping in the grips. Consequently, the value of the peak area after this point could not reliably be compared with those before the load drop since the exact effect on the sample remained unknown. For example, it is suspected that the jump in the value of the applied load may have resulted in an increase in the dislocation density. Despite this, it is interesting to note that the $(021)_{\alpha''}$ peak area was observed to decrease in value immediately after this load drop had occurred, and demonstrated how quickly these alloys can react to a change in stress state. After the load drop, the load was increased once more to a maximum stress of 300 MPa, and then fully unloaded, as shown in the corresponding stress curve at the bottom of figure 6.2a.

6.3.3 Stress-strain behaviour

To investigate the effect of niobium contents on the stress-strain behaviour in Ti-Nb alloys tensile tests to failure were conducted on Ti-Nb alloys containing 22, 26 and 28 at.% Nb, and are shown in figures 6.4a - c. The tensile curves to failure for the Ti-22Nb, Ti-26Nb and Ti-28Nb samples followed a similar shape, which began with a linear elastic region upon initial loading. All three curves were then observed to deviate from this straight line at a stress value that appeared to decrease with an increase in niobium contents.

To investigate this further, superelastic tensile loops were determine for each alloy, and are shown in figures 6.4 d - f. XRD patterns, which are shown in figures 6.5a - c, were determined for the each tensile sample both before and after the loading-unloading cycle to determine if any α'' had retained in the final, unloaded microstructure. Prior to loading, β reflections were observed in all samples, and additional shoulders that were attributed to the α'' phase could be seen in Ti-22Nb. Small deviations from the background could be observed in Ti-26Nb and Ti-28Nb at a diffraction angle of $\sim 42° \ 2\theta$, which could be attributed to the $(021)_{\alpha''}$ reflection, however, the intensity of this peak was so small this observation could not be stated with much confidence. Consideration of these XRD patterns, in addition to the M_s temperatures that were all measured to take values > 200°C, suggested that sensitivity of the laboratory based XRD pattern was insufficient to measure the presence of the small amounts of the α'' phase that should have been observed in Ti-26Nb and Ti-28Nb.

The load-unload cycles for each alloy are shown in figures 6.4. The loops corresponding to Ti-22Nb and Ti-28Nb showed full superelastic recovery at room temperature when loaded to 500 and 400 MPa respectively. The loop for Ti-26Nb showed almost complete recovery, suggesting that either a small amount of α'' had been retained after unloading, or that a small amount of plastic deformation had occurred. Therefore, it was suggested that all of the samples had undergone the stress induced $\beta \rightarrow \alpha''$ transformation during unloading, which had reversed upon unloading. Upon initial examination of the tensile tests to failure, the values for the critical stress appeared to follow a "V"-shaped dependence on the concentration of Nb, which was in agreement with the values that had been reported in previous work [12]. The critical stress values that were determined from the tensile curves to failure are shown in figure 6.6a, and are compared to those collected in the dataset published by Kim et al. [12].

However, a closer inspection of the stress-strain relationship of these alloys using the smaller-scaled hysteresis loops gave a different relationship, which is shown in figure 6.6b. It is suggested that some of the trends that were found in previous work may have resulted from the analysis of data on too large a scale, and, that a much closer examination of the tensile behaviour may be necessary to determine the true deformation behaviour in these alloys. These new values for the critical applied transformation stress followed a linear trend with niobium content, as shown in figure 6.6 and the increase in critical stress with niobium content, suggested that, at room temperature, alloys with more Nb required a larger total stress level to induce the $\beta \rightarrow \alpha''$ transformation.

The XRD patterns after the load-unload cycles are also shown in figure 6.5. Little difference was observed in the patterns that were recorded prior to and after loading in any of the samples, which confirmed the observation in the tensile loops that no α'' was retained after the complete removal of the applied stress.

6.4 Discussion

6.4.1 The effect of Nb content on the M_s and plateau temperatures

The effect on the M_s temperature

Overall, the M_s temperature was observed to decrease as the niobium content was increased in the binary Ti-Nb system. As the niobium content in a sample was increased, the β phase is expected to become more stable, since Nb is a commonly recognised β-stabiliser [14]. The Gibbs energy curve for the β phase is therefore expected to decrease with an increase in Nb, as shown in the schematic diagram in figure 6.7. Using this diagram, the concept of the plateau temperature can be discussed further. The black arrow represents the thermodynamic driving force that is required for the $\beta \rightarrow \alpha''$ transformation to occur at a given temperature. When a Ti-Nb alloy is cooled, the magnitude of the internal stress level in the material is expected to change as a result of additional thermal mismatches between grains or phases. In the schematic diagram, the magnitude of the internal stress is represented by the red arrow. If the internal stress level (red arrow) does not exceed the required critical stress (black arrow),

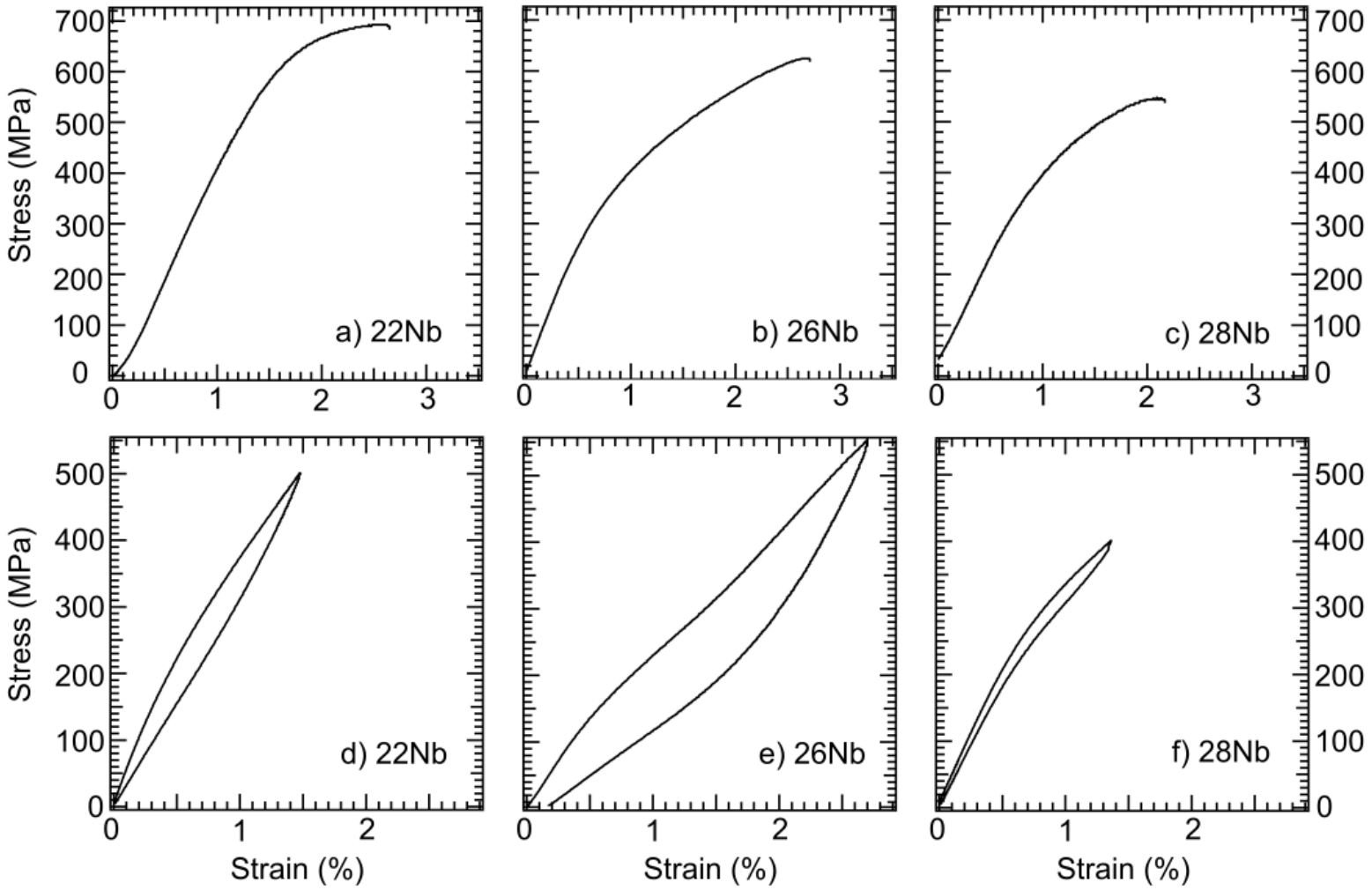

Fig. 6.4 Tensile curves to failure for Ti-Nb alloys containing a) 22, b) 26 and c) 28 at.% Nb. Cyclic tensile curves to a maximum stress approximately 100 MPa below the yield stress of Ti-Nb alloys containing d) 22, e) 26, and f) 28 at.% Nb

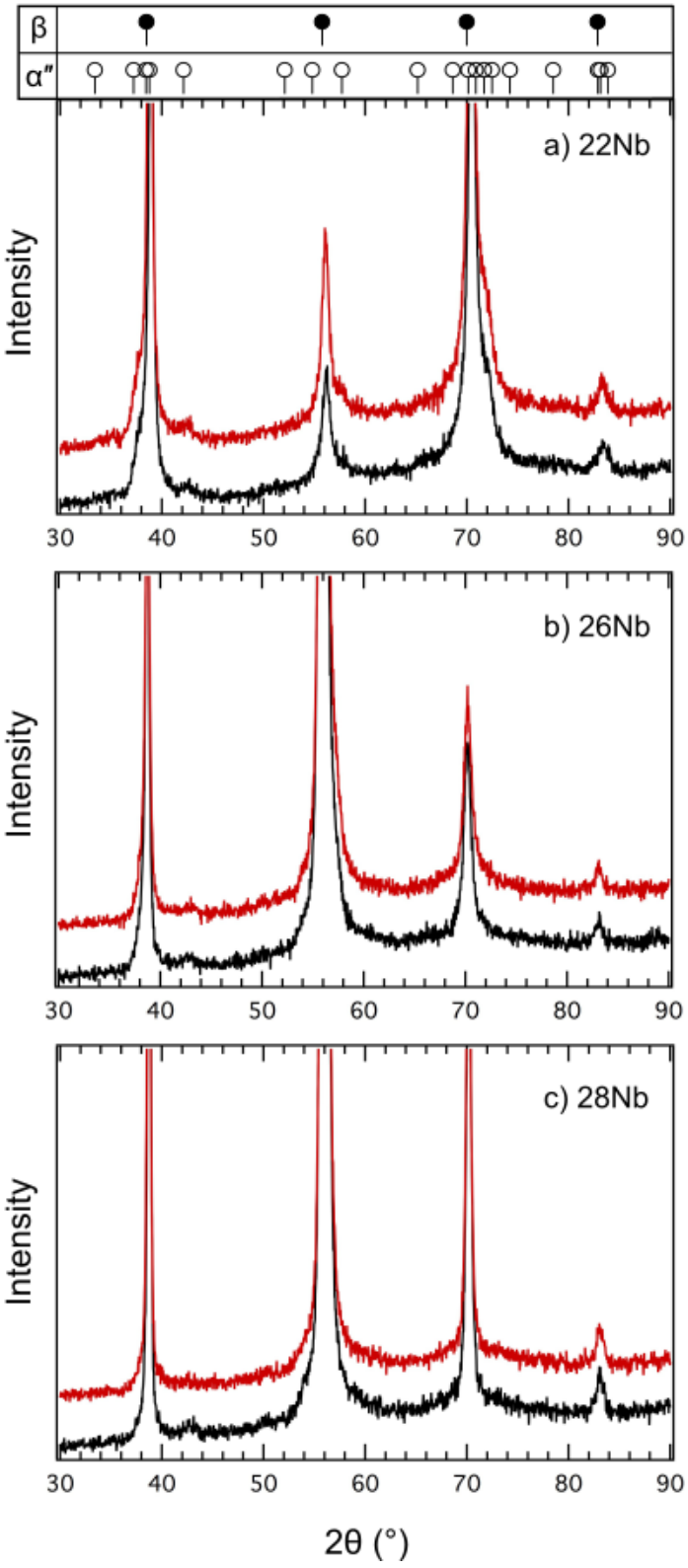

Fig. 6.5 A comparison of the XRD patterns prior to and after the tensile hysteresis loop for a) Ti-22Nb, b) Ti-26Nb and c) Ti-28Nb. Peaks corresponding to the β phase are observed in all samples before and after loading. Some shoulders on these β peaks could be attributed to the α'' phase, but no significant changes were observed in any alloy after loading.

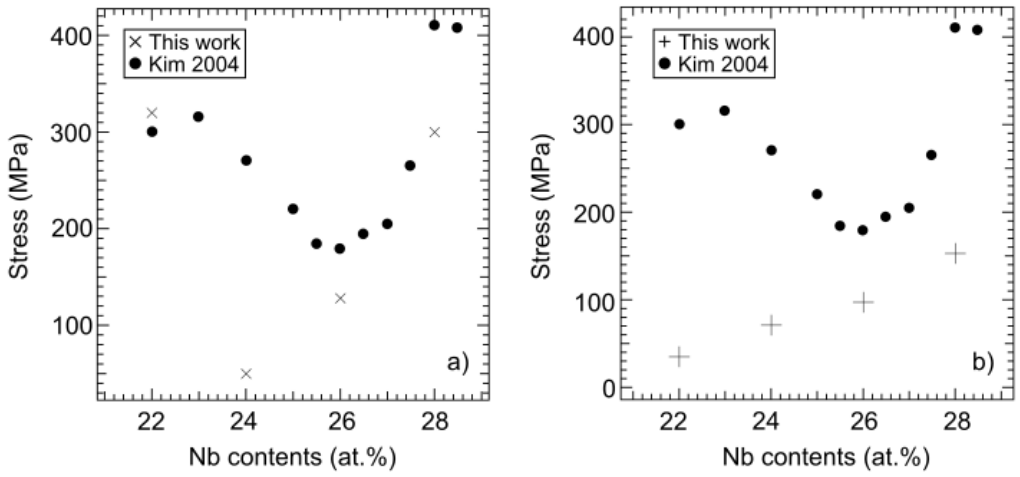

Fig. 6.6 The critical stress value where the tensile curves for Ti-(22-28)Nb alloys deviated from the linear elastic deformation as a function of niobium contents using a) the tensile tests to failure, and b) hysteresis loop data. Data collected from the larger scale tensile results lead to a "V"-shaped trend, similar to previous work [12]. However, data collected from the hysteresis loops, which focus more on the non-linear elastic behaviour showed a linear behaviour.

the $\beta \rightarrow \alpha''$ transformation will not occur. Above the M_s temperature, the magnitude of the internal stress level (red arrow) does not exceed the critical stress (defined by the black arrow) and the thermally driven transformation does not occur. Below M_s, the internal stress level exceeds the critical stress, and the transformation can take place. As the niobium content of an alloy is increased, the Gibbs energy curve decreases as the β phase becomes more stable. Hence, the magnitude of the force required to drive the $\beta \rightarrow \alpha''$ transformation increases, and, consequently, so does the critical stress required. Therefore, samples that contain more niobium need to be reduced to lower temperatures for the transformation to become favourable. This is because at lower temperatures the difference between the Gibbs energy curves for the β and α'' phases gets smaller and the internal stress level of the sample is more likely to exceed the critical stress that is required for the transformation. Hence, the decrease in M_s can be explained in terms of both thermodynamics and the total stress based mechanism that was proposed in chapters 3 and 4.

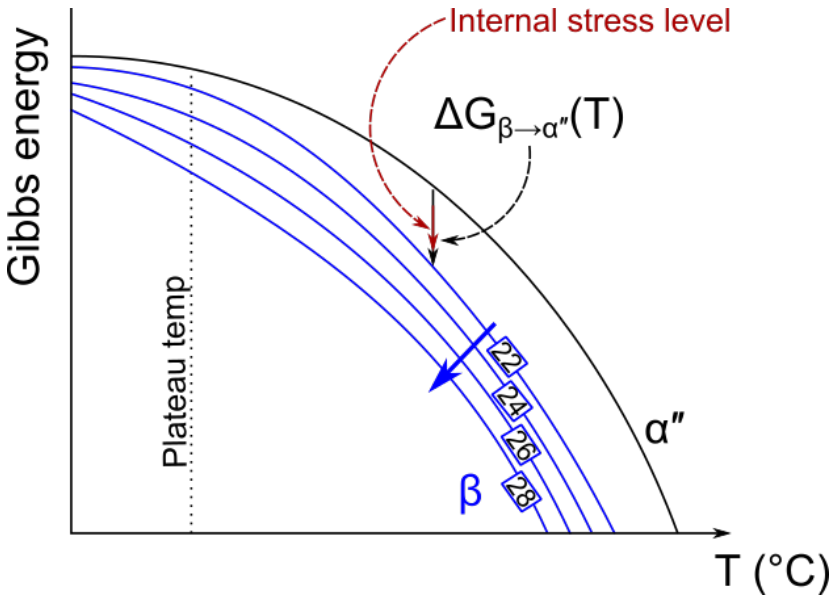

Fig. 6.7 A schematic diagram showing the Gibbs energy as a function of temperature for Ti-Nb alloys with an increasing amount of Nb. The black arrow represents the difference in Gibbs energy values that correspond to the critical stress required to induce the $\beta \rightarrow \alpha''$ transformation. The red arrow shows an example of how the magnitude of the internal stress level may not exceed this critical value, and, hence, the $\beta \rightarrow \alpha''$ transformation will not occur if this is the case. The plateau temperature represents the temperature when the magnitude of the red arrow is smaller than the black arrow during cooling. For simplicity, this plot does not consider the effect of increasing enthalpy as the temperature is increased.

The effect on the plateau temperature

The plateau temperature refers to the temperature where the intensity of the $(021)_{\alpha''}$ diffraction peak appeared to reach a constant value when a Ti-Nb sample in the CR condition was cooled from 350°C to -196°C. The value of this temperature was observed to decrease in Ti-Nb alloys with an increasing niobium content, as shown in figure 6.8. This observation can also be explained using the schematic diagram in figure 6.7. At temperatures below the plateau temperature, the intensity of the $(021)_{\alpha''}$ diffraction peak was observed to remain constant, indicating that the critical stress required to drive the $\beta \rightarrow \alpha''$ transformation had not been exceeded. Therefore, below the plateau temperature, the change in the magnitude of the internal stress level upon cooling, must not be sufficient enough to account for the revised difference in Gibbs energies at the new temperature. As the niobium content of a Ti-Nb alloy was increased, the Gibbs energy curve for the β phase decreased. As a result, the driving force to enable the $\beta \rightarrow \alpha''$ transformation is expected to increase at a given temperature with alloys that contain a larger amount of Nb. If the change in the internal stresses that result from thermal mismatches are assumed to be dependent on the microstructural condition only, and not the composition, the magnitude of the red arrow in figure 6.7 would not change between these alloys. Therefore, as the amount of Nb in Ti-Nb alloys was increased, the plateau temperature is expected to move to lower temperatures, because as the Gibbs energy curve decreases, the magnitude of the driving force is smaller at lower temperatures. Critically, the decrease in plateau temperature can also be explained in terms of the thermodynamics and the total stress based mechanism.

6.4.2 Stress-strain behaviour in Ti-Nb alloys

All of the Ti-Nb alloys that were used in this study were subjected to the same amount of cold rolling and the subsequent heat treatments. Whilst it could not be guaranteed that the exact conditions of these processing routes were the same, it is assumed that the internal stress level within the samples was similar. Since the total stress level of a sample can be expressed as a sum of the internal and external stresses, the values for the applied stresses of the Ti-Nb samples that contained different amounts of niobium can be directly compared with the critical transformation stresses at room temperature.

The M_s temperatures that were recorded for the cold rolled Ti-Nb alloys suggested that at room temperature, a small amount of α'' should be present in all cases prior to loading, even though laboratory based XRD measurements were unable to detect its presence. This indicated that at room temperature, the internal stress level in each material must lie just below the critical transformation stress that is defined by the difference in Gibbs energy of the β and α'' phases at room temperature. Therefore, the $\beta \rightarrow \alpha''$ transformation was expected to occur soon after a stress was applied to all of the samples. Despite this, a linear elastic response was still observed in the stress-strain curves recorded in all cases. It is suggested that in order to see the occurrence of the $\beta \rightarrow \alpha''$ transformation in these stress-strain curves, a significant amount of the transformation must have occurred. Whilst the critical stress value where these stress-strain curves began to deviate from a linear relationship cannot be attributed to the initial onset of the $\beta \rightarrow \alpha''$ transformation, it is thought that this value may provide an indication of the ease of the transformation in these alloys. Since the critical stress was observed to increase for alloys that contained more Nb, it is suggested that more additional stress is required to reach similar amounts of transformation strain. This indicated that the $\beta \rightarrow \alpha''$ transformation was less favourable in alloys that contained more Nb. This was unsurprising, since the difference in the Gibbs energies of the phases increases with an increased niobium content, which meant that that $\beta \rightarrow \alpha''$ transformation was less thermodynamically favourable.

6.4.3 A comparison of the datasets collected here with those in the literature

Difference in M_s

When alloys that contain between 22 to 28 at.% Nb were cooled from 350°C, the intensity of the $(021)_{\alpha''}$ diffraction peak increased when the temperature was cooled below a critical start temperature. In the literature this is often referred to as the M_s temperature for the alloy compositions. However, the work in chapters 3, 4 and 5 have conclusively shown that the microstructural condition of the sample will have an effect upon this value. Therefore, for clarity, in this discussion the M_s temperature will be used to refer to the start temperature for a given sample, which includes the microstructural condition as well as the alloy composition.

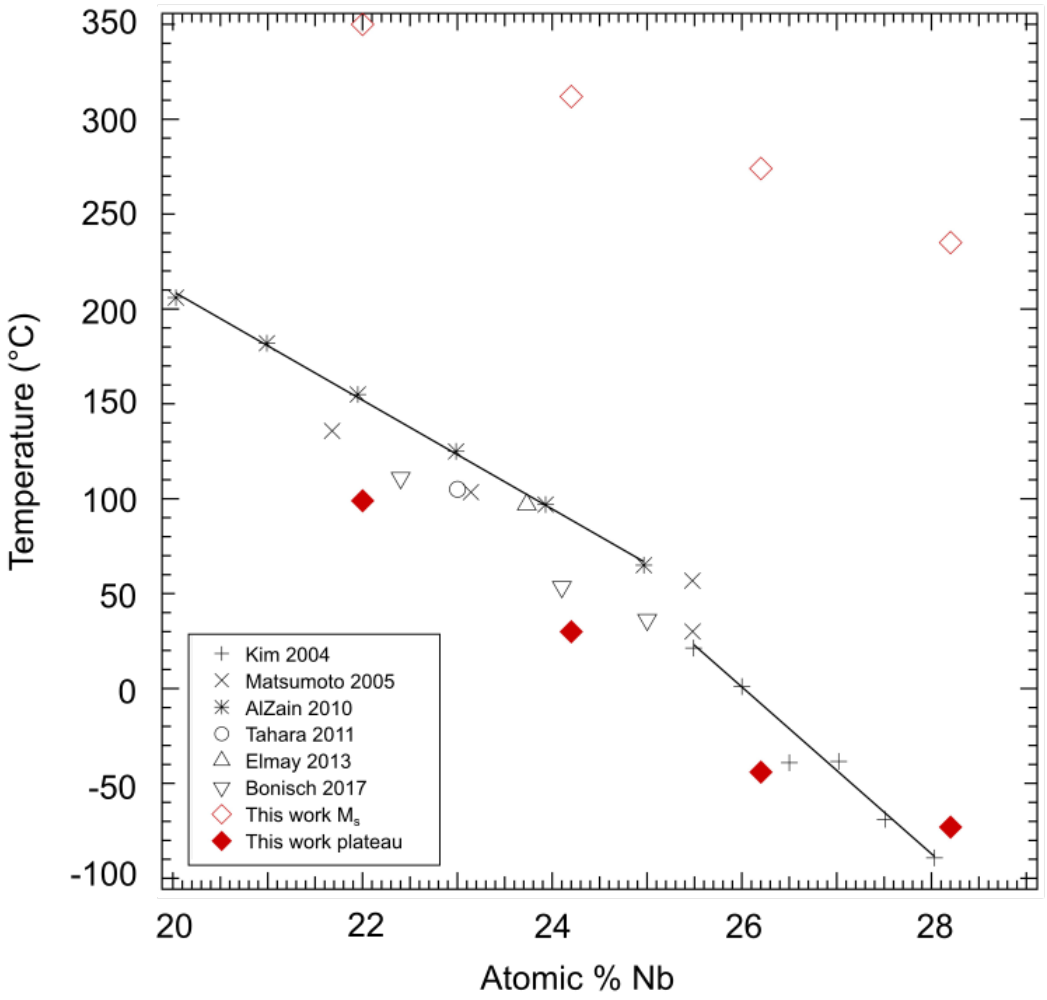

Fig. 6.8 Summary of the M_s temperatures reported in previous studies for the Ti-Nb system. The data from this work has been added to enable comparisons between datasets.

Table 6.3 Examples of manufacturing processes used in previous literature to make Ti-Nb alloys.

Study reference	Manufacturing process
Kim 2004 [12]	Arc melted, cold rolled to 95%, heated at 900°C for 30 minutes and water quenched
Al-Zain 2010 [19]	Arc melted, homogenised at 1000°C for 2 hours, cold rolled to 98.5%, heated at 700°C for 10 minutes and water quenched
Bönisch 2017 [20]	Cold crucible cast, homogenised at 1000°C for 24 hours and water quenched

The M_s temperatures that were determined in this work are compared with those reported within the literature in figure 6.8. The current values that are reported in the literature showed a maximum discrepency of $\sim$ 50°C within the composition range shown. Therefore, it seemed surprising that the M_s values that were determined here, were over 150°C larger than the highest values that had been reported in the current literature. The total stress based mechanism would suggest that the samples in this study had a larger internal stress level than those in previous work, since the M_s temperature was higher. To investigate the potential reasons for this difference in the internal stress level, the processing routes that were used to make the alloys in three studies are compared with the processes used here.

Table 6.3 summarises the amount of cold work and the subsequent heat treatments that were used in three of the most referenced pieces of work that have investigated the M_s temperatures of Ti-Nb alloys [12, 19, 20]. Before the effect of the microstructural condition of the samples in these studies are compared, it is important to consider the effects of any differences in the alloy compositions on the M_s temperatures that have been reported. However, this was difficult to identify accurately because out of the three studies, Bönisch et al [20] were the only authors to measure the actual composition of the alloys after they were processed, rather than assuming that the nominal compositions were suitable approximations. Despite this, over the next few sections in this discussion, the differences in the M_s temperatures that have been reported in these pieces of work have been justified in terms of the differences in composition as well as their microstructural condition.

Example 1 Figure 6.8 shows the three values for the M_s temperature that were measured by Bönisch et al [20]. These values formed a straight line trend that decreased in value with an increasing niobium content. As an example, the alloy with the composition Ti-24.9Nb-0.39O will be compared to the Ti-24.2Nb-0.2O used here. The difference in M_s that should result from this composition difference can be approximated using previously determined values of -43°C/at.% [12] (for niobium) and -160°C/at.% [45] (for oxygen), which predict Ti-24.9Nb-0.39O to have an M_s 66°C below that of Ti-24.2Nb-0.2O. Therefore, the discrepency of > 300°C must originate from the contrasting internal stress levels in the samples. The homogenisation at 1000°C compared with the CR condition here, is expected to have resulted in a microstructure that contained a much larger grain size and a lower dislocation density. Consequently, it is suggested that the more equiaxed grain structure and fewer dislocations in the solution treated alloy, reduced the internal stress level, which, in turn, reduced the value for M_s.

Additionally, the Ti-24.2Nb-0.25O sample in chapter 3 that was heated to 900°C for 5 minutes, showed no evidence for the $\beta \rightarrow \alpha''$ transformation when cooled to -196°C, indicating that the M_s temperature was below -196°C.

There were two main differences between this sample, and the Ti-24.9Nb-0.39O studied by Bönisch et al [20]. The first, was the β grain size of the samples, which were found to be 30 μm and 200 μm respectively, and, the second, was the initial phase constitution of the samples. Since data in chapter 5, suggested that the grain size did not have a significant effect upon the stress-induced transformation behaviour in a Ti-2448 alloy, it is suggested that the difference in the initial phase constitution of these samples had resulted in the measured difference in the M_s temperatures. The methods that are shown in table 6.3, indicated that the sample that was investigated by Bönisch et al [20] had been quenched from 1000°C. Therefore, since the M_s temperature that corresponded to this alloy was much higher than that value that had been recorded for the solution treated Ti-24.2Nb-0.25O, the additional internal stress is thought to have resulted from this quench.

Example 2 In a similar study by Al-Zain et al. [19], the target compositions were assumed to be the same as the actual composition of the alloy that had been arc melted. Neither the true values for the contents of Nb or O were known for the samples that were investigated,

and, discrepencies from the following predicted differences in M_s using the differences in compositions between alloys are inevitable.

A comparison of the concentrations of the Ti-24Nb alloy studied by Al-Zain et al. [19] with Ti-24.2Nb-0.2O in the CR condition studied here is predicted to result in a difference in M_s of 34.7°C. However, the majority of this value originated from the difference in O, which required the assumption that the alloy that was studied contained no O. However, this assumption cannot be true, since an oxide layer was removed from the surface after the heat treatment, suggesting that oxygen must have been present in the samples [19]. Despite this, the predicted difference of 34.7°C cannot solely account for the significantly larger differences that were shown in figure 6.8.

The alloys studied by Al-Zain et al. [19] were arc melted, and homogenised at 1000°C prior to cold rolling to a reduction ratio slightly higher than used here. After this, the alloys were heat treated at 700°C for 10 minutes followed by a final water quench. The resultant M_s value was reported as 97°C, which was 43°C above the Ti-24.9Nb-0.39O sample studied by Bönisch et al [20], 258°C below CR Ti-24.2Nb-0.2O, and over 200°C above the M_s for ST Ti-24.2Nb-0.25O.

The solution treatment that was used by Bönisch et al [20] was at a higher temperature, and for a considerably longer amount of time. Therefore, it is suggested that the difference in 43°C had arisen from the compositional differences as well as the expected lower internal stress level of the alloy that was heat treated for much longer.

The difference of 258°C between the Ti-24Nb alloy studied by Al-Zain et al. [19] and the CR Ti-24.2Nb-0.2O sample studied here is expected to have arisen from the much larger dislocation density in the CR sample. It is suggested that the solution treatment at 700°C allowed more time for dislocation motion in the Ti-24Nb sample to occur, which, may have resulted in the internal stress level of the sample decreasing.

In addition to this, the sample studied by Al-Zain et al. [19] was measured to have an M_s value over 200°C higher than that of the Ti-24.2Nb-0.25O in the ST condition. It is suggested that the alloys studied by Al-Zain et al. [19], that was quenched, contained a higher level of internal stress than the solution treated alloy that was studied here, which was cooled at

a much slower rate from 900°C, therefore, accounting for the increase in the recorded M_s temperature.

Critically, the effect of niobium content on the value of M_s showed a similar linear trend between the dataset collected in this study for cold rolled Ti-Nb alloys, and the results reported by Al-Zain et al. [19]. Both linear trendlines were observed to take a similar gradient, and the values of M_s were offset by ~ 215°C, which could be attibuted to the additional internal stress level introduced through the higher dislocation density in the cold rolled alloys. The slight difference between the gradients of the linear trends are suggested to be as a result of the different oxygen content between the alloys in the separate studies.

Example 3 The final example that will be used here, compares the M_s values for the cold rolled Ti-26.1Nb-0.22 and Ti-28Nb-0.22 alloys studied here, with the solution treated Ti-26Nb and Ti-28Nb alloys that were studied by Kim et al. [12]. Once again, the target compositions were used to describe the final compositions for these alloys. Therefore, the effects of any differences in the alloy composition are difficult to determine. Despite this, as in the previous two examples, the large difference between the M_s values are expected to have resulted from the different microstructural conditions of the samples. The cold rolled Ti-26.1Nb-0.22 and Ti-28Nb-0.22 alloys are expected to contain a much higher internal stress level than the Ti-26Nb and Ti-28Nb alloys that were solution treated at 900°C for 30 minutes, which justified their higher M_s values. It may be expected that the M_s temperature for the Ti-26Nb and Ti-28Nb alloys studied by Kim et al. [12] should be similar to that of the solution treated Ti-24.2Nb-0.25O alloy studied in chapters 3 and 4, which was shown to have an M_s value below -196°C. However, alloys studied by Kim et al. [12] were quenched from 900°C, which is expected to have introduced more internal stresses than in the alloys in this work, which were cooled at a slower rate. Hence, the quench-induced are thought to have resulted in the higher values for M_s.

Another noticeable difference between datasets in this work, and by Kim et al. [12] is the gradient of the linear trendline shown in figure 6.8. The gradient of their trendline appears much steeper than those that have been reported in other studies [19, 20], suggesting that these results may be anomalous. However, nothing in the paper concerning the processing methods, or the measurement techniques used to determine the M_s values provide an indication why

they might be incorrect. Since only two alloy compositions investigated in this work overlap with those that were also studied in the work by Kim et al. [12], it is proposed that additional data is required to make further statements with respect to the difference in the trendline gradient.

6.5 Conclusion and future work

The M_s temperatures that were recorded for Ti-Nb alloys in the cold rolled condition decreased as the niobium content was increased. The linear trendline took a negative gradient that was similar in value to those previously reported in the literature, however, the magnitudes of the M_s temperatures were $\sim$ 150 MPa larger than any of the values reported in the current literature. This difference was attributed to the higher dislocation density in the cold rolled samples, compared with samples in the literature, which had been solution treated and quenched. The internal stresses that had resulted from these rapid cooling rates justified why the M_s temperatures that were recorded in the current literature were above -196°C, whereas the solution treated Ti-24Nb alloy that was studied in chapter 4, which was cooled at a much slower rate in was not.

Three case studies were used to demonstrate that the range in the transformation temperatures that have been presented in the current literature for Ti-Nb alloys can be explained using the total stress based mechanism and the relative Gibbs energies of the β and α'' phases.

In future work, the M_s temperature for more Ti-Nb alloys below 22 at.% Nb and above 28 at.% Nb should be determined using *in situ* diffraction measurements. It is critical that the manufacturing procedure is replicated as close as possible to the methods used here, to maintain a similar level of internal stress. These experiments should provide more information on the dependence of the transformation temperatures on the niobium content of alloys that form the α'' martensite phase.

Chapter 7

Conclusions and future work

7.1 The new total stress based mechanism and its meaning for the future of engineering applications

Current temperature based theories cannot explain the differences in the transformation behaviour of Ti-24Nb (at.%) in two different microstructural conditions. The lack of the $\beta \rightarrow \alpha''$ transformation when solution treated Ti-24Nb (at.%) was cooled from 350°C to -196°C indicated that above -196°C, the Gibbs energy curve of the β phase must lie below that of the α'' phase. The same alloy in the cold rolled condition began to transform when the temperature was reduced below 190°C in the study in chapter 3, indicating that the internal stress level of the cold rolled material was sufficient to make the $\beta \rightarrow \alpha''$ transformation thermodynamically favourable below 190°C. When the temperature was reduced below -60°C, the $\beta \rightarrow \alpha''$ transformation ceased, and the internal stress level below this temperature was insufficient to drive the transformation any further. A total stress based approach was proposed to explain the difference in the transformation start temperatures in these two sample conditions, and the lack of additional transformation below a critical temperature.

This new total stress based mechanism was further validated by applying a stress to the Ti-24Nb (at.%) alloy in the cold rolled condition over a temperature range from -196°C to 30°C. In this study, the martensite start temperature was observed to increase to 312°C as detailed in chapter 4. The tensile samples that were used in the studies described in chapters

3 and 4 were cut from different cold rolled strips of material, which may have accounted for this difference. For example, the microstructural condition of the individual tensile samples may have been different for two tensile samples that were cut from different parts of the cold rolled strip. A tensile specimen that was cut from the very end of the strip may have been cold rolled to a different extent than a specimen that was cut from the centre. The image that was shown in figure 2.1 demonstrated how bent a cold rolled strip could be, which could also have indicated that the internal stress level of different specimens that were cut from different sections of the strip could differ.

Despite the difference in the martensite start temperature, the *in situ* diffraction data indicated the immediate occurrence of the $\beta \rightarrow \alpha''$ transformation when Ti-24Nb (at.%) in the cold rolled condition was subjected to an externally applied load at all temperatures that were tested between -196°C and 30°C. The significance of this result from an engineering point of view is very promising. Previously, the current temperature based theories suggested that a stress-induced transformation could only occur if a metastable β-Ti alloy was loaded above its M_s temperature [33], which limited the temperature range over which these alloys was thought to be able to be used. However, these results, that showed that full superelastic recovery of these materials can occur > 450°C below their recorded start transformation temperature thereby allowing these alloys to be considered for a much wider range of applications.

7.2 Microstructural features that give rise to the difference in transformation behaviour

The microstructural condition of metastable β-Ti alloys has been shown to significantly affect the temperatures when the $\beta \rightarrow \alpha''$ transformation can occur. The work in chapter 5 detailed the effect of dislocation density and grain size on the transformation behaviour. Problems arose in the study that considered the dislocation density of Ti-2448 (wt.%), because the α'' was unexpectedly retained in the microstructure despite a number of different heat treatments being conducted to remove it prior to loading. Additionally, the use of a laboratory based X-ray diffraction did not allow the dislocation densities of the samples that were rolled to different reduction ratios to be numerically evaluated. The investigations into the effect of

the grain size on the tensile behaviour were more successful, and indicated that the grain size did not significantly change the stress-induced transformation behaviour. These conclusions are critically important to understanding the effect of the microstructural condition on the $\beta \rightarrow \alpha''$ transformation in metastable β-Ti alloys. Additional investigations into which microstructural features contribute most to the value of the internal stress level must be prioritised in future work. In particular, the effect of the dislocation density and grain structure must be investigated further. In this work, the small, elongated grain structure of Ti-2448 (wt.%), which contained a high dislocation density, was observed to begin to transform as soon as an external load was applied and exhibit full superelastic recovery at room temperature. However, the transformation strain that was achieved during the tensile tests was $\sim \frac{1}{3}$ smaller than the magnitude of strain that was achieved when the solution treated Ti-2448 (wt.%) samples were loaded. If, in the future, the effect of the orientation and size of the grain structure on the transformation strains can be understood further, the superelastic properties of metastable β-Ti alloys may be able to be optimised towards a given stress condition. The engineering implications of being able to adjust the microstructural condition of a metastable β-Ti alloy towards specific applications may open up the potential use of these alloys in a wide range of new industries. This is especially the case if the key transformation temperatures are no longer a part of the alloy design.

7.3 The ω phase

The effect of the ω phase on the transformation behaviour has not been considered in depth in this work. Some studies have reported that during cooling, the transformation from the β phase to α'' and ω phases compete, and are dependent upon the cooling rate [84, 106]. The $\beta \rightarrow \alpha''$ transformation reportedly favours fast cooling rates, whilst the $\beta \rightarrow \omega$ transformation favours slower rates. Here, both the α'' and ω phases have been shown to increase in volume fraction in Ti-24Nb (at.%) during the cool from 350°C. The form of this ω phase remained unclear since similar observations within the literature are in their infancy [83]. Therefore, to understand the effect of this cooled form of the ω phase, the ω itself must be understood. Whilst the effect of the ω phase is vitally important if metastable β-Ti alloys are going to be

applied to engineering applications, the amount of work that this would entail could not be considered any further in this work. Therefore, in this work, since both the thermally induced and the stress-induced $\beta \rightarrow \alpha''$ transformation were observed in a sample that contained a significant amount of ω, the effect of the ω phase was not considered any further. It is strongly recommended that the effect of this form of ω, and the isothermal form on the martensitic transformation are considered in detail in the future, since this phase is an integral part of many titanium microstructures.

7.4 Final comments

In summary, the data that has been presented in this work has concluded that current temperature based theories that are used to describe the superelastic behaviour in Ni-Ti alloys cannot be used to explain the similar behaviour that is observed in Ti-Nb-based alloys. *In situ* diffraction data has been vital to pinpointing the exact temperatures where the martensitic transformation began to occur during cooling, and when the reverse transformation started upon heating. It is suggested that *in situ* experiments are used as the foundation for further investigations into the transformation behaviour in metastable beta-titanium alloys, since other indirect measurements have led to inaccurate conclusions. Following work should focus on investigating the effect of the omega phase on the martensitic transformation to identify if its presence could be used to improve the superelastic properties.

References

[1] C. Lexcellent. *Shape-memory alloys handbook*. 2013.

[2] K. Yamauchi, T. Ohkata, and S. Miyazaki. *Shape memory and superelastic alloys: technologies and applications*. 2011.

[3] L. Lecce and A. Concilio. *Shape memory alloy engineering for aerospace, structural and biomedical applications*. 2015.

[4] D. J. Hartl and D. C. Lagoudas. Aerospace applications of shape memory alloys. *Proc. Inst. Mech. Eng. Part G J. Aerosp. Eng.*, 221(4):535–552, 2007.

[5] A. Mamoozadeh. The aerospace applications of Ni-Ti as a superelastic material. pages 1–9, 2018.

[6] W. J. Buehler, J. V. Gilfrich, and R. C. Wiley. Effect of low-temperature phase changes on the mechanical properties of alloys near composition Ti-Ni. *J. Appl. Phys.*, 34(5):1475–1477, 1963.

[7] T. W. Duerig, A. Pelton, and D. Stöckel. An overview of nitinol medical applications. *Mater. Sci. Eng. A*, 273-275:149–160, 1999.

[8] M. Baumann. Nickel-titanium: Options and challenges. *Dent. Clin. North Am.*, 48(1):55–67, 2004.

[9] K. Otsuka and X. Ren. Physical metallurgy of Ti-Ni-based shape memory alloys. *Prog. Mater. Sci.*, 50(5):511–678, 2005.

[10] D. Kapoor. Nitinol for medical applications: A brief introduction to the properties and processing of Nickel-Titanium shape memory alloys and their use in stents. *Johnson Matthey Technol. Rev.*, 61(1):66–76, 2017.

[11] S. Miyazaki, H. Y. Kim, and H. Hosoda. Development and characterization of Ni-free Ti-base shape memory and superelastic alloys. *Mater. Sci. Eng. A*, 438-440(SPEC. ISS.):18–24, 2006.

[12] H. Y. Kim, H. Satoru, J. Il Kim, H. Hosoda, and S. Miyazaki. Mechanical Properties and Shape Memory Behavior of Ti-Nb Alloys. *Mater. Trans.*, 45(4):1090–1095, 2004.

[13] H. Y. Kim, Y. Ikuhara, J. Il Kim, H. Hosoda, and S. Miyazaki. Martensitic transformation, shape memory effect and superelasticity of Ti-Nb binary alloys. *Acta Mater.*, 54(9):2419–2429, 2006.

[14] H. Y. Kim, J. Il Kim, T. Inamura, H. Hosoda, and S. Miyazaki. Effect of thermomechanical treatment on mechanical properties and shape memory behavior of Ti-(26-28) at.% Nb alloys. *Mater. Sci. Eng. A*, 438-440(SPEC. ISS.):839–843, 2006.

[15] H. Y. Kim, S. Miyazaki, Y. Ikuhara, J. Il Kim, and H. Hosoda. Martensitic transformation and superelastic properties of Ti-Nb base alloys. *Mater. Trans.*, 56(5):625–634, 2015.

[16] K. Otsuka and C.M. Wayman. *Shape Memory Materials*. Cambridge University Press, 1998.

[17] J. Ma, I. Karaman, and R. D. Noebe. High temperature shape memory alloys. *Int. Mater. Rev.*, 55(5):257–315, 2010.

[18] H. Matsumoto, S. Watanabe, and S. Hanada. Beta Ti-Nb-Sn Alloys with Low Young's Modulus and High Strength. *Mater. Trans.*, 46(5):1070–1078, 2005.

[19] Y. Al-Zain, H.Y. Kim, H. Hosoda, T. H. Nam, and S. Miyazaki. Shape memory properties of Ti-Nb-Mo biomedical alloys. *Acta Mater.*, 58(12):4212–4223, 2010.

[20] M. Bönisch, A. Panigrahi, M. Calin, T. Waitz, M. Zehetbauer, W. Skrotzki, and J Eckert. Thermal stability and latent heat of Nb-rich martensitic Ti-Nb alloys. *J. Alloys Compd.*, 697:300–309, 2017.

[21] A. D Pelton. *Thermodynamics and phase diagrams of materials*. American Cancer Society, 2013.

[22] C. Leyens and M. Peters. *Titanium and Titanium Alloys: Fundamentals and applications*. Wiley-VCH Verlag GmbH & Co. KGaA, 2003.

[23] R. Kolli and A. Devaraj. A review of metastable beta Titanium alloys. *Metals (Basel).*, 8(7):506, 2018.

[24] P. J Bania. Beta titanium alloys and their role in industry. *J. Miner. Met. Mater. Soc.*, 46:16–17, 1994.

[25] G. Lütjering and J. C. Williams. *Titanium: Engineering materials and processes*. Springer Science & Business Media, 2007.

[26] B. Hatt and V G Rivlin. Phase transformations in superconducting Ti-Nb alloys. *J. Phys. D. Appl. Phys.*, 1(9):1145–1149, 2002.

[27] D. De Fontaine. Mechanical instabilities in the b.c.c. lattice and the beta to omega phase transformation. *Acta Metall.*, 18:275–279, 1970.

[28] S. K. Sikka, Y. K. Vohra, and R. Chidambaram. Omega phase in materials. *Prog. Mater. Sci.*, 27(3-4):245–310, 1982.

[29] Y. Yang. Investigation of the martensitic transformation and the deformation mechanisms occurring in the superelastic Ti-24Nb-4Zr-8Sn alloy. *Mater. Chem.*, 2015.

[30] T. W. Duerig, K.N. Melton, D. Stöckel, and C.M. Wayman. *Engineering Aspects of Shape Memory Alloys*. 1990.

[31] B. Sun, X. Meng, Z. Gao, and W. Cai. Crystallography study on the internal twinning of Ti–Nb-based shape memory alloys. *Cryst. Res. Technol.*, 53(8):1–5, 2018.

[32] K. Otsuka and K. Shimizu. On the crystallographic reversibility of martensitic transformations. *Scr. Metall.*, 11:757–760, 1977.

[33] K. Otsuka and K. Shimizu. Pseudoelasticity and shape memory effects in alloys. *Int. Met. Rev.*, 31(1):93–114, 1986.

[34] S. Miyazaki and K. Otsuka. Development of shape memory alloys. *ISIJ Int.*, 29(5):353–377, 1989.

[35] M. Wang, M. Jiang, G. Liao, S. Guo, and X. Zhao. Martensitic transformation involved mechanical behaviors and wide hysteresis of Ni-Ti-Nb shape memory alloys. *Prog. Nat. Sci. Mater. Int.*, 22(2):130–138, 2012.

[36] Y. Q. Zhang, S. Yong Jiang, Y.N. Zhao, and M. Tang. Influence of cooling rate on phase transformation and microstructure of Ti-50.9%Ni shape memory alloy. *Trans. Nonferrous Met. Soc. China (English Ed.*, 22(11):2685–2690, 2012.

[37] H. C. Tong and C. M. Wayman. Characteristic temperatures and other properties of thermoelastic martensites. *Acta Metall.*, 22(7):887–896, 1974.

[38] L. Kaufman and M. Cohen. Thermodynamics and kinetics of martensitic transformations. *Prog. Met. Phys.*, 7(C):165–246, 1958.

[39] H. Y. Kim and S. Miyazaki. Several issues in the development of Ti–Nb-based shape Memory alloys. *Shape Mem. Superelasticity*, 2(4):380–390, 2016.

[40] T. W. Duerig, R.M. Middleton, G.T. Terlinde, and J. C. Williams. Stress assisted transformation in Ti-10V-2Fe-3Al. *Titanium 1980, Science and Technology - Proceedings of the 4th International Conference on Titanium*, 1980.

[41] H. Matsumoto, Sadao Watanabe, Naoya Masahashi, and Shuji Hanada. Composition dependence of Young's modulus in Ti-V, Ti-Nb, and Ti-V-Sn alloys. *Metall. Mater. Trans. A Phys. Metall. Mater. Sci.*, 37(11):3239–3249, 2006.

[42] R. Davis, H. M. Flower, and D. R.F. West. Martensitic transformations in Ti-Mo alloys. *J. Mater. Sci.*, 14(3):712–722, 1979.

[43] M.J. Blackburn and J.A. Feeney. Stress-induced transformation in Ti-Mo alloys. 1970.

[44] N. T.C. Oliveira, G. Aleixo, R. Caram, and A. C. Guastaldi. Development of Ti-Mo alloys for biomedical applications: Microstructure and electrochemical characterization. *Mater. Sci. Eng. A*, 452-453:727–731, 2007.

[45] J. Il Kim, H. Y. Kim, H. Hosoda, and S. Miyazaki. Shape memory behavior of Ti-22Nb-(0.5-2.0)O(at%) biomedical alloys. *Mater. Trans.*, 46(4):852–857, 2005.

[46] Y. Al-Zain, H. Y. Kim, T. Koyano, H. Hosoda, and S. Miyazaki. A comparative study on the effects of the ω and α phases on the temperature dependence of shape memory behavior of a Ti-27Nb alloy. *Scr. Mater.*, 103:37–40, 2015.

[47] H. Y. Kim, Jie Fu, Hirobumi Tobe, J. Il Kim, and S. Miyazaki. Crystal structure, transformation strain, and superelastic property of Ti-Nb-Zr and Ti-Nb-Ta alloys. *Shape Mem. Superelasticity*, 1(2):107–116, 2015.

[48] M. Hansen, E. L. Kamen, H. D. Kessel, and D. J. McPhersen. Systems Titanium-Molybdenum and Titanium-Columbium. *Trans. AIME*, 191:881–888, 1951.

[49] R.I. Jaffee. The physical metallurgy of titanium alloys. *Prog. Met. Phys.*, 7:65–163, 1958.

[50] P. Duwez. The martensite transformation temperature in Ti binary alloys.pdf, 1953.

[51] A. B. Greninger. The martensite thermal arrest in iron-carbon and plain carbon steels. *Trans. Am. Soc. Met.*, 30:1, 1942.

[52] T. Sato, H. Seikiti, and Y.C. Huang. The Ms points of binary Titanium alloys. *J. Aust. Inst. Met.*, 5(2):149, 1960.

[53] K. S. Jepson, A. R. G. Brown, and J.A. Gray. The effect of cooling rate on the beta transformation in Titanium–Niobium and Titanium–Aluminium alloys, 1970.

[54] A. R. G. Brown, D. Clark, J. Eastabrook, and K. S. Jepson. The Titanium-Niobium System. *Nature*, 201:914–915, 1964.

[55] Y.C. Huang, S. Suzuki, H. Kaneko, and T. Sato. Thermodynamics of the Ms points in Titanium alloys. *Sci. Technol. Appl. Titan.*, pages 691–693, 1970.

[56] J.L. Murray. Phase diagrams of binary titanium alloys: The Niobium-Titanium system. *ASM Int.*, pages 188–194, 1987.

[57] M. Tahara, H. Y. Kim, T. Inamura, H. Hosoda, and S. Miyazaki. Lattice modulation and superelasticity in oxygen-added β-Ti alloys. *Acta Mater.*, 59(16):6208–6218, 2011.

[58] W. Elmay, F. Prima, T. Gloriant, B. Bolle, Y. Zhong, E Patoor, and Pascal Laheurte. Effects of thermomechanical process on the microstructure and mechanical properties of a fully martensitic titanium-based biomedical alloy. *J. Mech. Behav. Biomed. Mater.*, 18:47–56, 2013.

[59] M. Tahara, T. Inamura, H. Y. Kim, S. Miyazaki, and H. Hosoda. Role of oxygen atoms in α'' martensite of Ti-20 at.%Nb alloy. *Scr. Mater.*, 112:15–18, 2016.

[60] M. Tahara, H. Y. Kim, T. Inamura, H. Hosoda, and S. Miyazaki. Effect of nitrogen addition on superelasticity of Ti-Zr-Nb alloys. *Nippon Kinzoku Gakkaishi/Journal Japan Inst. Met.*, 72(12):955–959, 2008.

[61] M. Abdel-Hady, K. Hinoshita, and M. Morinaga. General approach to phase stability and elastic properties of beta-type Ti-alloys using electronic parameters. *Scr. Mater.*, 55(5):477–480, 2006.

[62] P. Castany, A. Ramarolahy, F. Prima, P. Laheurte, C. Curfs, and T. Gloriant. In situ synchrotron X-ray diffraction study of the martensitic transformation in superelastic Ti-24Nb-0.5N and Ti-24Nb-0.5O alloys. *Acta Mater.*, 88:102–111, 2015.

[63] R. Salloom, D. Reith, R. Banerjee, and S. G. Srinivasan. First principles calculations on the effect of interstitial oxygen on phase stability andmartensitic transformation in Ti–Nb alloys. *J. Mater. Sci.*, 53(16):11473–11487, 2018.

[64] P. Laheurte, A. Eberhardt, and M. J. Philippe. Influence of the microstructure on the pseudoelasticity of a metastable beta titanium alloy. *Mater. Sci. Eng. A*, 396(1-2):223–230, 2005.

[65] F. Sun, S. Nowak, T. Gloriant, P. Laheurte, A. Eberhardt, and F. Prima. Influence of a short thermal treatment on the superelastic properties of a titanium-based alloy. *Scr. Mater.*, 63(11):1053–1056, 2010.

[66] F. Sun, Y. Hao, S. Nowak, T. Gloriant, P. Laheurte, and F. Prima. A thermo-mechanical treatment to improve the superelastic performances of biomedical Ti-26Nb and Ti-20Nb-6Zr (at.%) alloys. *J. Mech. Behav. Biomed. Mater.*, 4(8):1864–1872, 2011.

[67] B. Sun, X. L. Meng, Z. Y. Gao, W. Cai, and L. C. Zhao. Effect of annealing temperature on shape memory effect of cold rolled Ti-16 at.%Nb alloy. *J. Alloys Compd.*, 715:16–20, 2017.

[68] A. Helth, S. Pilz, T. Kirsten, L. Giebeler, J. Freudenberger, M. Calin, J. Eckert, and A. Gebert. Effect of thermomechanical processing on the mechanical biofunctionality of a low modulus Ti-40Nb alloy. *J. Mech. Behav. Biomed. Mater.*, 65:137–150, 2017.

[69] T. Saito, T. Furuta, J. H. Hwang, S. Kuramoto, K. Nishino, N. Suzuki, R. Chen, A. Yamada, K. Ito, Y. Seno, T. Nonaka, H. Ikehata, N. Nagasako, C. Iwamoto, Y. Ikuhara, T. Sakuma. Multifunctional alloys obtained via a dislocation-free plastic deformation mechanism. *Science*, 300(5618):464–467, 2003.

[70] T. Furuta, S. Kuramoto, J. Hwang, K. Nishino, and T. Saito. Elastic deformation behavior of multi-functional Ti-Nb-Ta-Zr-O alloys. *Mater. Trans.*, 46(12):3001–3007, 2005.

[71] X. M. Ma and W. Sun. Characterization of deformation localization in cold-rolled metastable β-Ti-Nb-Ta-Zr alloy. *J. Alloys Compd.*, 509:294–298, 2011.

[72] Y. F. Xu, D. Q. Yi, H. Q. Liu, X. Y. Wu, B. Wang, and F. L. Yang. Effects of cold deformation on microstructure, texture evolution and mechanical properties of Ti-Nb-Ta-Zr-Fe alloy for biomedical applications. *Mater. Sci. Eng. A*, 547:64–71, 2012.

[73] C. Lan, Y. Wu, L. l. Guo, and F. Chen. Effects of cold rolling on microstructure, texture evolution and mechanical properties of Ti-32.5Nb-6.8Zr-2.7Sn-0.3O alloy for biomedical applications. *Mater. Sci. Eng. A*, 690(August 2016):170–176, 2017.

[74] F. Prima, F. Sun, W. El May, T. Gloriant, P. Laheurte, L. Jordan, P. Vermaut, R. Portier, and Y. L. Hao. Optimization of superelastic properties in Titanium-Niobium alloys using short-time thermal treatments. *Mater. Sci. Forum*, 738-739:554–558, 2013.

[75] B.E.O. Hall. The deformation and ageing of mild steel: III discussion of results. *Proc. Phys. Soc. Sect. B*, 64:747, 1951.

[76] N.J. Petch. The cleavage strength of polycrystals. *J. Iron Steel Inst.*, 173, 1953.

[77] E. S.N. Lopes, A. Cremasco, C. R.M. Afonso, and R. Caram. Effects of double aging heat treatment on the microstructure, Vickers hardness and elastic modulus of Ti-Nb alloys. *Mater. Charact.*, 62(7):673–680, 2011.

[78] E. L. Pang. *The effect of Zirconium additions on phase stability in metastable beta titanium-niobium alloys*. MPhil Thesis, University of Cambridge, 2016.

[79] A. P. Hammersley, S. O. Svensson, and A. Thompson. Calibration and correction of spatial distortions in 2D detector systems. *Nucl. Inst. Methods Phys. Res. A*, 346(1-2):312–321, 1994.

[80] H. Y. Kim. Texture and shape memory behavior of Ti-22Nb-6Ta alloy. *Acta Mater.*, 54:423–433, 2006.

[81] A. Josephine Prabha, S. Raju, B. Jeyaganesh, Arun Kumar Rai, Madhusmita Behera, M. Vijayalakshmi, G. Paneerselvam, and I. Johnson. Thermodynamics of $\alpha'' \rightarrow \beta$ phase transformation and heat capacity measurements in Ti-15 at.%Nb alloy. *Phys. B Condens. Matter*, 406(22):4200–4209, 2011.

[82] J. Il Kim, H. Y. Kim, T. Inamura, H. Hosoda, and S. Miyazaki. Shape memory characteristics of Ti-22Nb-(2-8)Zr (at.%) biomedical alloys. 403:334–339, 2005.

[83] S. Dubinsky, A. Korotitskiy, S. Prokoshkin, and V. Brailovski. In situ X-ray diffraction study of athermal and isothermal omega-phase crystal lattice in Ti-Nb-based shape memory alloys. *Mater. Lett.*, 168:155–157, 2016.

[84] N. B. D'yakonova, I. V. Lyasotskii, and Yu. L. Rodionov. Orthorhombic martensite and the ω phase in quenched and deformed titanium alloys with 20–24 at % Nb. *Russ. Metall.*, 2007(1):51–58, 2007.

[85] L. Héraud, P. Castany, D. Laillé, and T. Gloriant. In situ synchrotron X-ray diffraction of the martensitic transformation in superelastic Ti-27Nb and NiTi alloys: A comparative study. *Mater. Today Proc.*, 2(November):S917–S920, 2015.

[86] T. Grosdidier, Y. Combres, E. Gautier, and M. J. Philippe. Effect of microstructure variations on the formation of deformation-induced martensite and associated tensile properties in a β metastable Ti alloy. *Metall. Mater. Trans. A Phys. Metall. Mater. Sci.*, 31(4):1095–1106, 2000.

[87] A. Bhattacharjee, S. Bhargava, V. K. Varma, S. V. Kamat, and A. K. Gogia. Effect of β grain size on stress induced martensitic transformation in β solution treated Ti-10V-2Fe-3Al alloy. *Scr. Mater.*, 53(2):195–200, 2005.

[88] A. Paradkar, S.V. Kamat, A.K. Gogia, and B.P. Kashyap. Trigger stress for stress-induced martensitic transformation during tensile deformation in Ti-Al-Nb alloys: effect of grain size. *Metall. Mater. Trans. A*, 39(3):551–558, 2008.

[89] M. H. Cai, C. Y. Lee, and Y. K. Lee. Effect of grain size on tensile properties of fine-grained metastable β titanium alloys fabricated by stress-induced martensite and its reverse transformations. *Scr. Mater.*, 66(8):606–609, 2012.

[90] D. L. Moffat and U. R. Kattner. The stable and metastable Ti-Nb phase diagrams. *Metall. Trans. A*, 19(10):2389–2397, 1988.

[91] W. Y. Guo, M. Z. Quadir, and M. Ferry. The mode of deformation in a cold-swaged multifunctional Ti-Nb-Ta-Zr-O alloy. *Metall. Mater. Trans. A Phys. Metall. Mater. Sci.*, 44(5):2307–2318, 2013.

[92] R J Talling, R. J. Dashwood, M. Jackson, D. Dye On the mechanism of superelasticity in Gum metal. *Acta Mater.*, 57(4):1188–1198, 2009.

[93] V.A. Vorontsov, N. G. Jones, K.M. Rahman, and D. Dye. Superelastic load cycling of Gum Metal. *Acta Mater.*, 88:323–333, 2015.

[94] N G Jones, V.A. Vorontsov, and D. Dye. The behaviour of GUM metal (Ti-36Nb-2Ta-3Zr-0.3O wt.%) during superelastic cycling. In *Proc. 13th World Conf. Titan.*, pages 899–904, 2016.

[95] Y. Mantani and M. Tajima. Phase transformation of quenched α'' martensite by aging in Ti-Nb alloys. *Mater. Sci. Eng. A*, 438-440(SPEC. ISS.):315–319, 2006.

[96] A Nyayadhish, B C Maji, and M Krishnan. Martensitic transformation, omega transformation and pseudoelasticity in aged Ti-24 at.%Nb alloy. *Proc. Int. Conf. Martensitic Transform. ICOMAT-08*, pages 493–497, 2009.

[97] N.G. Jones, S L Raghunathan, and D. Dye. In-situ synchrotron characterization of transformation sequences in TiNi-based shape memory alloys during thermal cycling. *Metall. Mater. Trans. A Phys. Metall. Mater. Sci.*, 41:912–921, 2010.

[98] N. G. Jones and D. Dye. Martensite evolution in a NiTi shape memory alloy when thermal cycling under an applied load. *Intermetallics*, 19(10):1348–1358, 2011.

[99] J. Coakley, K. M. Rahman, V.A. Vorontsov, M. Ohnuma, and D. Dye. Effect of precipitation on mechanical properties in the β-Ti alloy Ti–24Nb–4Zr–8Sn. *Mater. Sci. Eng. A*, 655:399–407, 2016.

[100] C. H. Wang, M. Liu, P. F. Hu, J. C. Peng, J. A. Wang, Z. M. Ren, and G. H. Cao. The effects of α'' and ω phases on the superelasticity and shape memory effect of binary Ti-Mo alloys. *J. Alloys Compd.*, 720:488–496, 2017.

[101] Q. Li, J. Li, G. Ma, X. Liu, and D. Pan. Influence of ω phase precipitation on mechanical performance and corrosion resistance of Ti-Nb-Zr alloy. *Mater. Des.*, 111:421–428, 2016.

[102] E. L. Pang, E. J. Pickering, S. I. Baik, D. N. Seidman, and N G Jones. The effect of zirconium on the omega phase in Ti-24Nb-[0-8]Zr (at.%) alloys. *Acta Mater.*, 153:62–70, 2018.

[103] R J Talling, R. J. Dashwood, M. Jackson, and D. Dye. Compositional variability in gum metal. *Scr. Mater.*, 60(11):1000–1003, 2009.

[104] J. Zhang, Y. Liu, Y. Ren, Y. Huan, S. Hao, C. Yu, Y. Shao, Y. Ru, D. Jiang, and L. Cui. In situ synchrotron X-ray diffraction study of deformation behaviour and load transfer in a Ti2Ni-NiTi composite. *Appl. Phys. Lett.*, 105(4), 2014.

[105] J. Zhang, Y. Liu, Y. Huan, S. Hao, D. Jiang, Y. Ren, Y. Shao, Y. Ru, Z. Wang, and L. Cui. High damping NiTi/Ti3Sn in situ composite with transformation-mediated plasticity. *Mater. Des.*, 63:460–463, 2014.

[106] D. L. Moffat and D. C. Larbalestier. The competition between martensite and omega in quenched Ti-Nb alloys. *Metall. Trans. A*, 19:1677–1686, 1988.

[107] T Ahmed and H. J. Rack. Martensitic transformations in Ti-(16-26 at %) Nb alloys. *J. Mater. Sci.*, 31(16):4267–4276, 1996.

[108] E. Bertrand, P. Castany, and T. Gloriant. Investigation of the martensitic transformation and the damping behavior of a superelastic Ti-Ta-Nb alloy. *Acta Mater.*, 61(2):511–518, 2013.

[109] N. Sakaguchi, M. Niinomi, T. Akahori, J. Takeda, and H. Toda. Relationships between tensile deformation behavior and microstructure in Ti-Nb-Ta-Zr system alloys. 25:363–369, 2005.

[110] Y. Hao, S. J. Li, S. Y. Sun, and R. Yang. Effect of Zr and Sn on Young's modulus and superelasticity of Ti-Nb-based alloys. *Mater. Sci. Eng. A*, 441(1-2):112–118, 2006.

[111] W. Y. Guo, H. Xing, J. Sun, X. L. Li, J. S. Wu, and R. Chen. Evolution of microstructure and texture during recrystallization of the cold-swaged Ti-Nb-Ta-Zr-O alloy. *Metall. Mater. Trans. A Phys. Metall. Mater. Sci.*, 39 A(3):672–678, 2008.

[112] Q. Wei, Z. L. Pan, Y. H. Zhao, T. Topping, R. Z. Valiev, X. Z. Liao, E. J. Lavernia, and Y. T. Zhu. Effect of strain rate on the mechanical properties of a gum metal with various microstructures. *Acta Mater.*, 132:193–208, 2017.

[113] S. Kuramoto, T. Furuta, J. H. Hwang, K. Nishino, and T. Saito. Plastic deformation in a multifunctional Ti-Nb-Ta-Zr-O alloy. *Metall. Mater. Trans. A*, 37(3):657–662, 2006.

[114] Y. L. Hao, S. J. Li, S. Y. Sun, C. Y. Zheng, and R. Yang. Elastic deformation behaviour of Ti-24Nb-4Zr-7.9Sn for biomedical applications. *Acta Biomater.*, 3(2):277–286, 2007.

[115] S. J. Li, T. C. Cui, Y. L. Li, Y. L. Hao, and R. Yang. Ultrafine-grained ß-type titanium alloy with nonlinear elasticity and high ductility. *Appl. Phys. Lett.*, 92(4):5–8, 2008.